Robust Synchronization for PSK (DVB-S2) and OFDM Systems

Adegbenga B. Awoseyila

Submitted for the Degree of
Doctor of Philosophy
from the
University of Surrey

Centre for Communication Systems Research
Faculty of Engineering and Physical Sciences
University of Surrey
Guildford, Surrey, GU2 7XH, UK

December 2008

Abstract

The advent of high data rate (broadband) applications and user mobility into modern wireless communications presents new challenges for synchronization in digital receivers. These include low operating signal-to-noise ratios, wideband channel effects, Doppler effects and local oscillator instabilities. In this thesis, we investigate robust synchronization for DVB-S2 (Digital Video Broadcasting via Satellite) and OFDM (Orthogonal Frequency Division Multiplexing) systems, as these technologies are well-suited for the provision of broadband services in the satellite and terrestrial channels respectively.

DVB-S2 systems have a stringent frequency synchronization accuracy requirement and are expected to tolerate large carrier frequency offsets. Consequently, the existing techniques make use of a coarse acquisition and a fine-tracking stage. However, the use of two stages introduces extra synchronization delays. Therefore, we propose an improved technique for DVB-S2 frequency synchronization based on a novel method also proposed for single frequency estimation. The proposed method is single-stage, feed-forward, of practical complexity and has a wide estimation range. Consequently, a significant reduction in synchronization delays and a wider estimation range is achievable for DVB-S2 fixed and mobile systems.

On the other hand, OFDM systems are quite sensitive to symbol timing offsets and very sensitive to carrier frequency offsets due to orthogonality requirements. The existing techniques for timing and frequency synchronization suffer from various drawbacks in terms of overhead efficiency, computational complexity, accuracy and estimation range. Therefore, in this thesis, we propose two novel low-complexity techniques for timing and time-frequency synchronization in OFDM respectively. Both use only one training symbol with a simple and conventional structure to achieve a similar bit-error-rate (BER) performance to that of an ideal synchronized system and also a wide frequency estimation range. The improvement achieved translates into reduced overhead, higher power efficiency, lower hardware costs and higher reliability in OFDM receivers.

Keywords: autocorrelation, cross-correlation, normalization, threshold criterion.

E-mail: a.awoseyila@surrey.ac.uk

WWW: www.ee.surrey.ac.uk/ccsr

Acknowledgements

I wish to express my heartfelt gratitude to Prof. Barry Evans and Dr. Christos Kasparis for their supervision of this PhD research: your wealth of experience, availability, guidance, support and belief in me has been greatly helpful. My profound appreciation also goes to CCSR (and the European MOWGLY and SatNEx projects) for the financial support provided for my PhD study.

My love and appreciation is extended to my darling wife and my beloved son who have both been a strong motivation for me to complete my PhD successfully in a timely manner. I also deeply appreciate my parents and siblings for all their love and moral support. Thank you mum for funding my MSc., otherwise I probably would never have embarked upon a PhD degree.

I am grateful to all staff and students in CCSR for their friendliness, support and encouragement throughout my study. My gratitude is also extended to my friends and loved ones everywhere; and all those whose negative actions motivated me to aspire to the greatest heights of self-development.

Most importantly, my deepest appreciation goes to my saviour and lord, the bread of life, the prince of peace, the shepherd of my soul, my source and my joy, the sound of my music and the song that I sing. To him be all the glory.

Contents

List of Figures

List of Tables

Acronyms

1D	One Dimensional
2D	Two Dimensional
3G	3rd Generation
3GPP	3G Partnership Project
ACM	Adaptive Coding and Modulation
A/D	Analogue-to-Digital
ADSL	Asymmetric Digital Subscriber Line
AWGN	Additive White Gaussian Noise
B3G	Beyond 3G
BCH	Bose-Chaudhuri-Hochquenghem
BER	Bit Error Rate
BLUE	Best Linear Unbiased Estimation
CDF	Cumulative Distribution Function
C/N	Carrier-to-Noise
CP	Cyclic Prefix
CRLB	Cramer-Rao Lower Bound
DA	Data-Aided
D/A	Digital to Analogue Conversion
DAB	Digital Audio Broadcasting
DD	Decision Directed
DVB	Digital Video Broadcasting
DVB-H	DVB Handheld
DVB-RCS	Digital Video Broadcasting Return Channel via Satellite
DVB-S	DVB via Satellite (1st generation standard)
DVB-S2	DVB via Satellite (2nd generation standard)
DVB-SH	DVB via Satellite to Handhelds
DVB-T	DVB Terrestrial
FD	Frequency Domain
FEC	Forward Error Correction
FED	Frequency Error Detector
FF	Feed Forward

FFT	Fast Fourier Transform
GI	Guard Interval
ICI	Inter Carrier Interference
IFFT	Inverse Fast Fourier Transform
ISI	Inter Symbol Interference
LDPC	Low Density Parity Check
LO	Local Oscillator
LOS	Line-Of-Sight
LS	Least Squares
LTE	Long Term Evolution
MAP	Maximum A Posteriori
MAX	Maximum
MCRB	Modified Cramer-Rao Bound
ML	Maximum Likelihood
MOWGLY	Mobile Wideband Global Link System
MMSE	Minimum Mean Square Error
MSE	Mean Square Error
MVU	Minimum Variance Unbiased
NCO	Number Controlled Oscillator
NDA	Non-Data-Aided
NLOS	Non-Line-Of-Sight
OFDM	Orthogonal Frequency Division Multiplexing
OFDMA	Orthogonal Frequency Division Multiple Access
PDP	Power Delay Profile
PED	Phase Error Detector
PER	Packet-Error-Rate
PL	Physical Layer
PLSC	Physical Layer Signalling Code
PN	Pseudo-random Noise
PSK	Phase Shift Keying
QoS	Quality of Service
QPSK	Quadrature PSK
RMS	Root Mean Square
RMSE	Root-Mean-Square-Error

SNR	Signal-to-Noise-Ratio
SOF	Start of Frame
TD	Time Domain
TC	Threshold Crossing
UMTS	Universal Mobile Telephony Service
VCM	Variable Coding and Modulation
VCO	Voltage Controlled Oscillator
WiFi	Wireless Fidelity (for WLAN)
WLAN	Wireless Local Area Networks
WMAN	Wireless Metropolitan Area Networks
WiMAX	Worldwide Interoperability for Microwave Access
WPA	Weighted Phase Averager
WLP	Weighted Linear Predictor
WNALP	Weighted Normalized Autocorrelation Linear Predictor
WNLP	Weighted Normalized Linear Predictor

Notations

a	Angle of arrival
A	Amplitude
$B(g)$	Integer frequency metric (post-FFT)
c	Speed of light
$c(k)$	Transmitted data symbol
$c(t)$	Transmitted signal
d	Symbol timing index/instant
$\hat{d}$	Symbol timing estimate
$\hat{d}_{check}(n)$	Operational timing checkpoint
$e(k)$	Error signal
E_b	Energy per bit
E_s	Energy per symbol
f_0	Frequency
$\hat{f}_0$	Frequency estimate
f_c	Carrier frequency
f_d	Doppler frequency shift
f_m	Maximum Doppler frequency shift
Δf	Normalized carrier frequency offset
$\Delta\hat{f}$	Normalized carrier frequency offset estimate
F_{th}	Integer frequency threshold
g	Channel gain
G	Length of cyclic prefix/guard interval
$h(m)$	Discrete-time impulse response of the wideband channel
$h(t,\tau)$	Continuous-time impulse response of the wideband channel
$I(\hat{d}_{check})$	Integer frequency metric (pre-FFT)
$I(f)$	Frequency periodogram

I_0	Modified Bessel function of the first kind and zeroth-order
k	Rice k-factor
k	Sample index
l	Number of identical parts in training symbol
L	Number of pilot fields
L_s	Number of symbols contained in one DVB-S2 payload segment
m	Autocorrelation lag
M	Timing metric
$n(k)$	Zero-mean complex additive white Gaussian noise (samples)
$n(t)$	Zero-mean complex additive white Gaussian noise (continuous-time)
$n_{checkpoints}$	Maximum number of timing checkpoints
n'	Set of indices for previously determined checkpoints
N	Data record length/pilot field length/FFT size
N'	FFT resolution
N_0	Noise spectral density
N_{use}	Number of used OFDM subcarriers
$p(r)$	Probability density function
$P_x(d)$	Cross-correlation
P_{xNC}	Cross-correlation at non-coherent timing instants
$P_{dx}(d)$	Differential cross-correlation
P_{FA}	Probability of false alarm
$r(k)$	Received signal samples
$r(t)$	Continuous-time received signal
r_{cor}	Frequency-offset-corrected signal
R	Energy term
$R(m)$	Autocorrelation
$\breve{R}(m)$	Normalized autocorrelation
$R_T(m)$	Autocorrelation sum
S	OFDM training symbol
T	Symbol period
T_{th}	Timing adjustment threshold

v	Speed of mobile
$\bar{v}$	Frequency offset
V_n	Weighted differential of OFDM subcarriers
x_t	Received exponential in AWGN
$\breve{x}_t$	Normalized received exponential in AWGN
w_t	Smoothening function (weighting coefficients)
w_m	Smoothening function (weighting coefficients)
w_k	Smoothening function (weighting coefficients)
x_k	Transmitted signal samples
X_n	*nth* subcarrier data symbol (pre-FFT)
y_k	Discrete-time signal observations
$y(t)$	Wideband received signal without AWGN
Y	Data record vector
Y_n	*nth* subcarrier data symbol (post-FFT)
$z(k)$	Modulation-removed signal
δ	Threshold
ε	Integer symbol timing offset
θ	Signal/Carrier phase
λ	Expected channel delay spread
Λ	Likelihood function
σ^2	Variance of Gaussian random variable
τ	Sample timing offset
τ_n	Channel delay
$\omega(k)$	Zero-mean complex additive white Gaussian noise (OFDM samples)

Chapter 1

1 Introduction

1.1 Wireless Communications and Broadband Services

A current trend in modern digital communications is an increasing demand for high-speed/high-capacity (i.e. broadband) applications, wherein data rates of the order of Megabits/s are supported [1],[2]. This adds to another trend of increased user mobility in wireless communication systems. A high data rate implies that more of the scarcely available radio spectrum is required. Consequently, transmission techniques which can provide greater efficiency in bandwidth without comprising power efficiency are required. Another implication of broadband transmissions is that the mobile radio channel may transform from narrowband into wideband (frequency-selective) characteristics, depending on the profile of the surrounding clutter in such channels [3]-[5]. The satellite communication channel is more robust against the latter trend due to the high elevation angles of geostationary satellites with regard to ground-based receivers [6],[7]. However, the need for power efficiency is more critical in satellite systems due to their long transmission range. The second generation digital video broadcasting via satellite (DVB-S2) standard [1],[8],[9] has been designed to provide for broadcast and interactive broadband services in the satellite channel while orthogonal frequency division multiplexing (OFDM) modulation [10]-[17] has become the technique of choice in many terrestrial and satellite-mobile broadband systems due to its bandwidth efficiency and robustness in the wideband channel.

The DVB-S2 standard makes use of advanced modulation and coding techniques to achieve higher transmission efficiencies. It incorporates the techniques of 'adaptive coding and modulation' (ACM) and 'variable modulation and coding' (VCM) to achieve a high data throughput despite adverse satellite channel conditions. Its combination with the DVB standard for return channels via satellite (DVB-RCS) [18] provides two-way satellite communications for fixed terminals, which is well suited for interactive broadband services: a typical user demand nowadays. Based on this, the European project: mobile wideband global link system (MOWGLY) [19] has proposed the DVB-S2 standard for the downlink of internet broadband services to collective users of mobile platforms (such as airplanes, ships, and trains), with a quality of service (QoS) comparable to that of traditional terrestrial networks. Thus, DVB-S2 is likely to become the most used satellite standard for digital video broadcasting and broadband internet services to fixed and mobile terminals in the near future. Figure 1.1 illustrates the MOWGLY architecture for broadband communications.

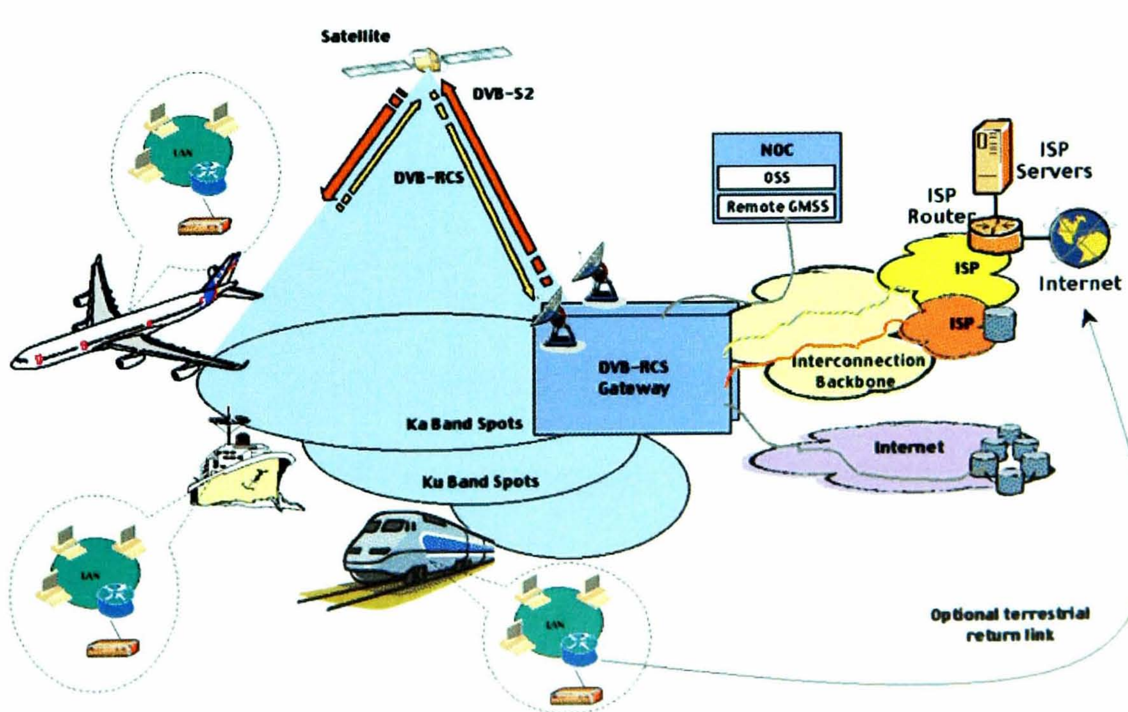

Figure 1.1: The MOWGLY architecture for mobile broadband via satellite [19]

Orthogonal Frequency-Division Multiplexing (OFDM) is a modulation technique, which uses many orthogonal sub-carriers to transmit/receive a high data rate signal [10]-[17]. Its use of orthogonal subcarriers which are closely spaced leads to great bandwidth efficiency, in addition to its robustness against frequency-selectivity in the multipath channel. Consequently, it has become an increasingly popular scheme for high data-rate applications and is already being applied in several wireless communication standards such DAB [20], DVB-T [21], DVB-H [22], DVB-SH [23], WiFi (IEEE.802.11a) [24], WiMAX(IEEE.802.16) [25] and 3GPP LTE [26]. OFDM is also likely to be incorporated into future broadband systems such as B3G and satellite-mobile standards. Figure 1.2 shows an example configuration of the WiMAX system for broadband communications.

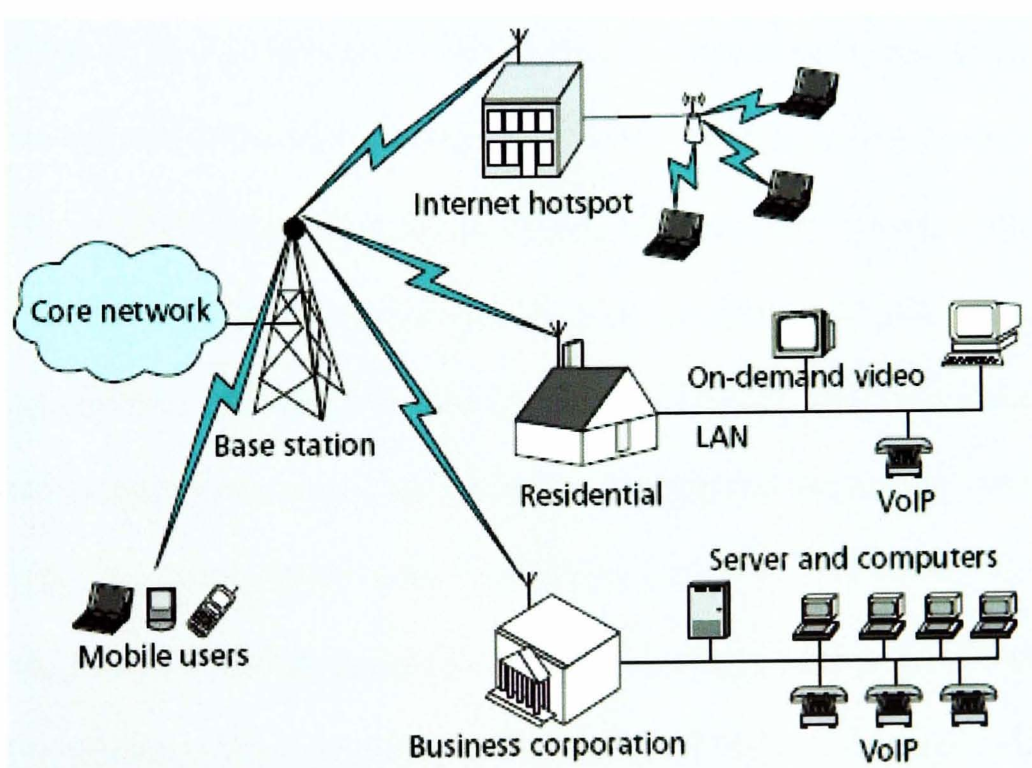

Figure 1.2: Example WiMAX configuration for broadband communications [27]

1.2 Synchronization Issues in DVB-S2 and OFDM Systems

Carrier frequency offset in the received signal of a digital modem arises from receiver oscillator instabilities and/or the Doppler effect [28]-[30]. The DVB-S2 system has a stringent frequency synchronization requirement due to its incorporated 'physical layer' frame structure and its operation at low SNR [31]. Moreover, in order to provide cheap receiver terminals to many consumers, DVB-S2 systems are expected to use low-cost oscillators which may cause large frequency offsets in the received signal [32]. These offsets will increase where mobility is introduced into DVB-S2 systems, due to Doppler frequency shifts. Hence, robust frequency synchronization at very low SNR is required for DVB-S2 systems in terms of both estimation accuracy and estimation range.

On the other hand, OFDM systems are quite sensitive to symbol timing errors and very sensitive to carrier frequency offsets due to orthogonality requirements [33], [34]. Although OFDM exhibits some tolerance to symbol timing errors when the cyclic prefix length is longer than the maximum channel delay spread, a timing error, wherein the FFT window is positioned to include copies of either preceding or succeeding symbols, will result in intersymbol interference (ISI) which destroys the orthogonality of the subcarriers and consequently degrades the decoder performance [33]. Carrier frequency offsets cause a shift in the OFDM subcarrier frequencies which leads to a loss of orthogonality, thereby resulting in inter-carrier interference (ICI) and degradation of the decoder performance [34]. Since consumer-grade crystal oscillators usually have a limit on the frequency accuracy they can provide and several OFDM systems support user mobility, it is expected that in practice, the frequency offset may be many multiples of the subcarrier spacing. As such, there is a need for frequency estimators having a wide acquisition range in order to keep receiver cost low.

Synchronization in DVB-S2 and OFDM systems has received significant attention in the literature. However, the existing techniques suffer from various drawbacks which inhibit an enhanced efficiency in receiver synchronization. Therefore, in this thesis, we focus on robust synchronization for DVB-S2 and OFDM systems. It is our objective to investigate the possibilities of low-complexity frequency and timing estimators which can achieve optimum accuracy, wide estimation range and minimal synchronization delay; such that these systems can have a decoder performance as close to an ideal synchronized system as possible.

1.3 Novel Achievements

- Two techniques are proposed in this thesis for *improved single frequency estimation with wide acquisition range*. The existing feed-forward techniques with optimal accuracy and practical computational complexity are unable to achieve the full theoretical frequency estimation range of ~50% the sampling rate. In contrast, our proposed methods achieve the full frequency estimation range without compromising optimal accuracy and with a lower computational complexity. This increased estimation range means that larger frequencies can be practically estimated in signal processing applications which include carrier frequency synchronization in wireless communications.
- A technique is proposed in this thesis for *improved carrier frequency synchronization in DVB-S2 systems*. The proposed technique achieves reduced synchronization delay and increased estimation range for DVB-S2 frequency synchronization as compared to the existing techniques, without

significant increase in computational complexity. The improvement achieved has even greater relevance in DVB-S2 mobile systems.

- A technique is proposed in this thesis for *improved frame/symbol timing estimation in OFDM systems*. The proposed low-complexity method uses only one training symbol, having a simple and conventional structure to achieve near-ideal accuracy for OFDM timing in contrast to the existing techniques. This results in a BER performance similar to that of an ideal time-synchronized system which is not achievable by existing techniques due to their associated timing errors. Consequently, the proposed method provides for greater power-efficiency in OFDM systems.
- A technique is proposed in this thesis for *robust and efficient time-frequency synchronization for OFDM systems*. The proposed low-complexity method uses only one training symbol, having a simple and conventional structure, to achieve robust, reliable and full-range time-frequency synchronization in OFDM systems. This all-in-one performance is not achievable by the existing techniques. Consequently, the proposed method achieves a BER performance similar to that of an ideal time-frequency-synchronized system in contrast to the existing methods. By using the proposed algorithm, OFDM receivers will be able to operate at lower SNR, with reduced hardware complexity and/or processing delay. Furthermore, the wide-range frequency estimation achieved provides for cheaper OFDM receivers, using low-grade oscillators, since they will be able to operate under large frequency offsets. An additional advantage is that the training symbol structure is compatible with current wireless network standards.

- Based on the research work presented in this thesis, a patent has been filed on OFDM timing and frequency synchronization, two conference papers published on DVB-S2 frequency synchronization [35],[36], a journal paper published on single frequency estimation [37] and another on OFDM timing estimation [38]. A journal paper has also now been submitted for publication on OFDM time-frequency synchronization [39], post the patent filing.

1.4 Structure of the Thesis

This thesis consists of seven chapters, which are organised in the following way:

Chapter 1 gives a basic introduction to the research work. This includes an overview of the crucial synchronization requirements of DVB-S2 and OFDM broadband systems and the novel achievements of this thesis.

Chapter 2 presents a basic review of the background theory used in the thesis. This includes a review of the wireless communication channel, parameter estimation theory and synchronization techniques in digital receivers.

Chapter 3 discusses single frequency estimation in complex additive white Gaussian noise. The existing techniques are reviewed and their shortcomings established. Consequently, two novel low-complexity techniques are proposed to improve frequency estimation performance. The methods are compared via computer simulations in the AWGN channel, with results shown in terms of frequency mean-square-error (MSE).

Chapter 4 discusses carrier frequency synchronization for DVB-S2 fixed and mobile systems. The DVB-S2 standard is reviewed and the existing techniques are presented. In order to improve performance, a low-complexity method is developed by modifying the novel technique proposed for single frequency estimation. The methods are compared via computer simulations in AWGN and Rician fading channels, with results shown in terms of frequency MSE.

Chapter 5 discusses timing synchronization in OFDM systems. The OFDM digital modulation technique is reviewed and the existing techniques for OFDM timing estimation discussed in order to establish their various shortcomings. Consequently, a novel low-complexity technique is proposed to improve timing performance. The methods are compared via computer simulations in AWGN and fading ISI channels, with results shown in terms of timing MSE, timing bias and bit-error-rate (BER).

Chapter 6 discusses combined timing and frequency synchronization in OFDM systems, within the context of wide-range frequency estimation. The existing techniques are presented and a novel low-complexity technique is proposed to improve performance. The methods are compared via computer simulations in terrestrial and satellite-terrestrial fading ISI channels, with results shown in terms of frequency MSE, timing MSE, BER and packet-error-rate (PER).

Chapter 7 presents a summary of the conclusions drawn from the chapters of this thesis and suggests some future research work.

Chapter 2

2 Signal Synchronization in the Wireless Channel

2.1 Introduction

This chapter reviews the background theory of signal synchronization in the wireless communication channel, which includes a basic review of the wireless channel characteristics, estimation theory and synchronization techniques for digital receivers. The issue of synchronization in a digital receiver is very important as it has a major impact on receiver hardware, costs and performance. It involves the estimation of some reference parameters associated with the received signal in order to ensure reliable data detection [28]-[30]. In a baseband system where received pulses are matched filtered and then sampled, there is a need to determine the optimum sampling time, which corresponds to the pulse peaks. In addition, passband digital systems need to perform carrier frequency synchronization in order to determine and correct the frequency offset introduced into the received signal by receiver oscillator instabilities and/or the Doppler effect arising from the wireless channel [40],[41]. After carrier frequency synchronization, the carrier phase offset arising from transmitter/receiver oscillator mismatch and/or the wireless channel response also needs to be corrected. Frame synchronization helps to determine the boundaries between blocks of data and is of key importance in digital transmissions that use block coding and/or burst multiplexing. Figure 2.1 shows the block diagram of an example digital receiver in the wireless channel wherein various synchronization tasks are implemented.

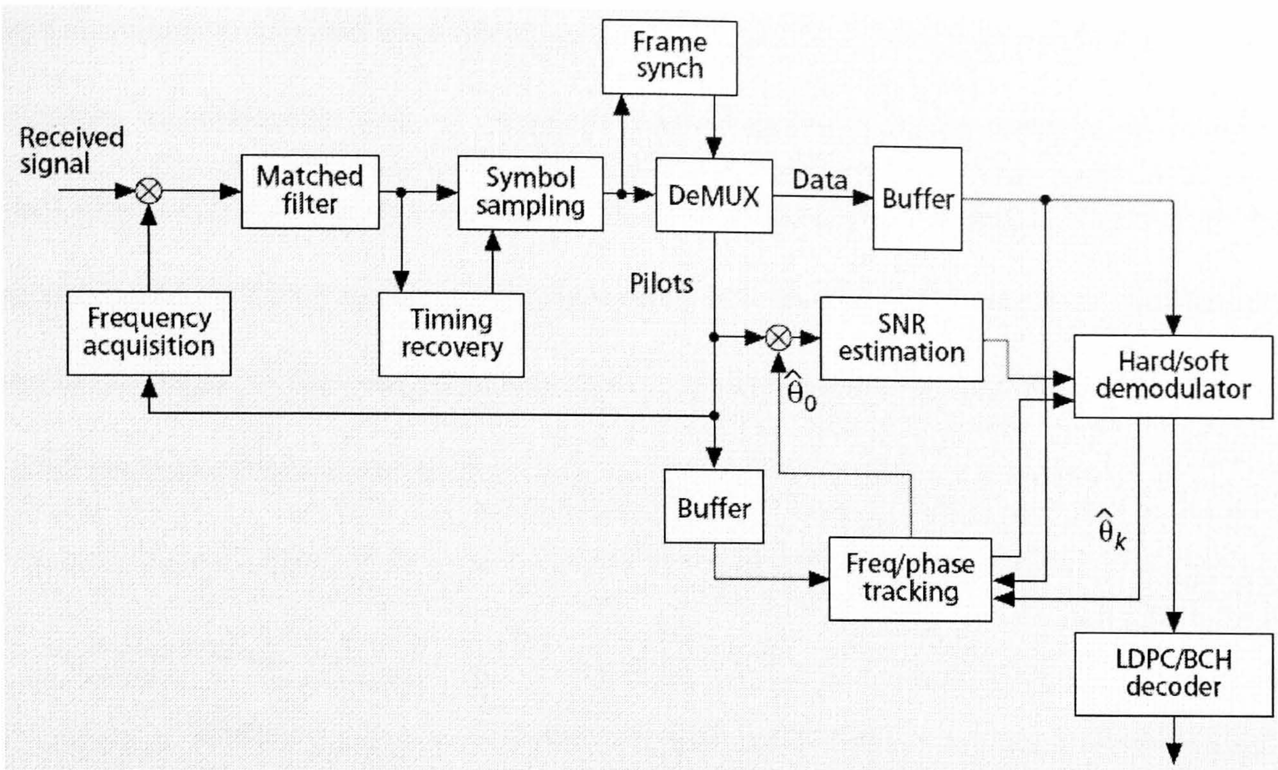

Figure 2.1: Block diagram of a DVB-S2 receiver [42]

The techniques used for synchronization are either based on ad-hoc reasoning or classical estimation theory such as the maximum likelihood (ML) principle. Also, there are data-aided (DA), decision-directed (DD) and non-data-aided (NDA) approaches to synchronization, depending on the application requirements. With the DA approach, known symbols (training pilots) are inserted into the transmitted sequence while the DD approach uses previous decisions on the demodulated data as a feedback into the estimation process.

2.2 The Wireless Communication Channel

Figure 2.2 shows a generic communication system as described by Claude Shannon [43]. This consists of an information source, a transmitter which inserts the information into a communications channel, a channel through which the transmitted signal propagates, a receiver which is used to recover the transmitted information from the channel and a destination which makes use of the information. The wireless communication channel is a radio wave propagation channel. This wireless channel consists of different type of noise sources, which include multiplicative fading processes (path loss, shadowing and fast fading) and additive noise (thermal and shot noise in the receiver, atmospheric noise and interference). Propagation mechanisms that contribute to the multiplicative noise include reflection, refraction, diffraction, scattering and absorption [3]-[5].

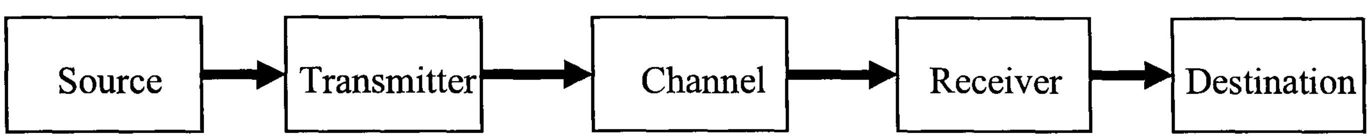

Figure 2.2: A generic communication system

2.2.1 The AWGN Channel

The simplest case of the wireless communication channel is the additive white Gaussian noise (AWGN) channel [3]-[7]. This is the type of channel that applies when the transmitter, receiver and their surrounding objects are not in relative motion and there is a line-of-sight propagation between transmitter and receiver. In this scenario, the received signal is given as follows:

$$r(t) = Ac(t) + n(t) \tag{2.1}$$

where A is the overall path loss, $c(t)$ is the transmitted signal and $n(t)$ represents the complex additive white Gaussian noise.

Where relative motion is involved between the transmitter, receiver and/or surrounding objects, the channel is referred to as a mobile radio channel. In addition to the path loss and additive noise experienced in the AWGN channel, the received signal from a mobile wireless channel experiences shadowing and fast-fading.

2.2.2 Narrowband Fast-Fading

Fast fading occurs due to the constructive and destructive interference between several (multipath) waves arriving at the mobile receiver from the transmitter due to the presence of surrounding objects (scatterers) in the channel. In the narrowband channel, fast fading is due to phase differences between these multipath waves which all arrive at practically the same time to the receiver. It is also referred to as frequency-flat fading because it affects all frequencies in the transmitted signal spectrum equally [3]. Equation (2.1) can therefore be rewritten as:

$$r(t) = A\alpha(t)\,c(t) + n(t) \tag{2.2}$$

where A represents the overall path loss and shadowing, $\alpha(t)$ is the complex time-dependent coefficient that accounts for fast-fading, $c(t)$ is the transmitted signal and $n(t)$ represents the complex additive white Gaussian noise.

2.2.2.1 Rayleigh Fading

Rayleigh fading is a type of narrowband fading experienced in non-line-of-sight (NLOS) multipath propagation i.e. where the direct wave between transmitter and receiver is completely blocked [5]. The received signal experiences amplitude fading whose probability density function (PDF) follows a Rayleigh distribution as shown in (2.3). This is because $\alpha(t)$ in this case is a complex Gaussian random variable whose magnitude r is Rayleigh-distributed with a PDF given as:

$$p_R(r) = \frac{r}{\sigma^2}\, e^{-\frac{r^2}{2\sigma^2}} \tag{2.3}$$

where σ^2 is the variance of either the real or imaginary components of $\alpha(t)$.

The Rayleigh channel can also be characterized in terms of the probability distribution of the instantaneous SNR (γ) which is a function of the mean SNR (Γ) of the received signal [3] as follows:

$$\begin{aligned} p_\gamma(\gamma) &= \frac{1}{\Gamma}\, e^{-\frac{\gamma}{\Gamma}} && \textit{for } \gamma > 0 \\ &= 0 && \textit{otherwise} \end{aligned} \tag{2.4}$$

2.2.2.2 Rician Fading

In line-of-sight (LOS) multipath propagation, the received signal is made of a coherent LOS component with constant power and a random part based on the Rayleigh distribution [3],[6]. The fading coefficient $\alpha(t)$ is now the sum of a real constant s and a complex Gaussian random variable with magnitude r. The magnitude of $\alpha(t)$ has a PDF which follows the Rice distribution as shown below:

$$p_R(r) = \frac{r}{\sigma^2}\, e^{-\frac{(r^2+s^2)}{2\sigma^2}}\, I_0\left[\frac{rs}{\sigma^2}\right] \tag{2.5}$$

where σ^2 is the variance of either the real or imaginary components of the random part and I_0 is the modified Bessel function of the first kind and zeroth-order [3]. The Rice k-factor gives a measure of how strong the LOS component is when compared with the multipath and the Rice PDF can be rewritten in terms of the k-factor as:

$$p_R(r) = \frac{r}{\sigma^2} e^{-\frac{r^2}{2\sigma^2}} e^{-k} I_0\left[\frac{r\sqrt{2k}}{\sigma}\right] \tag{2.6}$$

$$\mathrm{k} = \text{Power in constant part} \div \text{Power in random part} = s^2 / 2\sigma^2 \tag{2.7}$$

For k=0, the Rice distribution reverts back to Rayleigh while the channel becomes an AWGN channel as $\mathrm{k} \to \infty$.

2.2.3 Wideband Fast-Fading

Unlike the narrowband channel where fast fading is due to phase differences between multipath waves which arrive practically at the same time to the receiver, the differential delays between various multipath waves are large compared to the symbol duration of the transmitted signal in the wideband channel [3]-[5]. The transmitted signal experiences inter-symbol interference and frequency-selective fading, which further complicates the communication system design. The continuous-time received signal model in a wideband wireless system is given as:

$$r(t) = y(t) + n(t) \tag{2.8}$$

$$y(t)=\int_{-\infty}^{\infty} h(t,\tau)\, c(t-\tau)\, d\tau \tag{2.9}$$

where $h(t,\tau)$ is the time-variant impulse response of the wideband channel, also referred to as the input delay spread function with τ denoting the delay of the channel.

2.2.3.1 The Discrete-Time Wideband Channel Model

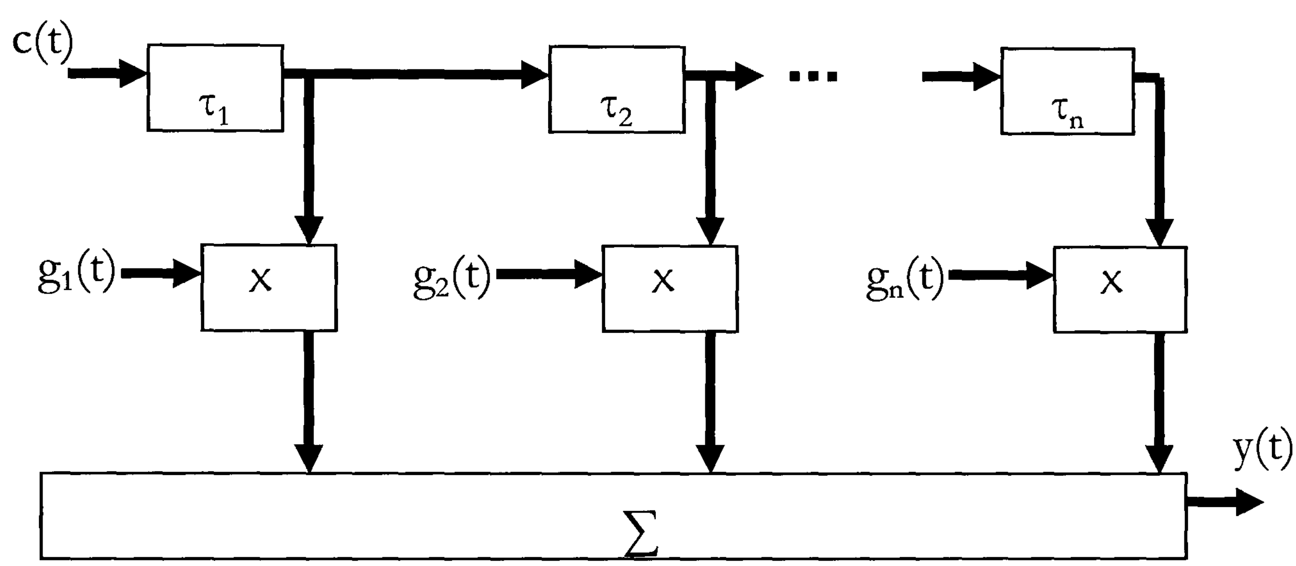

Figure 2.3: The tapped-delay-line wideband channel model

The wideband channel can be considered as a combination of several narrowband-fading paths, combined with appropriate delays. Thus it can be modelled using a tapped delay line, representing the effect of scatterers in discrete delay ranges, lumped together into distinct delay taps (τ_n) as shown in Figure 2.3. The taps are typically assumed to be uncorrelated and they have gain processes (g_n), which vary according to narrowband fading statistics [3]. Thus, the channel acts as a linear filter, having a time-variant impulse response.

The power delay profile (PDP) of a wideband channel can be used to characterize such channel. Table 2.1 shows an example PDP, standardized by ETSI [44] for the universal mobile telephony service (UMTS).

Table 2.1: PDP for ETSI vehicular test environment [44]

Tap	Relative delay (ns)	Mean relative power (dB)
1	0	0.0
2	310	-1.0
3	710	-9.0
4	1090	-10.0
5	1730	-15.0
6	2510	-20.0

The PDP of a wideband channel helps to specify some important practical parameters such as *excess delay*, *total excess delay*, *mean delay* and *RMS delay*. The excess delay of any tap is its delay relative to the first arriving tap while the total excess delay is the excess delay of the last arriving tap. The mean delay τ_0 and RMS delay τ_{RMS} are defined in equation (2.10) and (2.11) respectively. Whereas the mean delay gives an idea of the centre of gravity of the PDP, the RMS delay is an indicator of how dispersive a channel is.

$$\tau_0 = \sum_{i=1}^{n} P_i \tau_i \Big/ P_{total} \tag{2.10}$$

$$\tau_{RMS} = \sqrt{\left[\sum_{i=1}^{n} P_i \tau_i^2 \Big/ P_{total}\right] - \tau_0^2} \tag{2.11}$$

$$P_{total} = \sum_{i=1}^{n} P_i \tag{2.12}$$

where P_i denotes the power of each tap having delay τ_i.

The coherence bandwidth of a channel defines the frequency separation wherein the correlation between two frequency components is halved and this bandwidth is inversely proportional to the RMS delay spread [3]. Consequently, a system is classified as wideband if the signal bandwidth is large compared to the coherence bandwidth or if the RMS delay is significant in comparison to the symbol duration.

2.2.3.2 Inter-Symbol Interference

Inter-Symbol Interference (ISI) is the resultant effect of the wideband channel. This is because the energy arriving at the receiver (having traversed the channel) becomes spread in time due to multipath effects. Thus, the effective duration of a received symbol exceeds that of the transmitted symbol by the delay spread of the channel. Consequently, the last arriving taps of a current received symbol can overlap with the first arriving taps of the next received symbol, thus causing ISI [3]-[5].

2.2.4 Second-Order Fast-Fading Statistics

The second-order fading statistics deal with rate of change of fading i.e. how fast the signal level changes between different fade levels. These statistics are primarily determined by the Doppler effect and the Doppler spectrum.

2.2.4.1 The Doppler Effect

When a mobile is in relative motion to a transmitter, there occurs a shift in the frequency of the arriving wave due to the Doppler effect [3]. This apparent change in frequency called the Doppler shift f_d is given by equation (2.13) with a maximum shift f_m occurring when the angle of arrival $a = 0$.

$$f_d = f_c \frac{v}{c} \cos a \qquad (2.13)$$

where f_c is the carrier frequency of the arriving wave, v is the speed of the mobile and c is the speed of light.

It can be deduced from (2.13) that the bandwidth of the received signal is spread relative to that of the transmit signal when multipath propagation occurs, since the arriving waves will have different angles of arrival. This phenomenon is known as the Doppler spread, resulting in a Doppler spectrum whose greatest possible bandwidth is twice the maximum Doppler shift i.e. $2f_m$.

2.2.4.2 The Doppler Spectrum

The bandwidth and shape of the Doppler spectrum directly affects the rate of change of fading between different signal levels [3]. The classical Doppler spectrum assumes that all the multipath waves arrive horizontally at the mobile receiver with their azimuth angles uniformly distributed. This leads to a U-shaped Doppler spectrum as shown in Figure 2.4 due to the effect of 'cos a' in (2.13). The second-order fast-fading statistics helps to determine practical parameters such as the *level* *crossing rate (LCR)* and the *average fade duration (AFD)*. The LCR defines the rate at which the received signal rises above a reference level while the AFD indicates the mean duration of fades in the received signal below a reference level [3].

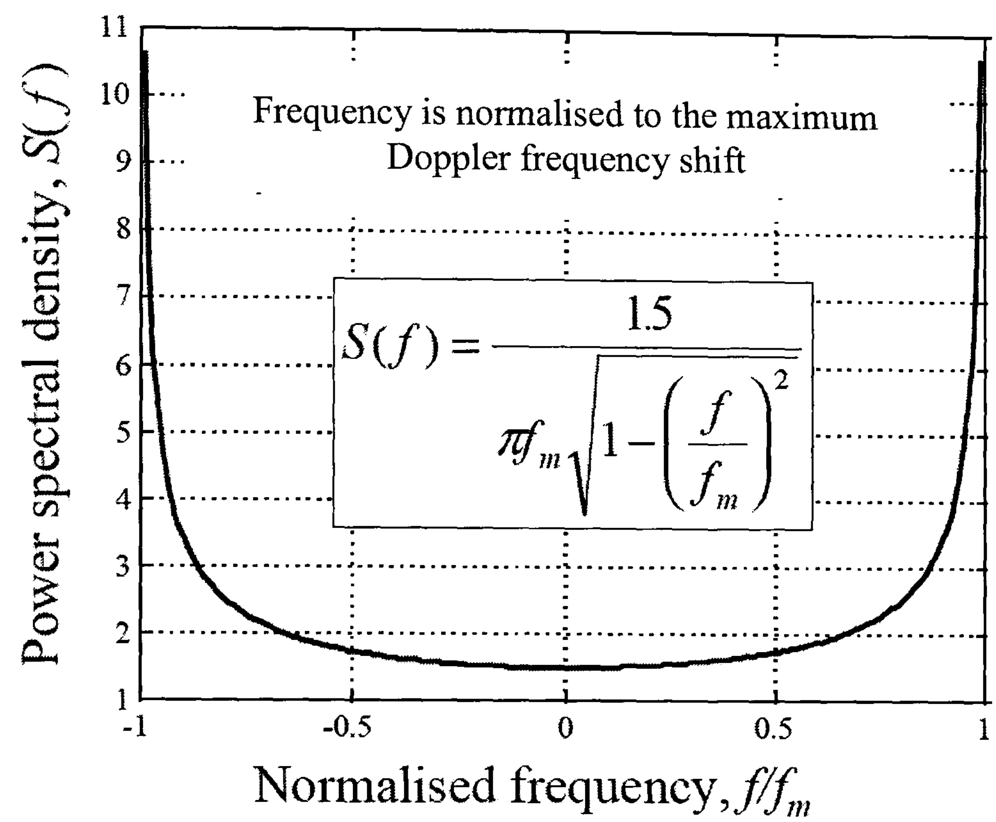

Figure 2.4: The classical Doppler spectrum [3]

2.2.5 Techniques for Overcoming Channel Impairments

The different types of wireless channel impairment can be overcome or their effects mitigated by the use of available communication techniques. Forward Error Control (FEC) coding can be used to overcome the effect of additive noise which causes random errors in the decoded data at low signal-to-noise ratios. It can also be used with/without interleaving to mitigate the effect of deep fades which causes bursty errors in the mobile channel [45]. Another technique used in overcoming the effect of channel fading is diversity, which includes space, frequency, polarisation and/or time diversity.

Equalisation techniques can be used to recover from the dispersive effects of a wideband channel, although the computational requirements of optimal equalisation can be very demanding [3-5]. An alternative approach is to restrict the transmitted data rate or to employ multicarrier modulation techniques such as Orthogonal Frequency Division Multiplexing (OFDM) [10]. This technique will be discussed further in Chapters 5 and 6.

2.3 Estimation Theory

2.3.1 Parameter Estimation in Signal Processing

Many signal processing applications such as radar, communications, biomedicine, seismology and control systems involve the estimation of parameters based on the observation of a continuous-time (analogue) signal [46]-[49]. An example is the estimation of carrier frequency offset in a digital communications receiver. A modern trend is to convert the received analogue signal into discrete-time observations y_k, in order benefit from the many advantages of digital signal processing. The problem therefore reduces to the estimation of a parameter λ based on N noisy observations/samples which depend on λ [46]. It should be noted that an estimator is a random variable and its performance can be predicted/analysed statistically since it depends on noisy observations. In general, a data record whose probability density function (PDF) depends strongly on the unknown parameter will yield good estimation accuracy whereas estimation becomes impossible where such PDF is independent of the parameter to be estimated.

2.3.2 Minimum Variance Unbiased Estimation

There are many different types of estimation techniques for an unknown deterministic parameter. In defining what makes a good estimator, two criteria of interest are the estimation bias and mean-square-error (MSE) of the estimator. An unbiased estimator will produce the correct value of the unknown parameter λ on average and is therefore desirable. In other words, the expected output of an unbiased estimator is the true value of the estimated parameter, i.e. $\mathrm{E}(\hat{\lambda}) = \lambda$. In general,

$$\mathrm{E}(\hat{\lambda}) = \lambda + f(\lambda) \tag{2.14}$$

where $\mathrm{E}(\cdot)$ is the expected value operator and $f(\lambda)$ is a function which represents the bias of the estimator.

Estimators which have a small MSE provide a consistent performance, wherein the produced estimates have a small deviation from the true value. The MSE and the variance of any estimator are defined as follows:

$$MSE(\hat{\lambda}) = \mathrm{E}\left(\left[\hat{\lambda} - \lambda\right]^2\right) = \mathrm{E}\left(\hat{\lambda}^2 - 2\hat{\lambda}\lambda + \lambda^2\right) \tag{2.15}$$

$$VAR(\hat{\lambda}) = \mathrm{E}\left(\left[\hat{\lambda} - \mathrm{E}(\hat{\lambda})\right]^2\right) = \mathrm{E}\left(\hat{\lambda}^2 - 2\hat{\lambda}\mathrm{E}(\hat{\lambda}) + \mathrm{E}(\hat{\lambda})^2\right) \tag{2.16}$$

Substituting equation (2.14) into (2.15) and (2.16) and rearranging gives:

$$MSE(\hat{\lambda}) = VAR(\hat{\lambda}) + f^2(\lambda) \tag{2.17}$$

It is seen from (2.17) that the MSE comprises the variance of the estimator and an additional error term arising from the bias in the estimator [46],[47]. For unbiased estimators, the MSE is equal to the variance of the estimator and designing to achieve a minimum MSE for such estimators leads to the concept of minimum variance unbiased (MVU) estimation. This is the ultimate target of every good estimator design, although the MVU estimator does not always exist [46].

2.3.3 The Cramer-Rao Lower Bound

A key design issue for an estimator is its accuracy, i.e. how small its variance can be made. This accuracy limit is defined by the Cramer-Rao Lower Bound (CRLB) for unbiased estimators [46]-[49] and an estimator that achieves this bound is said to be efficient in terms of accuracy.

The CRLB is determined based on the likelihood function Λ which is the conditional PDF expressed as a function of the parameter λ with the data record being fixed [46]. Consider for example a Gaussian PDF; it is known that the sharpness of such PDF is inversely related to the associated variance of the Gaussian random variable. This sharpness therefore determines the bound on estimation accuracy and can be measured by the curvature of the log-likelihood function which is equivalent to the negative of its second derivative.

$$CRLB(\lambda) \triangleq \frac{1}{-\mathrm{E}\left(\frac{\partial^2 \ln \Lambda(Y|\lambda)}{\partial \lambda^2}\right)} = \frac{1}{\mathrm{E}\left(\left[\frac{\partial \ln \Lambda(Y|\lambda)}{\partial \lambda}\right]^2\right)} \tag{2.18}$$

where $Y = [y_0, y_1 \ldots\ldots y_{N-1}]$ is the data record. Consequently, the variance of any given estimator of the parameter λ can be expressed as:

$$VAR(\hat{\lambda}) \geq CRLB(\lambda) \tag{2.19}$$

An approximation of the CRLB which is easier to determine is the modified Cramer-Rao Bound (MCRB) which was proposed in [50] and discussed further in [28]. The CRLB for frequency estimation has been defined in [51] while its MCRB counterpart is presented in [28].

2.3.4 Maximum Likelihood Estimation

The maximum likelihood (ML) principle is one fundamental approach to parameter estimation [29],[46] based on the set task of estimating a non-random (i.e. deterministic) parameter λ from some of its noisy discrete-time observations y_k. The ML approach determines the value of λ that maximizes the conditional probability density function (PDF) of the observed data, as the value that most likely caused the observed data to occur. The ML estimate is therefore given as:

$$\hat{\lambda}_{ML} = \arg\max_{\lambda}\{p(Y \mid \lambda)\} \tag{2.20}$$

where $p(Y \mid \lambda)$ is the conditional PDF of Y.

In general, the ML estimator is asymptotically unbiased and asymptotically optimal in accuracy [46], although the issue of complexity may affect its practical implementation depending on the parameter to be estimated and the length of the data record.

2.3.5 Best Linear Unbiased Estimation

A practical estimation approach is to constrain the estimator to be linear within the data set and subsequently find the best estimator that is unbiased and uses a linear combination of the data record to achieve minimum variance. Such an estimator is referred to as the best linear unbiased estimator (BLUE) and is equivalent to the MVU estimator if it is also linear within the data set.

$$\hat{\lambda}_{BLUE} = \sum_{k=0}^{N-1} \omega_k y_k \tag{2.21}$$

where ω_k represents the linear combination coefficients and y_k represents the data.

To find the BLUE, the unbiased constraint i.e. $\mathrm{E}(\hat{\lambda}) = \lambda$ is used and the weighting coefficients ω_k are determined such as to minimize the variance of the estimator. It is noted that the unbiased constraint can only be achieved by a linear estimator if the expected value of the data set y_k is linear in the unknown parameter λ, otherwise there would be a need for non-linear transformation of the original data (where possible) to achieve this.

Unlike the ML estimator wherein the PDF of the data needs to be completely known, only the mean and covariance are required in order to determine the BLUE. This makes this estimation approach of increased practical value. A more detailed explanation of how to find the BLUE estimator is given in [46]. Where the PDF of the data is Gaussian, the BLUE is also equivalent to the MVU estimator. An example of a BLUE frequency estimator based on non-linear transformation of the received data is Kay's method [52].

2.3.6 Least Squares Estimation

The least squares (LS) estimation approach can be considered as a curve-fitting process [46], wherein the observed data is closely-fitted to a curve (signal model) which is a function of the unknown parameter λ. The LS approach does not assume any PDF for the observed data; rather it seeks to minimize the squared difference between the assumed signal model and the observed data as shown in (2.22). This makes it well suited to situations where statistical information is lacking or where other approaches fail.

$$\hat{\lambda}_{LS} = \arg\min_{\lambda}\left\{ \sum_{k=0}^{N-1} \left(y_k - s_k(\lambda) \right)^2 \right\} \tag{2.22}$$

where $s_k(\lambda)$ represents the samples of the assumed signal model.

The LS approach does not guarantee the best estimation performance since it uses curve-fitting rather than the PDF of the data. Moreover, the choice of signal model plays a very important role in its performance. Nonetheless, if a correct signal model is assumed and the associated noise is Gaussian, the LS estimator becomes equivalent to the ML estimator.

2.3.7 Minimum Mean Square Error Estimation

The minimum mean square error (MMSE) estimation approach is based on Bayesian philosophy [46]. In contrast to the classical approach where the unknown parameter λ is assumed to be deterministic, the Bayesian approach assumes the parameter λ to be random and seeks to estimate its specific realization through the use of a prior knowledge of λ. The difference between the two approaches is shown in mathematical terms as follows:

$$MSE_{classical}\left(\hat{\lambda}\right)=\mathrm{E}\left\{\left(\hat{\lambda}-\lambda\right)^2\right\}=\int\left(\hat{\lambda}-\lambda\right)^2 p(Y\mid\lambda)\,dY \tag{2.23}$$

$$MSE_{Bayesian}\left(\hat{\lambda}\right)=\mathrm{E}\left\{\left(\lambda-\hat{\lambda}\right)^2\right\}=\iint\left(\lambda-\hat{\lambda}\right)^2 p(Y,\lambda)\,dY\,d\lambda \tag{2.24}$$

where the classical estimator makes use of the conditional PDF $p(Y\mid\lambda)$ while the Bayesian estimator uses the joint PDF $p(Y,\lambda)$ since it assumes that λ is random. The joint PDF of the unknown parameter and the observed data can be derived by making use of Baye's theorem [47] which can be stated as follows:

$$p(Y,\lambda)=p(Y\mid\lambda)p(\lambda)=p(\lambda\mid Y)p(Y) \tag{2.25}$$

where $p(\lambda)$ is the prior PDF and $p(\lambda\mid Y)$ is the posterior PDF which can be obtained as:

$$p(\lambda\mid Y)=[p(Y\mid\lambda)p(\lambda)]/p(Y) \tag{2.26}$$

$$p(Y) = \int p(Y \mid \lambda) p(\lambda) d\lambda \tag{2.27}$$

Equation (2.26) can be substituted into (2.24) to give:

$$MSE_{Bayesian}\left(\hat{\lambda}\right) = \int \left[\int \left(\lambda - \hat{\lambda}\right)^2 p(\lambda \mid Y)\, d\lambda \right] p(Y) dY \tag{2.28}$$

The minimization of the Bayesian MSE shown in equation (2.28) leads to the MMSE estimator which is given as:

$$\hat{\lambda}_{MMSE} = \int \lambda\, p(\lambda \mid Y) d\lambda = \mathrm{E}(\lambda \mid Y) \tag{2.29}$$

It can be seen from (2.25) to (2.29) that the prior PDF plays a very important role in Bayesian estimation and a wrong choice will result in poor estimation. Also, by using prior information, Bayesian techniques, such as the MMSE estimator, tend to be biased towards the prior mean and they perform a trade-off between bias and variance to achieve the overall goal of reducing the mean square error [46]. The MMSE estimator can improve on the estimation accuracy where applicable and it can be used for unknown deterministic parameters in the case where no MVU exists.

2.3.8 Maximum A Posteriori Estimation

The maximum a posteriori (MAP) estimation approach also makes use of Bayesian philosophy and assumes that the unknown parameter λ is random in similar fashion to the MMSE estimator. The MAP estimator can be explained as the ML estimator presented earlier but now incorporating prior information. As its name suggests, it find the value of λ that maximizes the posterior PDF as follows:

$$\hat{\lambda}_{MAP} = \arg\max_{\lambda}\{p(\lambda|Y)\} \tag{2.30}$$

Equation (2.30) is combined with (2.26) to yield:

$$\hat{\lambda}_{MAP} = \arg\max_{\lambda}\{p(Y|\lambda)p(\lambda)\} \tag{2.31}$$

The difference between the MMSE and MAP approaches lies in the cost profile assigned to estimation errors i.e. the cost function. Where such cost functions penalize errors proportionally, the MMSE estimator is optimal; whereas the MAP is optimal where the cost function has a hit-or-miss profile [46]. This is because the MAP approach finds the mode of the posterior PDF while the MMSE finds its mean.

2.3.9 Ad-hoc Estimation Techniques

While the classical and Bayesian estimation approaches may provide a systematic and conceptual guide to the development of estimation techniques in solving new problems, ad-hoc techniques (e.g. based on *heuristic reasoning*) are also applicable in the discovery of new techniques and can be used to refine the performance of existing ones. In addition, ad-hoc techniques can be designed to minimize computational complexity and/or achieve a sub-optimum performance which is tailored to satisfy the known requirements of an application. This approach features prominently in digital receiver synchronization [41],[52]-[54] and can be applied to both carrier frequency offset estimation and frame detection.

2.4 Synchronization Techniques for Digital Receivers

2.4.1 Received Signal Model

For a single-carrier passband digital communication system in an AWGN wireless channel [28], the received signal after matched filtering and sampling can be represented as follows:

$$r(k) = c(k)e^{j[2\pi\bar{v}(kT+\tau)+\theta]} + n(k) \tag{2.32}$$

where $c(k)$ represents the transmitted symbols, $\bar{v}$ is the frequency offset, k represents the sample index in a symbol period T, τ is the sample timing offset (ranges between 0 and T), θ is the phase offset and $n(k)$ represents the complex additive white Gaussian noise.

In a data-aided approach for phase-shift-keying (PSK), modulation can easily be removed by taking advantage of the PSK property: $c(k)c^*(k)=1$, where $c(k)$ represents the known data symbols [4]. $z(k) \underline{\underline{\Delta}} r(k)c^*(k)$ defines the modulation-removed signal and $\Delta f \underline{\underline{\Delta}} \bar{v}T$ is the frequency offset normalized to the symbol rate. Assuming ideal matched filtering and perfect sampling, we have:

$$z(k) = e^{j(2\pi\Delta f k+\theta)} + n'(k) \qquad k = 0,1,2,\ldots,N-1 \tag{2.33}$$

where N is the pilot field (or data record) length and $n'(k) = n(k)c^*(k)$ has the same statistics as $n(k)$ [4].

2.4.2 Frequency Synchronization

Carrier frequency offset in the received signal of a digital modem results from receiver oscillator instabilities and/or the Doppler effect and performance criteria for frequency estimators in general include estimation range, accuracy, stability, processing delay and computational complexity [52]-[56]. This section presents some typical frequency synchronizers for a single-carrier passband digital system using phase-shift-keying (PSK) modulation.

2.4.2.1 Closed-Loop Frequency Error Detector (FED) Estimators

Closed-loop techniques used for frequency estimation have a feedback structure that incorporates frequency error detectors (FED) as shown in Figure 2.5.

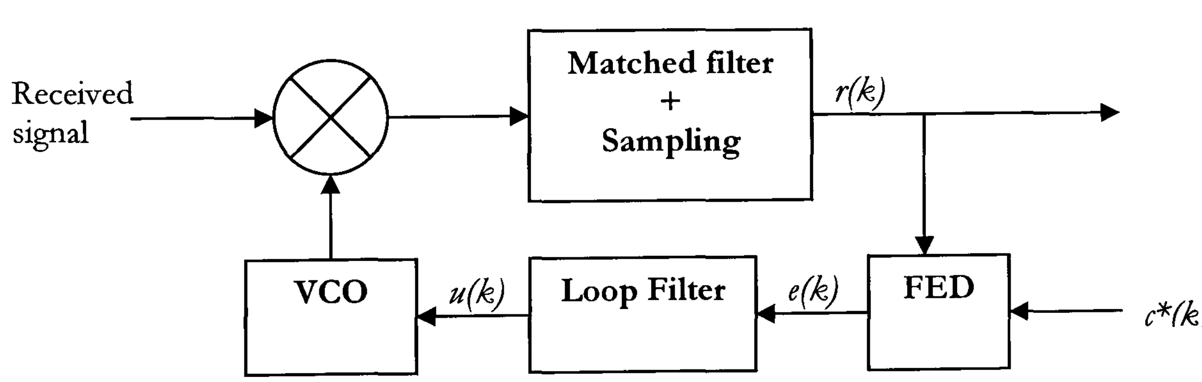

Figure 2.5: Block diagram of a closed-loop FED

The FED acts on the modulation-removed signal (via DA or DD techniques) to produce an error signal that is representative of the frequency offset. This error signal is filtered to remove noise via the loop filter and then used to steer the voltage controlled oscillator (VCO) towards the carrier frequency of the received signal [28],

[56]. FEDs, also called error generators implement algorithms that help to track frequency offset.

2.4.2.2 Kay's Estimator

Kay's method [52] is a feed-forward (FF) technique which makes use of the phase differences between adjacent samples of the modulation-removed signal. The frequency offset estimate is given as follows:

$$\Delta\hat{f} = \frac{1}{2\pi}\sum_{k=1}^{N-1} w_k \angle\left\{z(k)z^*(k-1)\right\} \tag{2.34}$$

where w_k represents weighting coefficients determined as follows:

$$w_k = \frac{3N}{2(N^2-1)}\left\{1-\left(\frac{2k-N}{N}\right)^2\right\}, \qquad k = 1,2,3,\dots\dots\dots N-1 \tag{2.35}$$

The estimator proposed by Kay observes the sequence $\chi(k) = \angle\left\{z(k)z^*(k-1)\right\}$, which can be viewed as a noisy measurement of $2\pi\Delta f$ [28]. It then uses the BLUE approach to determine the weights w_k, which enable the optimum linear combination of the sequence $\chi(k)$. Although Kay's method is computationally efficent and has a wide estimation range, it has an SNR threshold, below which its performance degrades significantly, compared to the Cramer-Rao lower bound [52].

2.4.2.3 Luise and Reggiannini's Estimator

The frequency offset estimate resulting from the Luise and Reggiannini (L&R) method [41] is given as follows:

$$\Delta\hat{f} = \frac{1}{\pi(M+1)} \angle\left\{\sum_{m=1}^{M} R(m)\right\} \tag{2.36}$$

$$R(m) \triangleq \frac{1}{N-m}\sum_{k=m}^{N-1} z(k)z^{*}(k-m), \qquad 1 \le m \le M \tag{2.37}$$

where *R(m)* is the autocorrelation of *z(k)*, computed over *m*=1,…,*M* autocorrelation lags and *M* is a design parameter. Even at low SNR, this feed-forward algorithm achieves the CRLB for *M=N/2* [41]. However, the value of *M* poses a constraint on the estimation range, i.e. $|\Delta f| \le\sim 1/(M+1)$.

2.4.3 Phase Synchronization

After the frequency offset has been compensated, there is need to estimate and compensate for the residual phase offset in the received signal especially for the purpose of coherent demodulation. This section presents two known phase estimators for coherent PSK. These are the feed-forward ML phase estimator and the decision-directed phase estimator (Costas loop). Both assume that sample timing and carrier frequency synchronization have been achieved.

2.4.3.1 Feed-Forward ML Phase Estimator

The ML phase estimator is a feed-forward technique that makes use of the modulation-removed signal to provide a phase estimate as shown in (2.38). It is shown to be an efficient estimator in [28], under the assumption of ideal matched filtering.

$$\hat{\theta} = \angle\left\{\sum_{k=0}^{N-1} z(k)\right\} \tag{2.38}$$

2.4.3.2 Decision-Directed Phase Estimator (Costas Loop)

The decision-directed (DD) phase recovery loop as shown in Figure 2.6 is a recursive non-data-aided phase synchronization technique and a version of the popular Costas loop for analogue applications [28],[57]. It makes use of symbol decisions $\hat{c}(k)$ from the detector instead of pilot symbols. The phase error detector (PED) in Figure 2.6 uses equation (2.39) to generate an error signal *e(k)* which is then used recursively to improve the phase estimate $\hat{\theta}(k)$ as shown in (2.40).

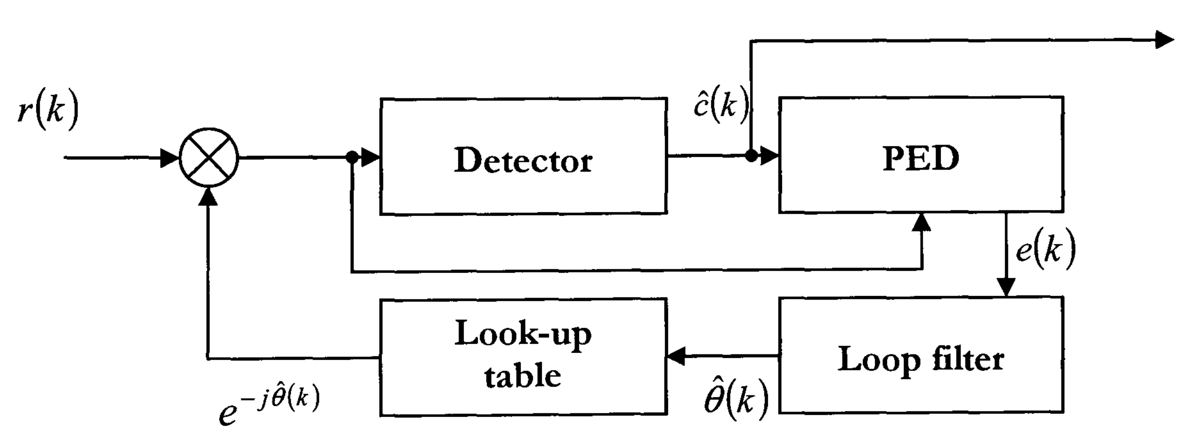

Figure 2.6: The decision-directed phase recovery loop

$$e(k) \triangleq \mathrm{Im}\left\{ \hat{c}^{*}(k) r(k) e^{-j\hat{\theta}(k)} \right\} \tag{2.39}$$

$$\hat{\theta}(k+1) = \hat{\theta}(k) + \gamma e(k) \tag{2.40}$$

where γ is a step-size parameter used with the error signal.

2.4.4 Frame Synchronization

Fast and reliable frame alignment is of key importance in digital transmissions that use block coding and/or burst multiplexing. It involves bringing the receiver into phase with the transmission format such that it knows the start of a frame or block. This enables data bits and/or symbols to be properly delimited for the purpose of decoding of blocks and/or de-multiplexing of bursts [28]. Frame synchronization usually involves the use of a unique pattern which is either intrinsically derived from the data stream or inserted into it and this is referred to as the marker concept [58],[59]. Where framing bits, symbols or preambles are inserted, the goal is to minimize the overhead that is introduced into the transmission stream.

The techniques of correlation [59] are then be used to detect this unique pattern, in order to achieve accurate frame alignment in the receiver. Key issues associated with frame detection are false alarm: where the frame is misaligned and yet successful synchronization is declared by the framing circuit, and missed detection: whereby a frame alignment goes unnoticed. Technically, the goal is to achieve a high reliability with fast response and as such balance the probability of false alarm with that of missed detection.

2.5 Conclusions

In this chapter, we have discussed the importance of signal synchronization in wireless communications and have reviewed the wireless channel in terms of additive white Gaussian noise, narrowband fast-fading (Rayleigh and Rician), wideband fast-fading and second-order fast fading statistics (Doppler spread and Doppler spectrum). The major signal impairments arising from the wireless channel and available techniques for overcoming them have also been noted. In addition, parameter estimation approaches such as MVU, ML, CRLB, BLUE, LS, MMSE, MAP and ad-hoc techniques were reviewed. Finally, the typical signal synchronization stages in a digital receiver were discussed with a focus on frequency, phase and frame synchronization. Some practical techniques were presented which include the BLUE Kay's frequency estimator, the ad-hoc Luise and Regiannini's frequency estimator and the ML phase estimator. The literature review in this chapter serves as a background for the research work of this thesis.

Chapter 3

3 Single Frequency Estimation

3.1 Introduction

Frequency estimation of a complex sinusoid in complex additive white Gaussian noise is a common problem in several fields such as radar, seismology, biomedicine and communications [48],[60] and this problem has been widely addressed in the literature [61]-[77]. An example application is carrier frequency synchronization for digital receivers operating in the wireless channel [28]. It is well known that the optimal maximum likelihood (ML) estimator [51] is specified by the location of the peak of a periodogram. It achieves the Cramer-Rao lower bound (CRLB) [51] even at low signal-to-noise ratios (SNR) and also has a full estimation range. However, the approach is considered to be too computationally intensive for real-time implementation, even with the use of FFT techniques [61] due to the resolution required to attain optimum accuracy for small data records.

Some methods try to approximate the ML estimator [61], [62] with an aim of reducing the amount of computations needed to achieve the CRLB. However, they incorporate significant processing delays due to their feedback structure/iterative procedures. Other methods such as the ones proposed in [41], [63] provide optimal accuracy within a specified range of SNR but are very limited in frequency estimation range. Consequently, they cannot be widely used as stand-alone single frequency estimators.

Computationally efficient frequency estimators with feed-forward structure and wide estimation range include that of Kay [52], who proposed the weighted phase averager which achieves the CRLB at moderate SNR.

Mengali and Morelli (M&M) [64] used a similar approach to Kay's method to derive the weighted autocorrelation phase averager which is more complex than Kay's method but not as complex as the ML approach, for small data records. M&M's method achieves the CRLB at lower SNR than Kay's method while maintaining a wide estimation range and its accuracy competes favourably with the ML approach. However, both Kay's and M&M's methods suffer from an increased threshold effect at frequencies approaching the full estimation range. Consequently, they do not achieve the full theoretical estimation range in contrast to the ML approach.

In order to solve this problem and achieve a full frequency estimation range with a computationally efficient feed-forward approach, two novel techniques are proposed based on weighted linear prediction. It is shown by theoretical analysis and computer simulations that the proposed methods achieve an optimal accuracy and have a lower complexity when compared with Kay's and M&M's methods respectively. Furthermore, the proposed methods achieve a full estimation range and do not involve processing delay arising from iterations and/or stepped frequency search as is the case with periodogram-based techniques.

3.2 Signal Model

Consider the observed signal to be a noisy exponential signal represented as

$$x_t = Ae^{j(2\pi f_0 t+\theta)} + n_t \qquad t = 0,1,2,\ldots,N-1 \tag{3.1}$$

where the amplitude A, frequency f_0 and phase θ are deterministic but unknown constants with $A > 0$ and $0 \le |f_0| < 0.5$, wherein f_0 is expressed as a fraction of the sampling frequency. N is the data record length (i.e. number of samples) and the noise $n_t = \alpha_t + j\beta_t$ is assumed to be a zero-mean complex white Gaussian process having variance σ^2, wherein α_t and β_t are real uncorrelated zero-mean Gaussian random variables having variance $\sigma^2/2$.

The set task is then to estimate the value of the frequency f_0 from a data record of N samples obtained from the observed sinusoid.

3.3 ML Frequency Estimator

In [51], Rife and Boorstyn derived the maximum likelihood frequency estimator (MLE) which is given as follows:

$$I(f) = \left| \sum_{t=0}^{N-1} x_t e^{-j2\pi f t} \right|^2 \tag{3.2}$$

$$\hat{f}_{0_{MLE}} = \arg\max_{f} \{ I(f) \} \tag{3.3}$$

where $I(f)$ is the frequency periodogram and f is a frequency value which falls within the range $-0.5 \le f \le 0.5$. The ML frequency estimate is obtained as that value of f which maximizes the periodogram.

The MLE can be implemented more efficiently via the fast Fourier transform (FFT) algorithm [61] as follows:

$$\hat{f}_{0_{MLE-FFT}} = \frac{1}{N'}\left(\underset{-N'/2 \le f' < N'/2}{\arg\max} \left\{ \left| \sum_{t=0}^{N-1} x_t \, e^{-j2\pi f' t/N'} \right|^2 \right\} \right) \tag{3.4}$$

where N' is the FFT resolution.

In order to achieve a frequency estimation accuracy that attains the CRLB, the value of N' must be sufficiently large to have an adequate resolution in the periodogram. When the data record is small as obtains in practice [52], $N' >> N$. Consequently, the data record is zero-padded to enable appropriate FFT processing, thus leading to a complexity in the order of $N' \log_2 N'$ complex multiplications. This complexity is practically undesirable for small data records [61],[62] and constitutes a major drawback for the MLE despite its ability to achieve optimum accuracy and a full estimation range.

Some methods have been proposed to approximate the MLE such as [61], [62], in order to reduce its computational complexity to a practical level. However, they involve processing delay due to their feedback/iterative procedures as compared to feed-forward techniques.

3.4 CRLB for Frequency Estimation

In addition to the ML frequency estimator, Rife and Boorstyn [51] also derived the Cramer-Rao lower bound (CRLB) for the variance of unbiased frequency estimation in an AWGN channel. The CRLB which is prominently used in several applications as a performance measure for frequency estimation is given in [51] as:

$$VAR\left(\hat{f}_0\right) \geq \frac{3}{2\pi^2 N\left(N^2-1\right)SNR} \qquad (3.5)$$

where N is the data record length and SNR is the signal-to-noise ratio.

3.5 Kay's Estimators

The feed-forward methods proposed by Kay in [52], were derived by replacing (3.1) with an approximate model under an assumption that the SNR $\left(A^2/\sigma^2\right)$ is large, yielding:

$$x_t \approx Ae^{j\left(2\pi f_0 t+\theta+\widetilde{\beta}_t\right)} \qquad t = 0,1,2,\ldots,N-1 \qquad (3.6)$$

where $\widetilde{\beta}_t$ is a real-valued zero-mean white Gaussian noise process [52] with a variance of $\sigma^2/2A^2$.

3.5.1 Weighted Phase Averager

An observation of (3.6) shows that the differenced phase data of x_t gives

$$\angle\left\{x_t x_{t-1}^*\right\} = 2\pi f_0 + \widetilde{\beta}_t - \widetilde{\beta}_{t-1} \qquad t = 1,2,3,\ldots,N-1 \qquad (3.7)$$

Based on the linear model of (3.7), the problem reduces to estimating the mean of a coloured Gaussian noise process. The ML estimator of the frequency f_0 based on this linear model is equivalent to the minimum variance unbiased (MVU) estimator for (3.7) and was derived by Kay as a weighted phase averager (WPA) shown as:

$$2\pi\hat{f}_0 = \sum_{t=1}^{N-1} w_t \angle\{x_t x_{t-1}^*\} \tag{3.8}$$

where w_t is a smoothening function given by:

$$w_t = \frac{3N}{2(N^2-1)}\left\{1-\left(\frac{2t-N}{N}\right)^2\right\}, \qquad t = 1,2,3,\ldots\ldots\ldots N-1 \tag{3.9}$$

Note that the sum of w_t over all values of t in (3.9) is equal to 1. This means that the BLUE (best linear unbiased estimation) weights do not introduce bias into the estimator. Unlike the linear regression LS (least squares) estimator proposed by Tretter [65] which achieves similar accuracy to Kay's WPA [52], the latter does not involve phase unwrapping and is therefore a preferred solution. The WPA has a wide estimation range and achieves the CRLB at moderate SNR. However, it has an SNR threshold below which it performance degrades significantly. Also, its estimation range is below the full range possible, as will be shown later.

3.5.2 Weighted Linear Predictor

It was also shown in [52] that when $(\tilde{\beta}_t - \tilde{\beta}_{t-1})<<1$ (i.e. at sufficiently large SNR), a similarly weighted linear predictor (WLP) formed by interchanging the angle and summation operations in (3.8) as shown below is identical to the WPA.

$$2\pi\hat{f}_0 = \angle\left\{\sum_{t=1}^{N-1} w_t x_t x_{t-1}^*\right\} \tag{3.10}$$

Although both estimators are shown to be analytically equivalent using Kay's signal model under the assumption of a sufficiently large SNR, the WLP produces a degraded accuracy at moderate SNR in contrast to the WPA [52]. As a result, the WPA is more widely known as Kay's estimator in the literature while the WLP is scarcely referenced.

3.6 Weighted Normalized Linear Predictor

In order to rectify the problem of degraded accuracy associated with the WLP at moderate SNR whilst at the same time achieving a full estimation range in contrast to the WPA, we propose a more accurate approximation for the signal model of equation (3.1) than that used to derive Kay's method. We re-write (3.1) as:

$$x_t = Ae^{j(2\pi f_0 t+\theta)} + n_t = Ae^{j(2\pi f_0 t+\theta)}\left[1+\tilde{n}_t\right] \tag{3.11}$$

where $\tilde{n}_t \triangleq n_t e^{-j(2\pi f_0 t+\theta)} / A$

Note that $A\tilde{n}_t = A(\tilde{\alpha}_t + j\tilde{\beta}_t)$ has the same statistics with n_t. Consequently, $\tilde{\alpha}_t$ and $\tilde{\beta}_t$ are real uncorrelated zero-mean Gaussian random variables having a variance of $\sigma^2/2A^2$. Equation (3.11) can be expanded as:

$$x_t = A(|1+\tilde{n}_t|)\, e^{j(2\pi f_0 t+\theta)} e^{j\angle\{1+\tilde{n}_t\}} \tag{3.12}$$

$$= A\sqrt{(1+\tilde{\alpha}_t)^2 + \tilde{\beta}_t^{\,2}}\, e^{j(2\pi f_0 t+\theta)} e^{j\left(\tan^{-1}\{\tilde{\beta}_t/(1+\tilde{\alpha}_t)\}\right)} \tag{3.13}$$

It should be noted that the parameter of interest to be estimated is the frequency and this is contained only in the phase of (3.13) and not in its amplitude. Also, the summation in (3.10) is equivalent to phase averaging in a weighted fashion. Consequently, the amplitude information in (3.13) is unnecessary for frequency estimation accuracy and at low/moderate SNR, the profile of the BLUE weights (w_t) used for the WLP can be significantly distorted by the noisy amplitude of the differenced phase data, thus degrading its performance. This can be easily seen when $w_t\left|x_t x^*_{t-1}\right|$ is simulated/plotted for different SNR values, with A=1 as shown in Figure 3.1.

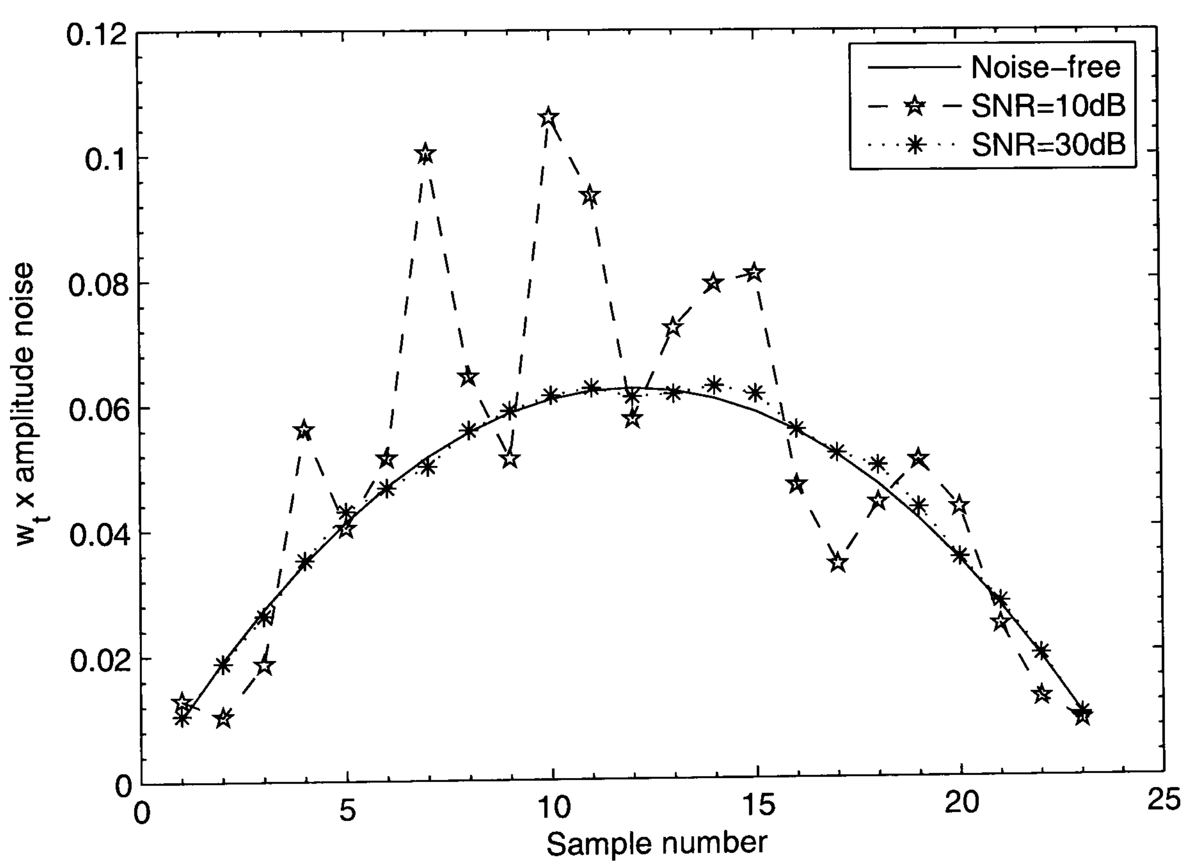

Figure 3.1: Plot of weighting factors multiplied by amplitude noise; N=24

The WPA does not encounter this problem as the amplitude information is already eliminated in (3.7) before the optimal weighting process in (3.8) is applied. Therefore we propose to normalize the observed data by its amplitude as $\breve{x}_t = x_t / |x_t|$. It is noted that under the assumption that $\widetilde{n}_t$<<1 (i.e. at sufficiently large SNR), the normalized version of equation (3.13) becomes:

$$\breve{x}_t \approx e^{j(2\pi f_0 t+\theta+\widetilde{\beta}_t)} \tag{3.14}$$

The equation shown above is essentially the same as that of (3.13) in terms of phase information. Therefore, an improved linear predictor, also referred to as the weighted 'normalized' linear predictor (WNLP) is proposed as follows:

$$2\pi\hat{f}_0 = \angle\left\{\sum_{t=1}^{N-1} w_t \breve{x}_t \breve{x}_{t-1}^*\right\} \tag{3.15}$$

The WNLP can be shown to be analytically equivalent to Kay's WPA using the same set of BLUE weighting factors derived in [52]. This proof is shown as follows:

Let $\delta_t = \widetilde{\beta}_t - \widetilde{\beta}_{t-1}$ and note that $\sum_{t=1}^{N-1} w_t = 1$. Substituting (3.6) into (3.8), we have

$$\sum_{t=1}^{N-1} w_t \angle\{x_t x_{t-1}^*\} = \sum_{t=1}^{N-1} w_t \angle\left(A^2 e^{j2\pi f_0} e^{j\delta_t}\right) \tag{3.16}$$

$$= \sum_{t=1}^{N-1} w_t \left(2\pi f_0 + \delta_t\right) = 2\pi f_0 + \sum_{t=1}^{N-1} w_t \delta_t \tag{3.17}$$

Assuming $|\delta_t| << 1$, i.e. at sufficiently large SNR, we have

$$\sum_{t=1}^{N-1} w_t \angle\{x_t x_{t-1}^*\} = 2\pi f_0 + \tan^{-1}\left\{\sum_{t=1}^{N-1} w_t\, \delta_t\right\} = 2\pi f_0 + \angle\left\{1 + j\sum_{t=1}^{N-1} w_t\, \delta_t\right\} \tag{3.18}$$

$$= 2\pi f_0 + \angle\left\{\sum_{t=1}^{N-1} w_t\,(1 + j\delta_t)\right\} = 2\pi f_0 + \angle\left\{\sum_{t=1}^{N-1} w_t\, e^{j\delta_t}\right\} \tag{3.19}$$

$$= \angle\, e^{j2\pi f_0} + \angle\left\{\sum_{t=1}^{N-1} w_t\, e^{j\delta_t}\right\} = \angle\left\{e^{j2\pi f_0}\sum_{t=1}^{N-1} w_t\, e^{j\delta_t}\right\} \tag{3.20}$$

$$= \angle\left\{\sum_{t=1}^{N-1} w_t\, e^{j2\pi f_0}\, e^{j\delta_t}\right\} = \angle\left\{\sum_{t=1}^{N-1} w_t \breve{x}_t \breve{x}_{t-1}^*\right\}. \tag{3.21}$$

3.7 Mengali and Morelli's Estimator

It is known that Kay's WPA exhibits a threshold effect at low SNR [52] and some other phase-based methods have been proposed to rectify this [66]-[70]. However, these methods incur an increase in complexity and still do not achieve an optimal accuracy as compared to the ML frequency estimator. In contrast, Mengali and Morelli (M&M) [64] proposed an autocorrelation-based frequency estimator to achieve optimal accuracy at low SNR. The autocorrelation of the received signal is given as:

$$R(m) \triangleq \frac{1}{N-m}\sum_{t=m}^{N-1} x_t x_{t-m}^*, \qquad 0 \le m \le N-1 \tag{3.22}$$

where m is the autocorrelation lag.

Substituting (3.11) into (3.22), as done in [64], we have the autocorrelation expressed as:

$$R(m) = e^{j2\pi m f_0}\left[1+\xi(m)\right] \tag{3.23}$$

$$\xi(m) \triangleq \frac{1}{N-m}\sum_{t=m}^{N-1}\left[\tilde{n}_t + \tilde{n}_{t-m} + \tilde{n}_t \tilde{n}^*{}_{t-m}\right] \tag{3.24}$$

An inspection of (3.24) shows that $\xi(m)$ is a zero-mean noise term whose variance is inversely proportional to $(N-m)$ and also smaller compared to that of $\tilde{n}_t$. Under the assumption that the SNR>>1, we have

$$R(m) \approx B_m e^{j(2\pi m f_0 + \xi_I(m))} \tag{3.25}$$

where B_m is a noisy amplitude

As can be deduced from (3.25), the autocorrelation can be used to design frequency estimators. However, the optimally-accurate autocorrelation methods proposed by Luise and Regiannini [41] and Fitz [63] suffer from a restricted estimation range while the single autocorrelation estimator proposed by Lank and Reed [71] suffers from sub-optimal accuracy. M&M's method achieves an optimal accuracy with wide estimation range by making use of the differenced phase of the autocorrelation as follows:

$$\angle\{R(m)R^*(m-1)\} = 2\pi f_0 + \xi_I(m) + \xi_I(m-1) \tag{3.26}$$

where $\xi_I(m)$ is the real-valued zero-mean imaginary part of $\xi(m)$ [64].

M&M use a similar approach to Kay's method to determine BLUE weights w_m for (3.26) and the resulting algorithm is given as:

$$2\pi\hat{f}_0 = \sum_{m=1}^{M} w_m \angle\{R(m)R^*(m-1)\}; \qquad 1 < m \leq M \tag{3.27}$$

where M is a design parameter whose optimal value is $N/2$ and w_m is the smoothening function given in [64] as:

$$w_m \triangleq \frac{3[(N-m)(N-m+1) - M(N-M)]}{M(4M^2 - 6MN + 3N^2 - 1)}; \qquad 1 < m \leq M \tag{3.28}$$

It is noted that the sum of w_m over all values of m in (3.28) is equal to 1. This means that the BLUE weights do not introduce bias into the estimator.

3.8 Weighted Normalized Autocorrelation Linear Predictor

Based on the proof provided in [52] and section 3.6 which shows the analytical equivalence of Kay's WPA and the WNLP, we propose a second frequency estimator derived from the Mengali and Morelli estimator, also referred to as the weighted 'normalized autocorrelation' linear predictor (WNALP) and given as:

$$2\pi\hat{f}_0 = \angle\left\{\sum_{m=1}^{M} w_m \breve{R}(m)\breve{R}^*(m-1)\right\} \tag{3.29}$$

where $\breve{R}(m) = R(m)/|R(m)|$ is the autocorrelation normalized by its amplitude.

3.9 Estimation Range and Complexity

Table 3.1 shows the frequency estimation range and computational complexity of the proposed methods in comparison to the existing methods. Unlike our proposed WNLP and WNALP where the noise has been averaged out by the optimal weights before taking the angle function, there is no noise averaging performed as yet when the angle function is used in Kay's and M&M's methods. This makes them more susceptible to large estimation errors as $|f_0|$ approaches 0.5 since the output of the angle (arg) function is always in the interval $[-\pi, \pi]$ and an un-averaged phase noise will increase the chances of crossover from $-\pi$ to π and vice-versa. Consequently, their estimation range falls below 35% of the sampling rate at low/moderate SNR while the proposed methods attain the full range.

Table 3.1: Estimation range and complexity of the estimators

Estimator	Estimation Range	Angle Operations	Complex Multiplications
MLE-FFT	$\|f_0\| \le \sim 0.5$	-	$N'\log_2 N'$
WPA	$\|f_0\| < 0.35$	$N-1$	$2(N-1)$
WNLP	$\|f_0\| \le \sim 0.5$	1	$2(N-1)$
M&M	$\|f_0\| < 0.35$	M	$2M + M(2N-M-1)/2$
WNALP	$\|f_0\| \le \sim 0.5$	1	$2M + M(2N-M-1)/2$

In terms of complexity, the MLE is shown to have the highest complexity of all the methods compared, since $N' >> N$ in practice. For example, assuming an FFT resolution of $N' = 1024$ points and a data record length of $N = 24$, the MLE requires 10,240 complex multiplications as compared to 234 needed by the proposed WNALP and M&M's method. The WNLP and WNALP make use of only one angle function in contrast to multiple angle functions used by the WPA and M&M's method. This constitutes a significant reduction in complexity for the proposed methods as the angle function is computationally intensive due to its non-linear arctangent operations. However, it is noted that the need to normalize data in the proposed methods will slightly increase complexity in comparison to their un-normalized linear prediction versions.

3.10 Application to PSK Communication Systems

The methods presented for single frequency estimation are easily applied to carrier frequency synchronization in PSK-modulated systems by employing modulation-removal techniques [28]. For coherent PSK transmissions where known training pilot symbols are used, modulation can easily be removed from the received signal by taking advantage of the PSK property: $c(k)c^*(k) = 1$, where $c^*(k)$ represents the complex conjugate of the known symbols. In other words, the received signal at the training pilot positions is multiplied by the complex conjugate of the known pilots. This effectively results in a signal of a similar form and statistics as in (3.1) wherein the estimated frequency is the value of the carrier frequency offset as normalized to the symbol rate.

3.11 Computer Simulations

Extensive computer simulations were performed to verify the performance of the proposed methods in comparison to the existing ones in an AWGN channel. A small data record of N=24 is chosen in similar fashion to [52],[61]. The MLE is implemented using FFT processing with a resolution of $N' = 1024$. Figure 3.2 shows the mean-square-error (MSE) of the frequency estimate for an initial frequency $f_0 = 0.05$. It can be seen that the proposed WNLP and WNALP attain the CRLB for frequency estimation in an AWGN channel, in a similar fashion to the WPA and M&M's methods respectively. The MLE-FFT is also shown to achieve an optimal accuracy which can be extended to lower SNR by increasing the resolution of the periodogram (i.e. the value of N'). Figure 3.3 and 3.4 show how the MSE performance of the WPA and M&M's estimators degrade as the frequency is progressively increased from 0.05 to 0.45. The proposed methods and the MLE-FFT maintain their MSE performance in the presence of a large frequency in contrast to Kay's and M&M's estimators as shown in Figure 3.5. However, it is noted that the MLE-FFT is significantly more complex than the proposed methods as discussed in section 3.9. The advantage of the proposed WNALP over M&M's method in terms of estimation range is illustrated further in Figure 3.6 for an initial frequency $f_0 = 0.48$.

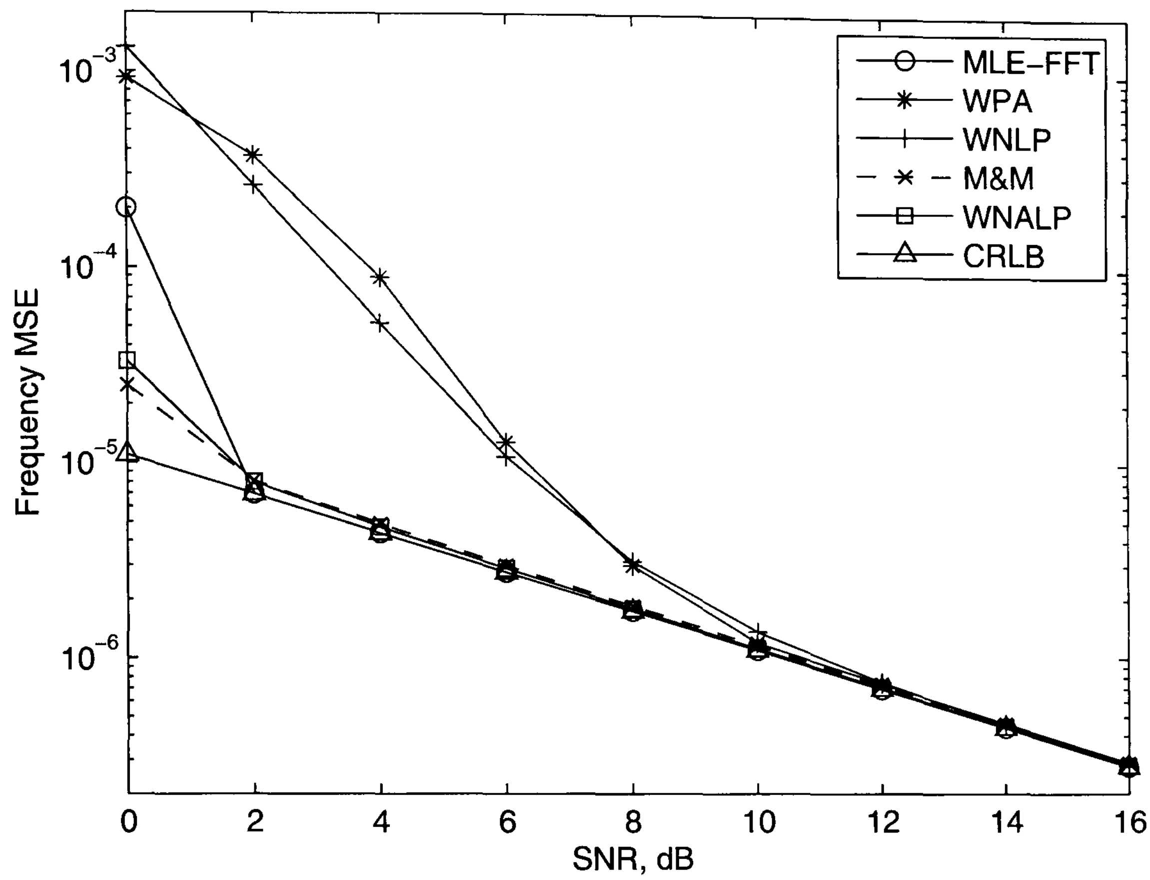

Figure 3.2: MSE for the different estimators; N=24 and f_0=0.05

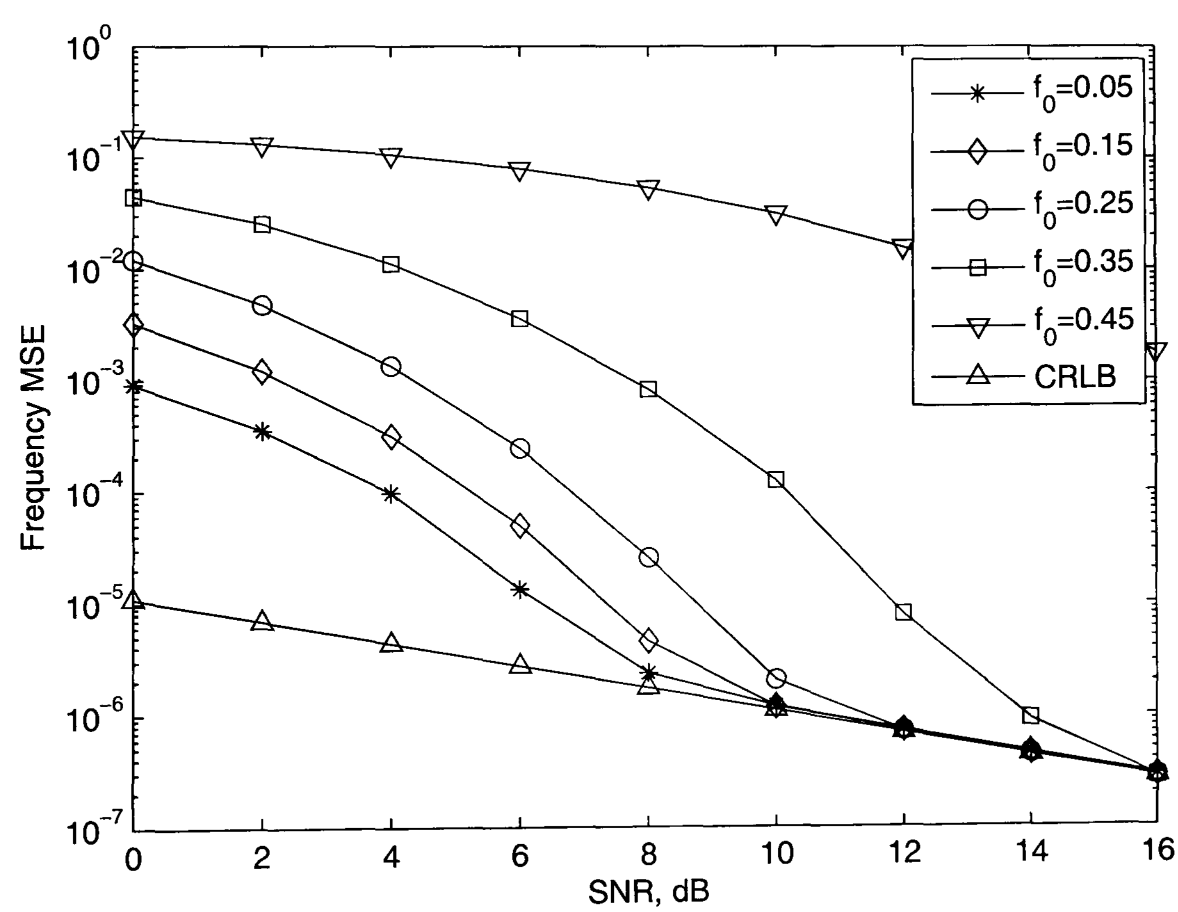

Figure 3.3: MSE for the WPA at different frequencies; N=24

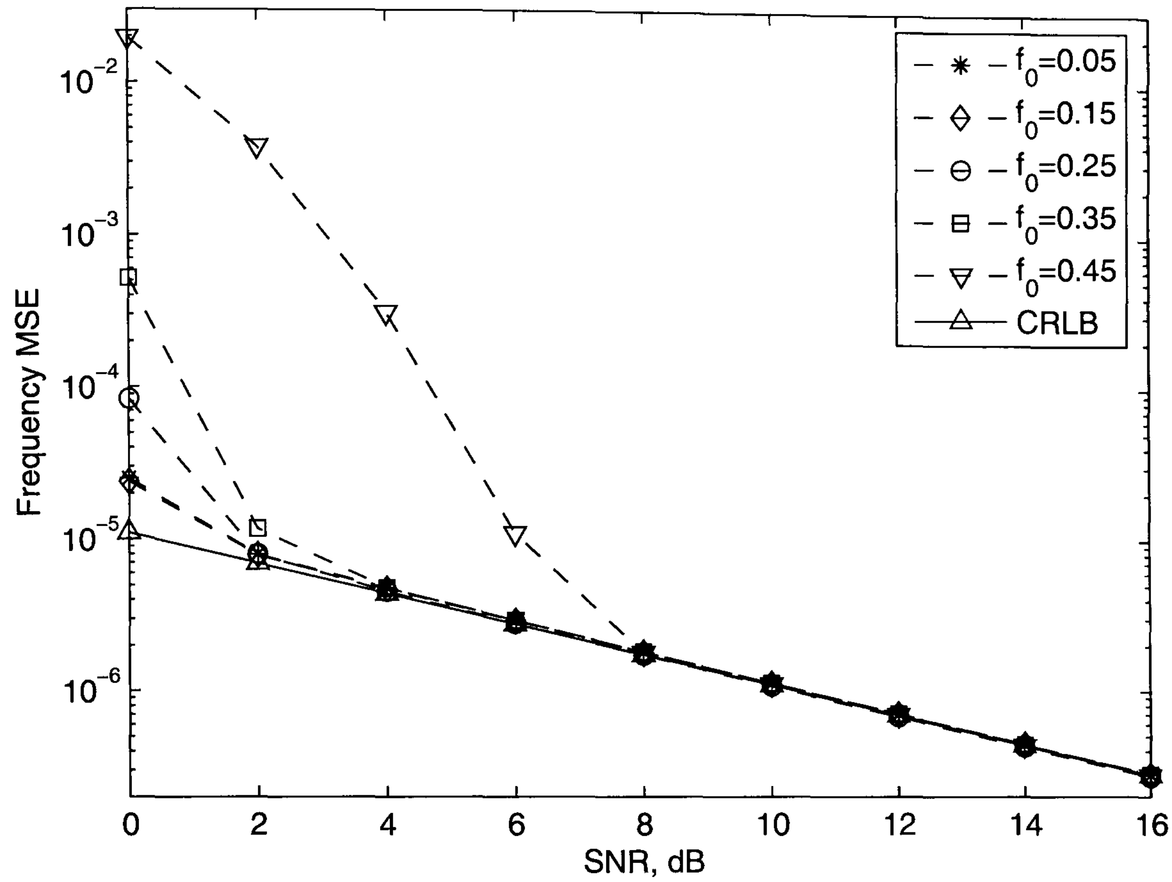

Figure 3.4: MSE for M&M's estimator at different frequencies; N=24

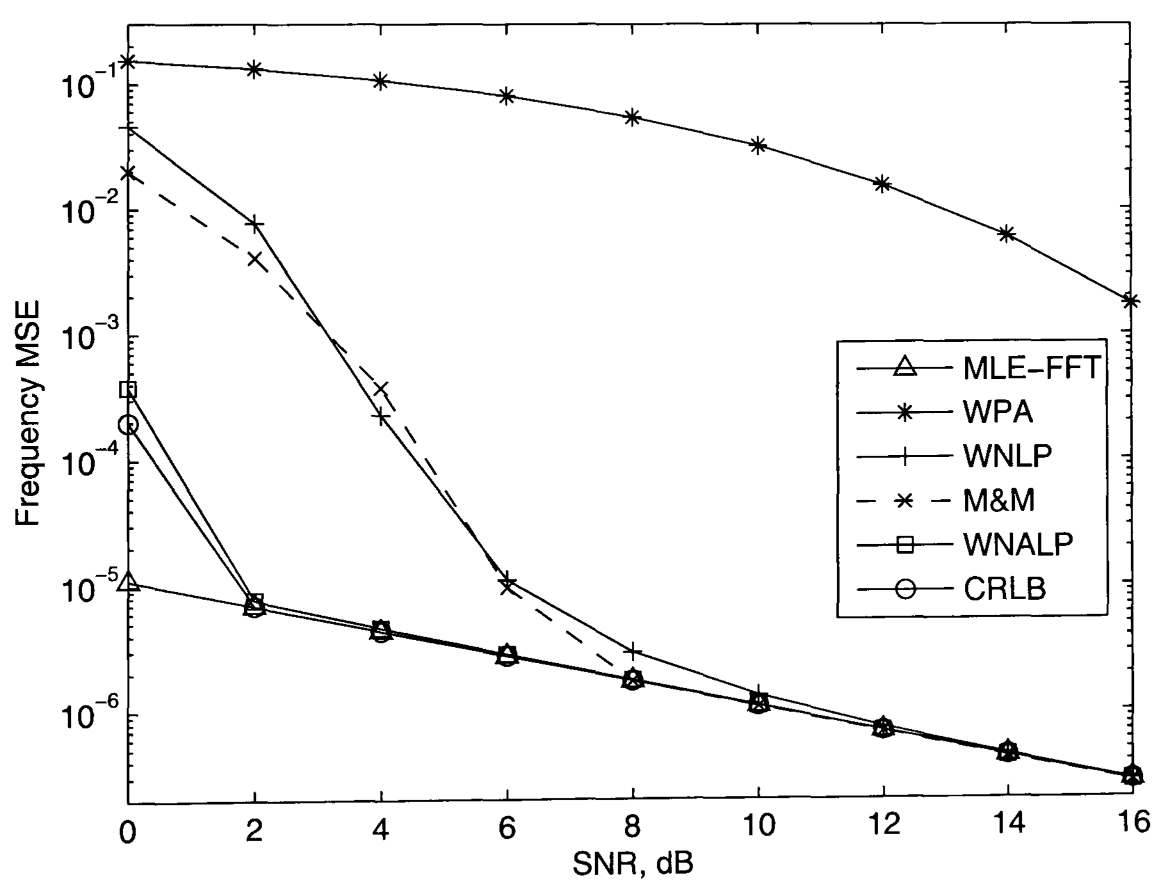

Figure 3.5: MSE for the different estimators; N=24 and f_0=0.45

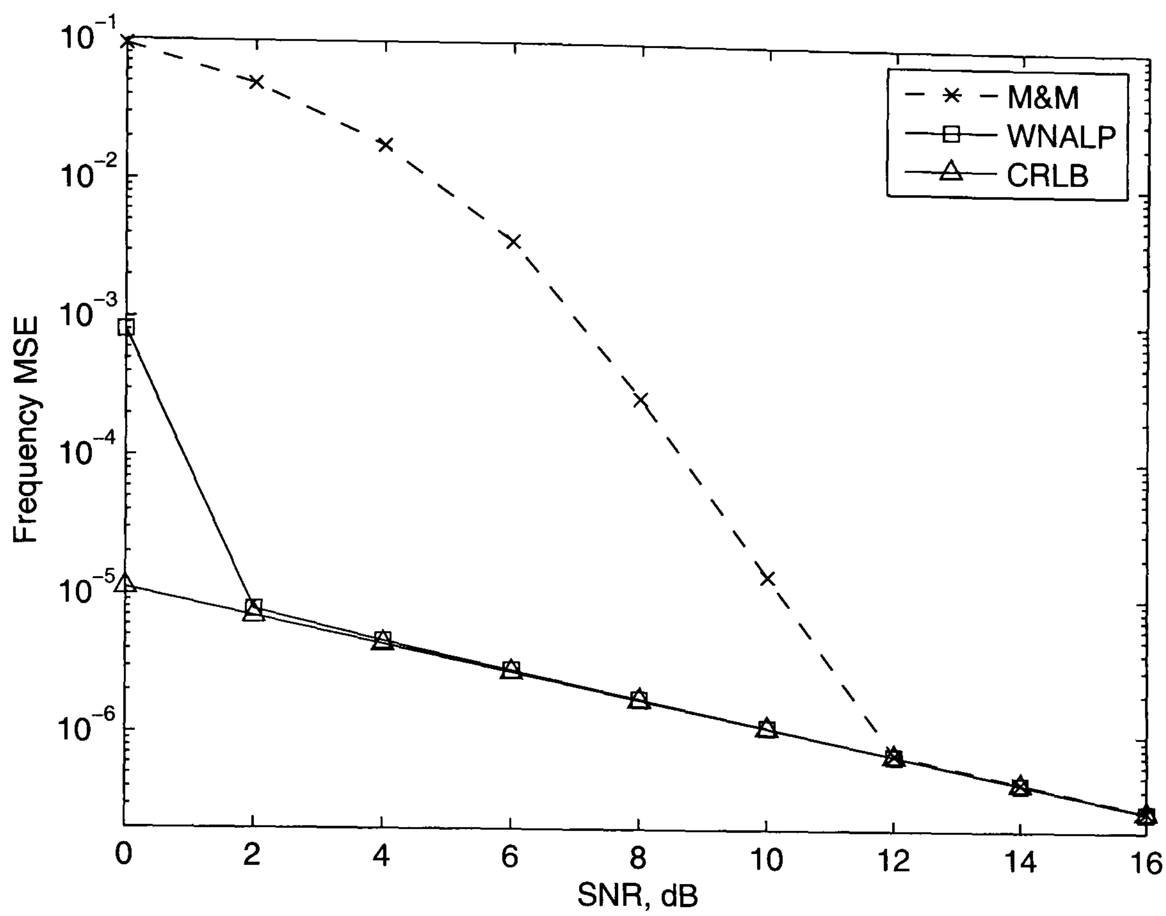

Figure 3.6: MSE comparison at a large frequency; N=24 and f_0=0.48

3.12 Conclusions

In this chapter, single frequency estimation as applicable to many fields including carrier frequency synchronization in communication systems has been discussed. The MLE is known to be very computationally intensive for small data records due to the resolution it requires, although it has a full estimation range and achieves the CRLB at low SNR. In contrast, feed-forward techniques with practical computational complexity, such as Kay's WPA and M&M's methods are unable to achieve a full estimation range. Therefore, we have proposed two new feedforward techniques for single frequency estimation, based on weighted linear prediction. The proposed WNLP and WNALP have a lower computational complexity than the existing WPA and M&M's methods respectively, yet they achieve the CRLB in similar fashion to the latter. Furthermore, the proposed methods are able to achieve the full frequency estimation range of ~0.5. Simulation results confirm the superior performance of the proposed methods in comparison to the existing methods. Consequently, the proposed techniques are more robust for single frequency estimation since they are computationally efficient, achieve optimal accuracy and have a full estimation range. Table 3.2 summarizes the improvement achieved by the proposed WNLP and WNALP over existing techniques for a data record length $N = 24$ and an FFT resolution $N' = 1024$.

Table 3.2: Summary table of improvement achieved by the proposed methods

Estimator	**Frequency MSE SNR=4dB, f_0=0.45**	**Angle Operations**	**Complex Multiplications**
MLE-FFT	4.38×10^{-6}	-	10,240
WPA	0.11	23	46
WNLP	2.29×10^{-4}	1	46
M&M	3.76×10^{-4}	12	234
WNALP	4.64×10^{-6}	1	234

Chapter 4

4 Frequency Synchronization for DVB-S2 Systems

4.1 Introduction

Carrier frequency offset in the received signal of a digital modem arises from receiver oscillator instabilities and/or the Doppler effect [28]-[30]. This problem has given rise to various techniques over the years, some of which have been discussed in the previous chapter, on single frequency estimation. However, the advancement in error control coding means that digital receivers can now function at very low signal-to-noise ratios (SNR) [78], resulting in the need for synchronization algorithms which can operate at such SNR.

An example system is the second generation standard for digital video broadcasting via satellite: DVB-S2 [1],[8],[9], which is designed to provide high-speed/high-capacity (i.e. broadband) downlink services to consumers spread over a wide geographical area, through the use of advanced modulation and coding techniques. Due to its ability to achieve a high data throughput, the DVB-S2 standard has also been proposed in the MOWGLY project [19] for the downlink of internet broadband services to collective users of mobile platforms such as airplanes, ships and trains. However, DVB-S2 systems have a stringent frequency synchronization accuracy requirement due to the incorporated frame structure. Moreover, its consumer-type terminals are expected to use low-cost oscillators which may drift and introduce large initial frequency offsets into the received signal [32]. Hence, robust frequency synchronization at very low SNR is required for DVB-S2 systems in terms of both estimation accuracy and estimation range.

Some techniques have been proposed for DVB-S2 frequency synchronization in [31],[32],[42]. In particular, Casini et al [31] proposed a low-complexity approach, wherein a closed-loop frequency-error-detector (FED) is used for coarse frequency synchronization while a modified version of the feed-forward Luise and Regiannini estimator is used for fine frequency synchronization. Both techniques make use of averaging over multiple pilot fields to achieve the required estimation accuracy.

In this chapter, we investigate the possibility of improving DVB-S2 frequency synchronization performance for both fixed and mobile terminals. The Cramer-Rao lower bound (CRLB) for the multiple pilot fields scenario is analytically derived based on simplifying assumptions. Consequently, a method is proposed to enhance DVB-S2 frequency synchronization performance in the AWGN channel, in terms of reduced synchronization delay and increased estimation range. The proposed method is investigated further in the Rician fading channel to establish its suitability for the deployment of DVB-S2 mobile systems as proposed by the MOWGLY project [19].

4.2 Digital Video Broadcasting via Satellite

The second generation digital video broadcasting via satellite (DVB-S2) was designed with a specific interest in high data throughput applications, including broadcast and interactive services. It improves on the first generation DVB-S system by making use of advanced modulation and coding techniques and a physical level framing structure [8]. It also incorporates the techniques of 'variable coding and modulation' (VCM) and 'adaptive coding and modulation' (ACM) to achieve a high throughput, despite adverse channel conditions. Consequently, it is able to achieve remarkable capacity increase over the preceding DVB-S system under similar transmission conditions and to provide a very wide range of services at reduced cost .

4.2.1 Coding and Modulation in DVB-S2

DVB-S2 is able to operate at very low SNR because it makes use of a powerful concatenated forward-error-correction (FEC) scheme, consisting of an outer BCH code and an inner LDPC (low density parity check) code. A wide range of code rates are used depending on the modulation and channel requirements. Two FEC frame lengths provide flexibility to optimise between carrier-to-noise (C/N) performance and latency reduction. The normal FEC frame has a code block length of 64,800 bits long while the short frame is 16,200 bits.

Four digital modulation modes are available in DVB-S2. QPSK and 8PSK are preferred for broadcast applications while 16APSK and 32APSK are aimed at professional applications [1]. The latter offer a higher spectral efficiency but are not as power efficient as the former and are used with advanced pre-distortion in the satellite uplink. Several different combinations of modulation and coding provide spectrum efficiencies ranging from 0.5 – 4.5 bits per symbol [8]. Table 4.1 summarizes the DVB-S2 parameters while Table 4.2 shows typical operating SNR values [78] for some combinations of modulation and coding in DVB-S2, wherein the operating SNR can be as low as -2dB.

Table 4.1: DVB-S2 parameters and options

Parameter	Options
Modulation	QPSK, 8-PSK, 16APSK or 32APSK
Roll-off factors	0.2, 0.25 or 0.35
FEC	outer BCH and inner LDPC
FEC code rates	1/4, 1/3, 2/5, 1/2, 3/5, 2/3, 3/4, 4/5, 5/6, 8/9 or 9/10
FEC frame length	16,200 bits (short frame) or 64,200 bits (normal frame)

Table 4.2: SNR for Quasi-Error-Free (QEF) DVB-S2 operation [78]

Modulation	FEC Rate	E_s/N_0 (dB)
QPSK	1/4	-2.00
QPSK	1/2	1.00
QPSK	2/3	3.10
8-PSK	2/3	6.62
8-PSK	3/4	7.91
8-PSK	5/6	9.35

4.2.2 Frame Structure in DVB-S2

The DVB-S2 standard makes use of physical layer (PL) frames to implement the techniques of VCM and ACM. Furthermore, the PL header helps to facilitate synchronization (e.g. frame detection) and signalling in the received signal. The PL frame consists of a PL header (90 symbols, $\pi/2$ BPSK modulated) and a payload consisting of a modulated FEC frame (an integer multiple of 90 symbols). Each PL header consists of a 26-symbol start of frame (SOF) and a 64-symbol physical layer signalling code (PLSC). Within each PL frame, the modulation and coding is constant but this may change in adjacent PL frames. Training pilot fields, each consisting of 36 symbols (unmodulated carriers with a phase-shift of $\pi/4$) are inserted into the payload at intervals of 16 slots (1 slot = 90 symbols), for the purpose of carrier synchronization [3]. Figure 4.1 illustrates the DVB-S2 physical level frame structure, showing the PL header and the training pilot fields.

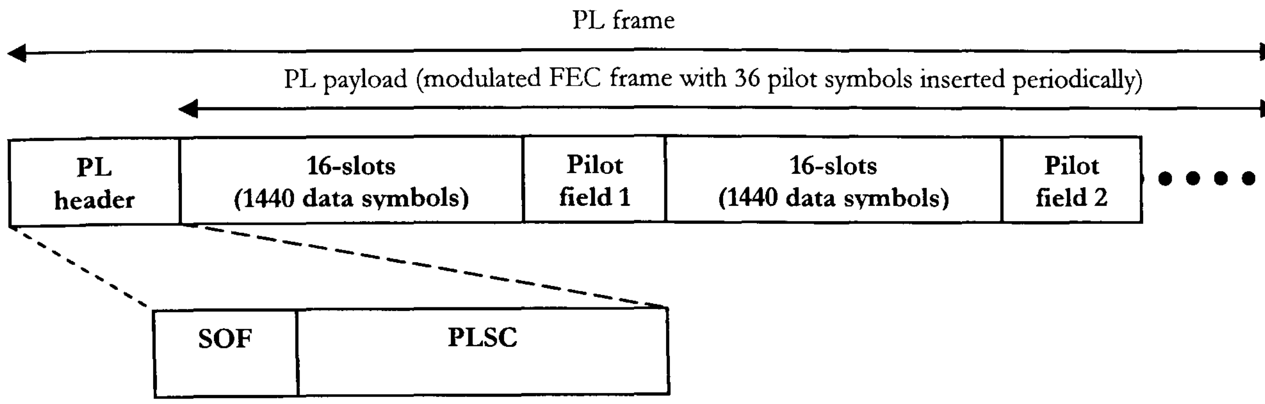

Figure 4.1: PL frame structure showing inserted pilot fields and PL header

4.3 Signal Model

Let $r(k)$ be the received signal after ideal matched filtering and perfect sample timing.

$$r(k) = c(k)e^{j(2\pi\Delta f k+\theta)} + n(k) \tag{4.1}$$

where $c(k)$ belongs to a sequence of statistically independent phase-shift-keying (PSK) symbols with unit-amplitude, $\Delta f \triangleq \bar{v}T$ is the carrier frequency offset $\bar{v}$ normalized to the symbol rate $1/T$, k represents the sample time index, θ is the carrier phase and $n(k)$ represents samples of the independent and identically distributed (i.i.d.) complex additive white Gaussian noise (AWGN) with zero mean and a variance equal to $1/(E_s/N_0)$.

In a data-aided approach, modulation can be easily removed by taking advantage of the PSK property: $c(k)c^*(k)=1$, where $c^*(k)$ represents the complex conjugate of the known preamble symbols. Thus, the modulation-removed signal $z(k) \triangleq r(k)c^*(k)$ is given as follows:

$$z(k) = e^{j(2\pi\Delta f k+\theta)} + n'(k), \qquad 0 \le k \le N-1 \tag{4.2}$$

where N is the pilot field length and $n'(k) = n(k)\, c^*(k)$ has the same statistics as $n(k)$.

4.4 Existing Techniques for DVB-S2 Frequency Synchronization

4.4.1 Overview of DVB-S2 Frequency Synchronization

As proposed in [31], the DVB-S2 receiver synchronization starts with symbol clock (sample timing) recovery. This is followed by frame synchronization in order to determine the start of frame and the location of the training pilot symbols which are then used to achieve coarse frequency acquisition, followed by fine frequency tracking and phase recovery (with fine phase tracking for higher-order modulations).

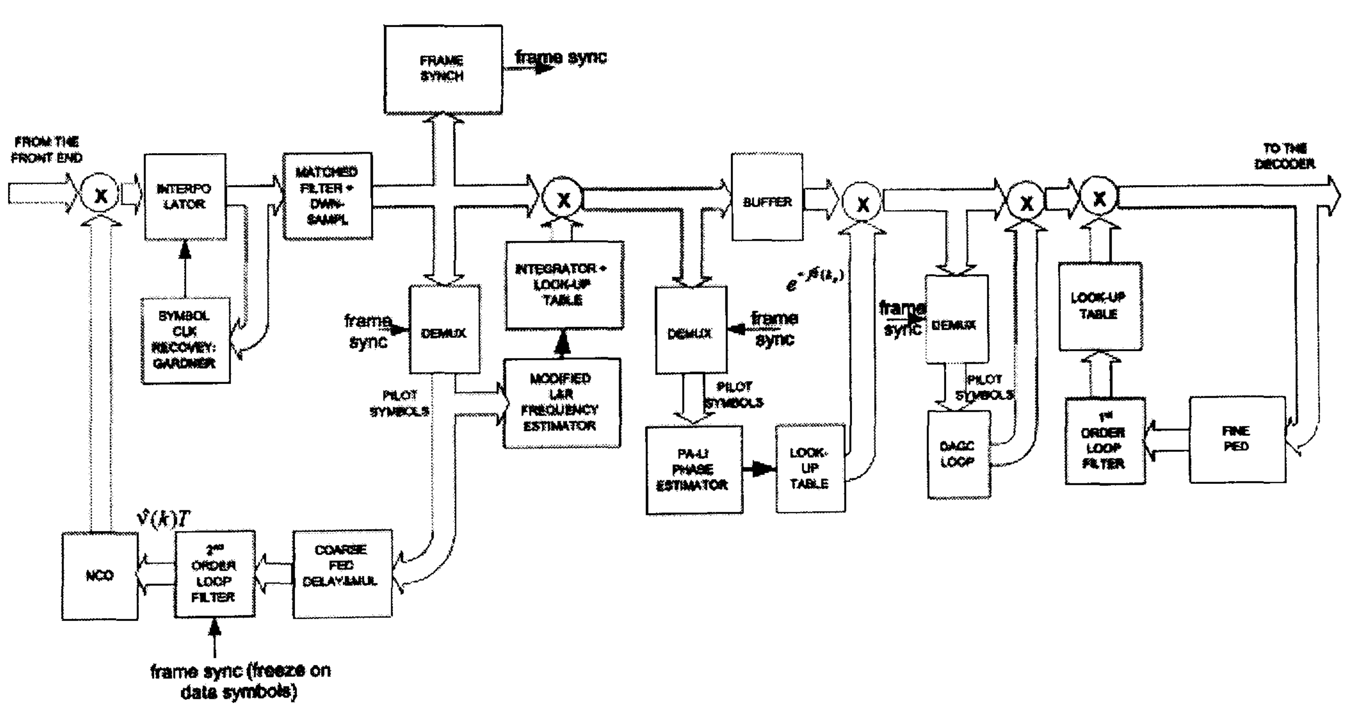

Figure 4.2: DVB-S2 receiver synchronization modules as proposed in [31]

In this thesis, we focus on the carrier frequency synchronization aspects of the DVB-S2 receiver with an implicit assumption that the preceding stages of sample timing recovery and frame synchronization have been achieved satisfactorily.

DVB-S2 consumer-type terminals are expected to incorporate low-cost oscillators. These low-grade oscillators may drift and consequently introduce large initial frequency offsets (e.g. 20% of the symbol rate) into the received signal. Hence, wide range frequency estimation is imperative in DVB-S2 systems. The phase recovery unit of DVB-S2 can tolerate residual frequency errors resulting from the accuracy limitations of frequency synchronizers via a linear interpolation process which tracks the phase trajectory over the data symbols using the phase estimates of adjacent pilot fields [31] but the maximum value of the residual frequency error allowable is determined by the need to avoid cycle slips in the interpolation process as shown in equation (4.3).

$$2\pi\Delta f L_s \leq \pi \Rightarrow \Delta f \leq \frac{1}{2L_s} \tag{4.3}$$

where L_s is the number of symbols contained in one payload segment. L_s is equivalent to 1476 symbols as specified in the DVB-S2 frame structure.

By substituting the value of L_s into (4.3), it can be deduced that the maximum acceptable frequency error in DVB-S2 is $\Delta f = 3.4\text{x}10^{-4}$. Consequently, this defines the carrier frequency synchronization accuracy requirement. Therefore, DVB-S2 frequency synchronization algorithms incorporate averaging over multiple pilot fields to improve estimation performance since one pilot field of 36 symbols is insufficient to achieve the desired accuracy.

4.4.2 Frequency Error Detector in Closed Loop

A pilot-aided frequency error detector (FED) with a feedback structure as shown in Figure 4.2 was proposed in [31] for coarse frequency acquisition in the DVB-S2 receiver. It can handle initial frequency offsets up to 20% of the symbol rate (i.e. $\Delta f \leq 0.2$). This is equivalent to a 5MHz frequency offset at a symbol rate of 25Mbaud. The FED implements a low-complexity 'delay and multiply' algorithm as shown in the following equation:

$$e(k) = \mathrm{Im}\{z(k)\, z^{*}(k-2)\} \tag{4.4}$$

Since the equation uses the modulation-removed signal $z(k)$, the loop is frozen over the data symbols and only active over pilot symbols. The result presented in [31] as shown in Figure 4.3 reflects the performance of the closed-loop FED for DVB-S2 coarse frequency acquisition in an AWGN channel, using a loop bandwidth of 10^{-4}, as normalized to the symbol rate. The estimation time needed to achieve this accuracy was given in [31] as 100ms at 25Mbaud, which is equivalent to the use of approximately 1650 DVB-S2 training pilot fields.

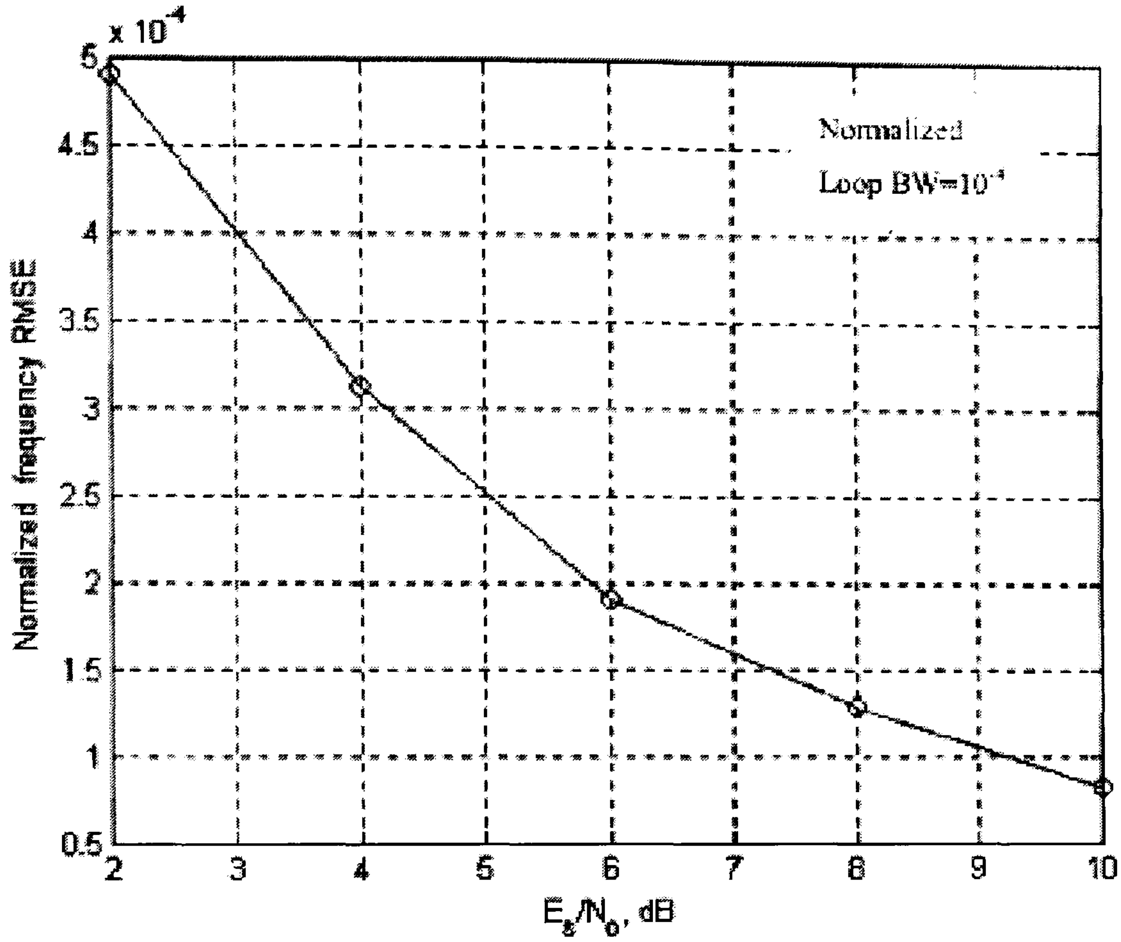

Figure 4.3: DVB-S2 coarse frequency estimation using a closed-loop FED [31]

4.4.3 Averaged Luise and Reggiannini's Estimator

A pilot-aided feedforward algorithm derived from the Luise and Reggiannini (L&R) estimator was also proposed in [31], for DVB-S2 fine frequency tracking. This is because the L&R estimator [41] has a practical computational complexity and achieves a near-optimal accuracy at very low SNR as shown in Figure 4.4. However, its estimation range is limited and the method must be preceded by a coarse frequency acquisition stage in digital receivers that experience large frequency offsets.

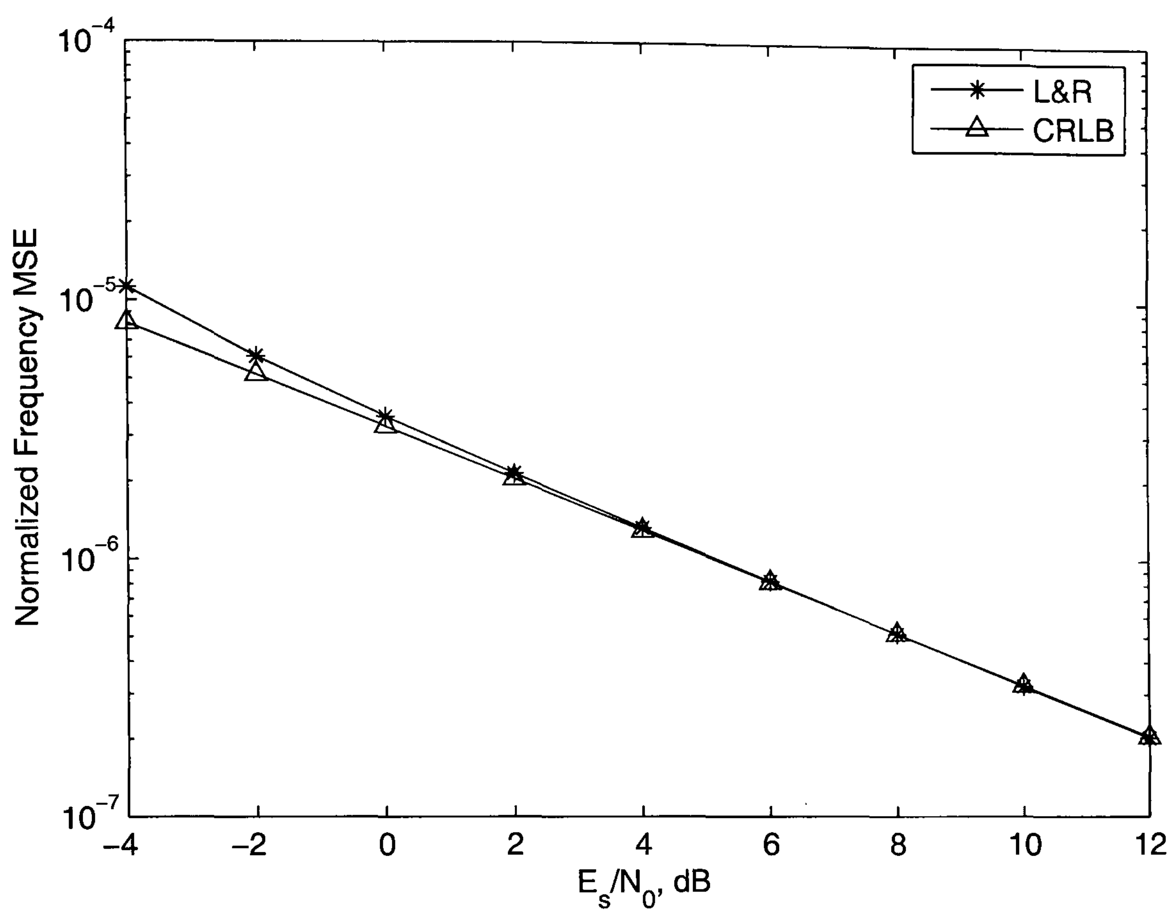

Figure 4.4: Frequency MSE for L&R's estimator; N=36 and Δf = 0.01

The averaged L&R estimator (ALRE) proposed in [31] incorporates an averaging of the autocorrelation $R(m)$ over L consecutive pilot fields, in order to satisfy the DVB-S2 frequency accuracy requirement. The algorithm is given as follows:

$$R(m) \triangleq \frac{1}{N-m}\sum_{k=m}^{N-1} z(k)z^*(k-m) \tag{4.5}$$

$$\Delta\hat{f} = \frac{1}{\pi(M+1)}\angle\left\{\sum_{l=1}^{L}\sum_{m=1}^{M} R_l(m)\right\} \tag{4.6}$$

where $R_l(m)$ is the autocorrelation of $z(k)$, computed for $m = 1,\cdots,M$ lags over the l^{th} pilot field and N is the length of each pilot field in samples. The optimal value for M is given as $N/2$ in [31],[41].

4.5 Improved Frequency Synchronization for DVB-S2 Systems

In this section, we derive the CRLB for frequency estimation in the multiple pilot field scenario and propose a method to improve frequency synchronization performance in DVB-S2 systems. The proposed technique is a modified version of the novel WNALP which was proposed in chapter 3 of this thesis. It can achieve a full-range frequency estimation (i.e. $\Delta f \leq\sim 0.5$), thereby eliminating the need for a coarse frequency acquisition stage. This leads to a desirable reduction in synchronization delay without significant increase in complexity.

4.5.1 CRLB for Frequency Estimation over Multiple Pilot Fields

The Cramer-Rao lower bound (CRLB) for the frequency estimation variance in the AWGN channel, over a single pilot field has already been defined in [51] as presented earlier in chapter 3. However, in a scenario where frequency estimation accuracy is increased by averaging estimates over multiple pilot fields such as in DVB-S2, it is desirable to know the improved bound on estimation variance. In order to define the CRLB over multiple pilot fields in the AWGN channel, we refer to basic statistical theory [46],[30].

Consider a set of uncorrelated and unbiased frequency offset estimates $\Delta\hat{f}_l$, each derived by using one pilot field of fixed length N and having the same variance. The averaged estimate over L pilot fields is given as:

$$\Delta\hat{f} = \frac{1}{L}\sum_{l=1}^{L}\Delta\hat{f}_l \tag{4.7}$$

$$E\left(\Delta\hat{f}\right) = \frac{1}{L}\sum_{l=1}^{L} E\left(\Delta\hat{f}_l\right) = \Delta f \tag{4.8}$$

$$VAR\left(\Delta\hat{f}\right) = \frac{1}{L^2}\sum_{l=1}^{L} VAR\left(\Delta\hat{f}_l\right) = VAR\left(\Delta\hat{f}_l\right)/L \tag{4.9}$$

Therefore, assuming that the L pilot fields are uncorrelated in noise, the CRLB in the averaging scenario can be derived from the CRLB for a single pilot field in (3.5) as:

$$VAR\left(\Delta\hat{f}\right) \geq \frac{3}{2\pi^2 N\left(N^2-1\right)SNR} \Big/ L \tag{4.10}$$

It is noted that the CRLB for frequency estimation over multiple pilot fields in a fading channel will be different from that of the AWGN channel. This is because the pilot fields will experience different fade levels and the effective SNR per pilot field will vary. A possible approach to derive the CRLB under this scenario may be the use of weighting coefficients for each pilot field, assuming the channel is constant over the pilot field duration.

4.5.2 Averaged WNALP

The novel 'weighted normalized autocorrelation linear predictor' (WNALP) proposed in chapter 3 of this thesis can be modified for wide-range DVB-S2 frequency synchronization, wherein the existing coarse and fine stages as proposed in [31] are fully replaced by the proposed single-stage algorithm. The WNALP as derived in chapter 3 is given as follows:

$$\Delta\hat{f} = \angle\left\{\sum_{m=1}^{M} w_m \breve{R}(m)\breve{R}^*(m-1)\right\} \tag{4.11}$$

$$w_m \triangleq \frac{3[(N-m)(N-m+1)-M(N-M)]}{M(4M^2-6MN+3N^2-1)} \tag{4.12}$$

where $\breve{R}(m) = R(m)/|R(m)|$ is the autocorrelation normalized by its amplitude, M is a design parameter whose optimal value is $N/2$ and w_m is a smoothing function.

A drawback of the WNALP is that its accuracy degrades significantly at very low SNR in contrast to L&R's estimator. This trend is illustrated in Figure 4.5 where the WNALP is used over one DVB-S2 pilot field in an AWGN channel with an initial frequency offset: $\Delta f = 0.2$.

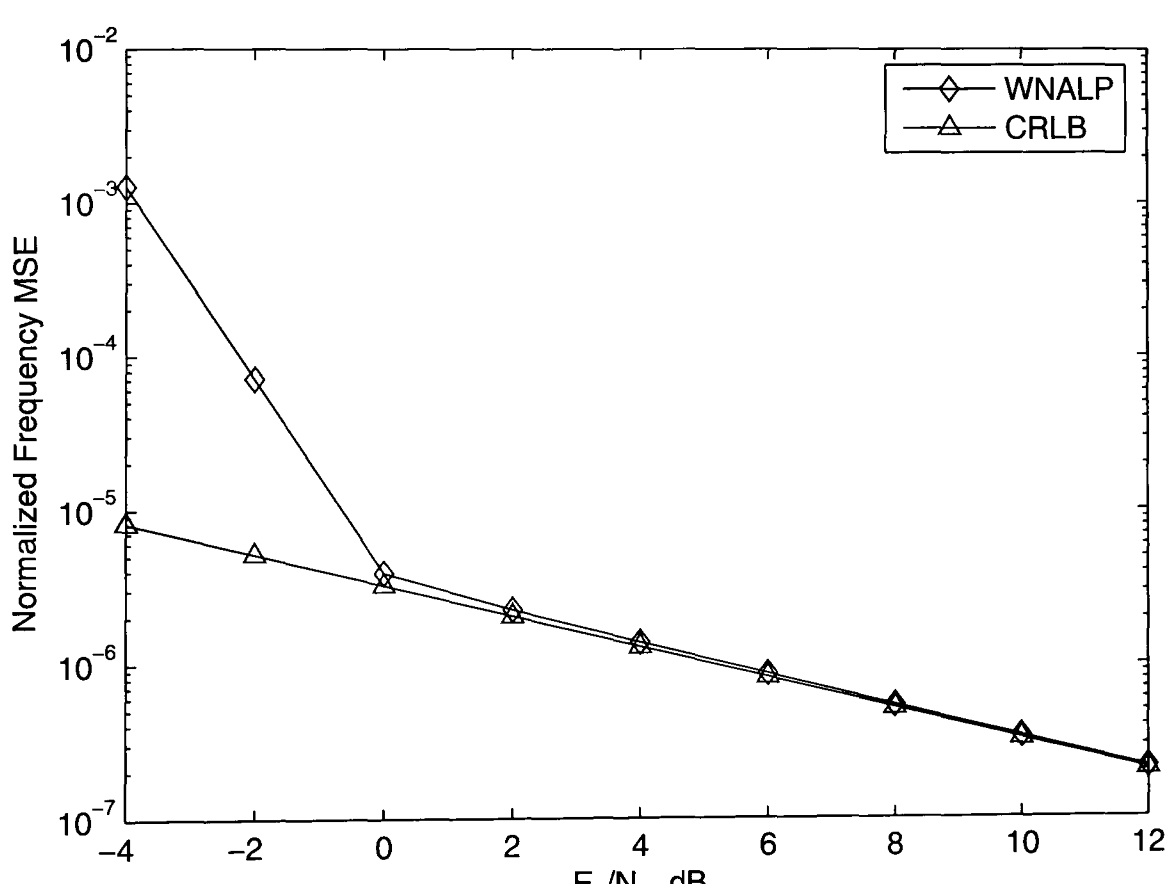

Figure 4.5: Frequency MSE for the WNALP; N=36 and $\Delta f = 0.2$

In order to solve this problem and achieve a wide-range DVB-S2 frequency synchronization with near-optimal accuracy at very low SNR, we re-examine the autocorrelation shown in (4.5). By substituting (4.2) into (4.5) and re-arranging terms as done in [28], the autocorrelation can be expressed as:

$$R(m) = e^{j2\pi m\Delta f}\left[1+\xi(m)\right] \tag{4.13}$$

$$\xi(m) \triangleq \frac{1}{N-m}\sum_{k=m}^{N-1}\left[\tilde{n}(k)+\tilde{n}(k-m)+\tilde{n}(k)\,\tilde{n}^*(k-m)\right] \tag{4.14}$$

where $\tilde{n}(k) = n(k)c^*(k)e^{-j(2\pi\Delta fk+\theta)}$ has the same statistics as $n(k)$ and $\xi(m)$ is a zero-mean noise term.

$$R(m) = e^{j2\pi m\Delta f}\left[1+\xi(m)\right] \approx B_m e^{j(2\pi m\Delta f+\xi_I(m))} \tag{4.15}$$

$$\breve{R}(m) \approx e^{j(2\pi m\Delta f+\xi_I(m))} \tag{4.16}$$

$$\breve{R}(m)\breve{R}^*(m-1) \approx e^{j(2\pi\Delta f+\xi_I(m)+\xi_I(m-1))} \tag{4.17}$$

where B_m is a noisy amplitude and ξ_I is the imaginary part of $\xi(m)$.

Equation (4.15)-(4.17) are based on the assumption that the SNR is sufficiently large. However, at very low SNR, the model is no longer accurate due to the presence of significant noise. Since the WNALP uses the differenced phase of the autocorrelation as shown in (4.17), the inaccuracies of the model at very low SNR are more prominent in the WNALP as compared to L&R's method. Therefore its accuracy degrades sharply as the SNR becomes very low. This problem can be rectified in scenarios where averaging over multiple pilot fields is used, as follows:

$$R_T(m)=\sum_{l=1}^{L}R_l(m) \tag{4.18}$$

where $R_l(m)$ is the autocorrelation of $z(k)$, computed at a fixed lag m over the l^{th} pilot field and L is the total number of pilot fields used in the estimation process. $R_T(m)$ is the autocorrelation sum at a fixed lag m.

The autocorrelation sum $R_T(m)$ has a lower noise variance than each individual autocorrelation $R_l(m)$. Even at very low SNR, the effective noise in $R_T(m)$ is significantly low due to the averaging process. Consequently, the model of (4.15)-(4.17) is re-validated for $R_T(m)$ even at very low SNR. By using $R_T(m)$ instead of $R_l(m)$, the proposed averaged WNALP (AWNALP) can provide accuracies which are similar to the ALRE as will be shown later in the simulation results. The AWNALP is therefore given as:

$$\Delta\hat{f}=\frac{1}{2\pi}\angle\left\{\sum_{m=1}^{M}w_m\breve{R}_T(m)\breve{R}_T^{*}(m-1)\right\} \tag{4.19}$$

where $\breve{R}_T(m)=R_T(m)/|R_T(m)|$.

4.6 Estimation Range and Complexity

Table 4.3 shows a comparison of the estimators in terms of estimation range and complexity. The complexity is quantified in terms of the number of complex multiplications and non-linear angle operations involved while the estimation range defines the maximum normalized frequency offset that can be tolerated by each estimator. The complexity of the proposed AWNALP is shown to compete favourably with that of the ALRE. For a pilot field length of N=36 samples as used is DVB-S2, the ALRE performs 477 multiplications for limited-range fine frequency estimation while the proposed method performs 513 multiplications for wide-range fine frequency estimation. Both methods perform only one non-linear angle operation. However, it is noted that the normalization process used in the AWNALP constitutes a minor increase in complexity. For M=18, the ALRE has a limited frequency estimation range of $|\Delta f| \leq\sim 0.05$ while that of the proposed method approaches the full theoretical range of $|\Delta f| \leq\sim 0.5$. However, it is noted that the imperfections of matched filtering may restrict the practical estimation range in communication systems to less than 30% of the symbol rate [28].

Table 4.3: Estimation range and complexity of the estimators

Estimator	Estimation Range	Angle Operations	Complex Multiplications
AWNALP	$\lvert\Delta f\rvert \leq \sim 0.5$	1	$2M + M(2N - M - 1)/2$
ALRE	$\lvert\Delta f\rvert \leq \sim 1/(M+1)$	1	$M(2N - M - 1)/2$

4.7 Computer Simulations

Computer simulations were run to assess the performance of the proposed method for DVB-S2 carrier frequency synchronization in comparison to the existing method. The simulation model incorporates QPSK-modulated DVB-S2 frames wherein pilot fields, each consisting of 36 symbols are inserted into the frame for the purpose of frequency synchronization. It assumes ideal matched filtering and perfect symbol timing. An initial normalized frequency offset of $\Delta f = 0.2$ is introduced into the received signal for the AWNALP while $\Delta f = 0.01$ is used for the ALRE due to its limited estimation range. The results are shown in terms of frequency mean-square-error (MSE) wherein the Cramer-Rao lower bound (CRLB) for frequency estimation in the multiple pilot field scenario as derived in section 4.5.1 is also shown.

4.7.1 Test case A: DVB-S2 Fixed Terminals

In the first set of simulations, the transmitted signal is received in complex additive white Gaussian noise, as this represents the channel condition for DVB-S2 fixed terminals [3],[6]. Figure 4.6 shows the frequency MSE achieved by the proposed AWNALP and the existing ALRE for DVB-S2 fine frequency synchronization. L=1000 pilot fields are used in similar fashion to [31], in order to achieve the desired estimation accuracy. The results show that AWNALP achieves a similar performance to that of the ALRE, wherein the accuracy of each method approaches the CRLB, even at low signal-to-noise ratios. However, the additional advantage of the AWNALP is its ability to estimate a wide-range of frequency offset in one stage, using the same number of pilot fields as the ALRE which can only estimate a limited range. Consequently, the closed-loop coarse acquisition stage proposed in [31] is not required for the AWNALP. This translates into a significant reduction in synchronization delay since the coarse stage requires the use of an additional 1650 pilot fields (equivalent to 100ms at 25MBaud) for sufficient accuracy [31].

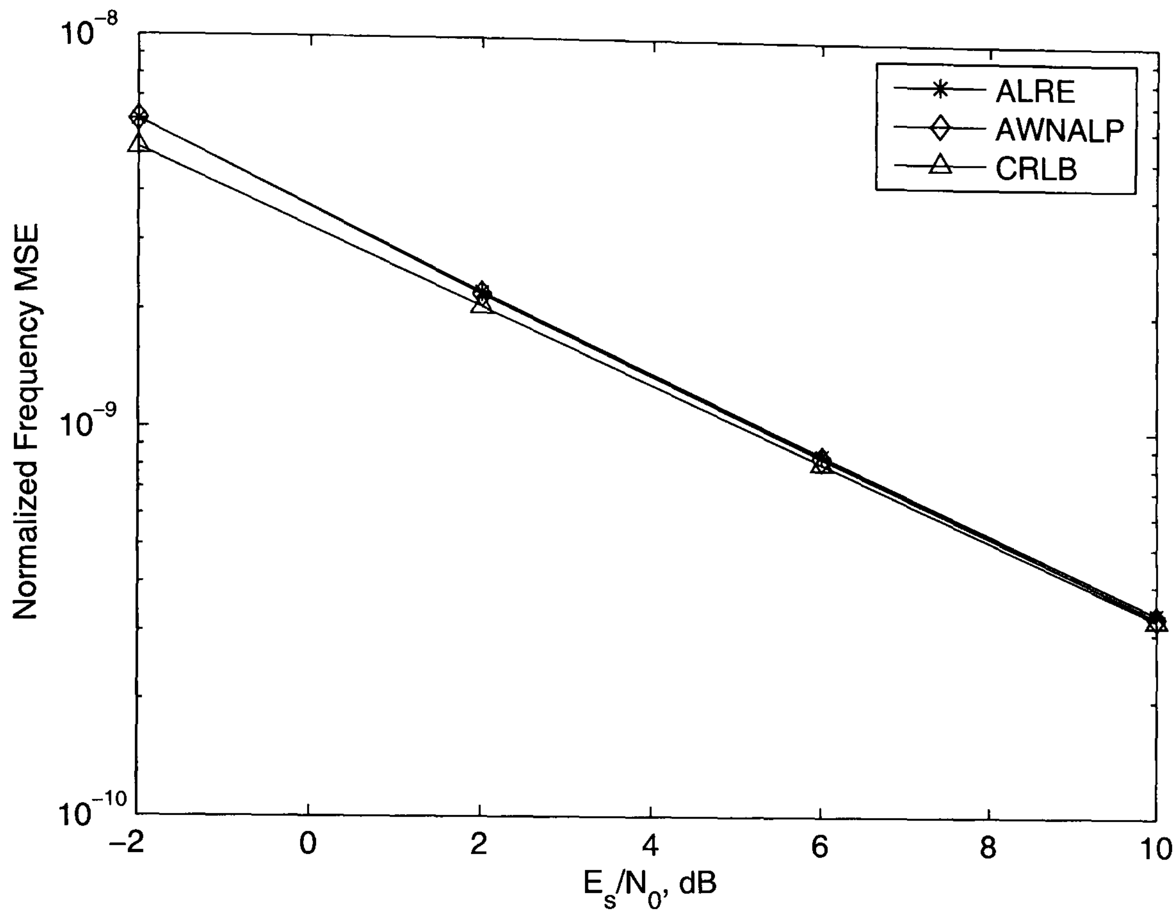

Figure 4.6: DVB-S2 fine frequency MSE in AWGN channel; N=36 and L=1000

4.7.2 Test Case B: DVB-S2 Mobile Terminals

In the second set of simulations, carrier frequency synchronization is investigated for DVB-S2 mobile systems as proposed by the MOWGLY project [19]. In modelling the mobile channel for satellite communication services to terminals such as airplanes, ships and trains, Doppler and fading effects are primarily considered [79]. The fading mechanisms can be classified into four main categories:

- Multipath propagation (aeronautical, maritime, rail)
- Shadowing due to vegetation (maritime, rail)
- Blockage due to building, tunnels, etc. (maritime, rail)
- Diffraction due to space-periodic power arches (rail)

For the aeronautical and maritime satellite channels, measurements have shown that they are narrowband, with fading statistics following a Rician distribution due to the strong line-of-sight (LOS) component at relatively high elevation angles [80]-[82]. A 3-state Markov channel model has been proposed for the railway environment in [83],[84]. These are the LOS, shadowing and blockage states. The situation with trains is considered as more critical of than that of the airplanes and ships. This is because of extended loss of signal (blockage) due to tunnels. A typical example used in [85] gives the signal blockage due to tunnels as occurring for a 44s duration at a train speed of 324km/h. This is expected to result in a loss of frequency synchronization and the need for reacquisition. Therefore, the speed of acquisition takes on a greater importance in the mobile environment in order to minimize service interruptions.

The LOS state is investigated for the three mobile scenarios as this is the preferred option for optimum synchronization purposes at the low SNR typical of DVB-S2. Based on the work done in [80]-[83], the following parameters were chosen for each scenario:

- Airplanes: Speed = 900km/h, k-factor = 30dB
- Ships: Speed = 30km/h, k-factor = 30dB
- Trains Speed = 300km/h, k-factor = 17dB

Computer simulations were run using similar parameters and assumptions as for the fixed terminals in combination with the Doppler and fading parameters specified for the mobile channel in this section. A transmission symbol rate of 25Mbaud is used similar to [31] and a Ku-band carrier frequency of 12GHz is assumed. Figure 4.7 shows that similar accuracy is achieved by the AWNALP for fixed and mobile terminals. This is made possible by the high k-factors of the tested satellite channels and the use of averaging over a large number of pilot fields in the estimation process. The results confirm the robust performance of the AWNALP for wide-range frequency estimation, even at very low SNR. By excluding a coarse frequency estimation stage and achieving the same accuracy as the existing ALRE without significant increase in complexity, the use of the proposed AWNALP leads to a significant reduction in synchronization delay. This improvement is maintained for the DVB-S2 mobile terminals where it has a greater relevance since frequent frequency re-synchronization may be required in the railway channel as discussed earlier.

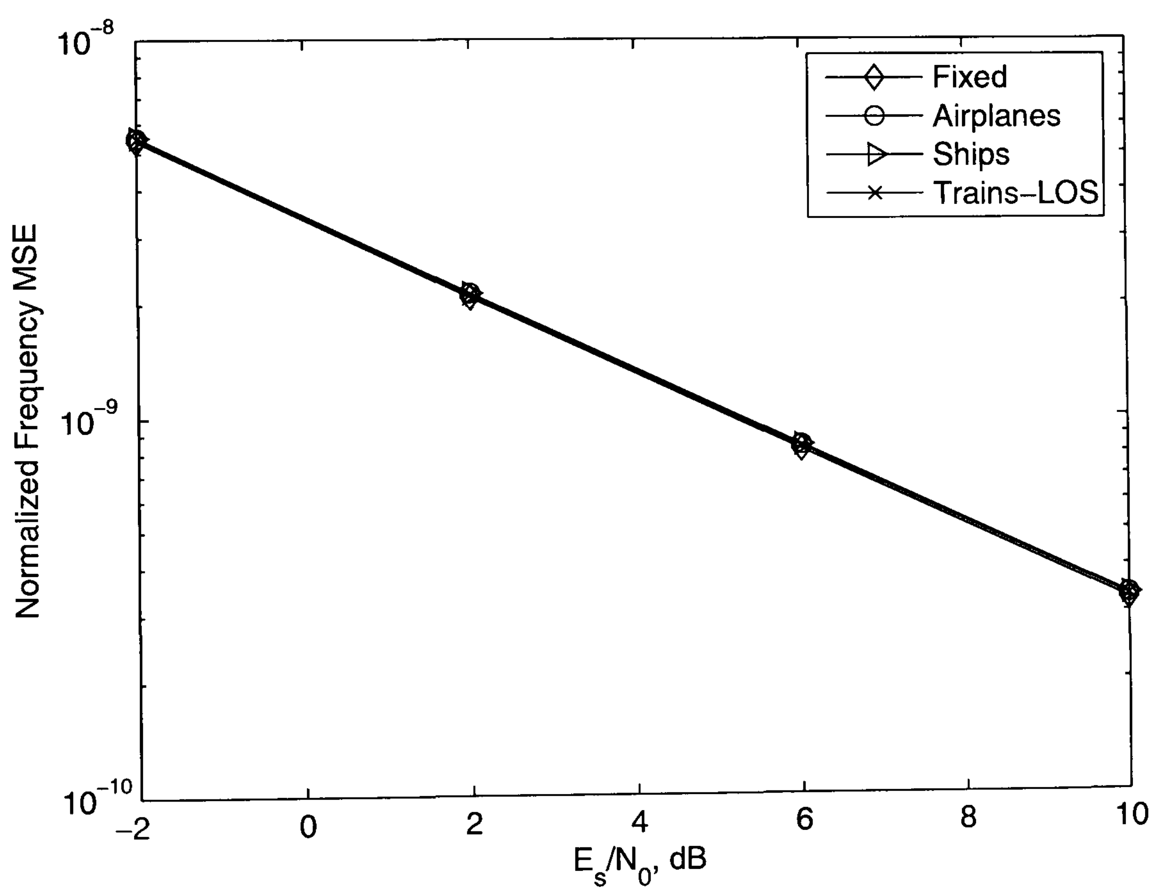

Figure 4.7: DVB-S2 frequency MSE using AWNALP ; *N*=36 and *L*=1000

4.8 Conclusions

In this chapter, we have discussed carrier frequency synchronization for DVB-S2 systems which operate at very low SNR, have a stringent frequency accuracy requirement and tolerate large frequency offsets. In order to improve frequency synchronization performance in comparison to the existing techniques, we have proposed a modified version of the 'weighted normalized autocorrelation linear predictor' for wide-range frequency synchronization in DVB-S2. The proposed AWNALP overcomes the degraded performance of the WNALP at very low SNR and achieves an improvement over the existing techniques in terms of reduced synchronization delays and increased estimation range.

The estimators were tested via extensive computer simulations for DVB-S2 operation in the AWGN channel for fixed terminals and also in the narrowband Rician fading channel for airplane, ship and train services as proposed in the MOWGLY project [6]. The AWNALP achieves a similar accuracy to the ALRE, wherein it is used for wide-range fine frequency synchronization while the ALRE is used for limited-range fine frequency synchronization. This implies that the delay-intensive coarse acquisition stage used in [31] is no longer needed and this translates into a significant reduction in synchronization time without any significant increase in hardware complexity since the AWNALP competes favorably with the ALRE in terms of complexity. The proposed method also maintains its performance in the mobile scenarios due to the strong LOS component in the channel and the effect of averaging over many pilot fields.

The improvement achieved by our proposed technique has increased significance for DVB-S2 mobile systems which may experience larger frequency offsets due to the Doppler effect and may require frequent carrier frequency re-synchronization due to severe signal fading (e.g. in railway tunnels). Table 4.4 summarizes the improvement achieved by the proposed single-stage AWNALP over the existing two-stage method for the same DVB-S2 synchronization accuracy.

Table 4.4: Summary table of improvement achieved by proposed method

Estimator	Number of Pilot Fields	Synchronization time at 25Mbaud
AWNALP	1000	60ms
FED+ALRE	1650+1000	(100+60)ms

Chapter 5

5 Timing Synchronization for OFDM Systems

5.1 Introduction

Orthogonal Frequency-Division Multiplexing (OFDM) is a digital multi-carrier modulation technique, which uses many orthogonal sub-carriers to transmit/receive a high data rate signal [10]-[17]. It has become an increasingly popular scheme for fixed and mobile applications and is already being applied in cable (ADSL), broadcasting (DVB-T/H/SH, DAB), wireless (WiFi, WiMAX) and mobile (3GPP LTE) network standards.

The primary advantage of OFDM over single-carrier transmissions is its robustness against frequency-selective fading occuring due to a multipath (wideband) channel, thus eliminating the need for complex time-domain equalization [4]. Indeed, OFDM may be viewed as a composite of many low data rate signals, each modulating a different subcarrier, rather than a single-carrier high data rate signal. This effectively changes the channel from a wideband transmission into many parallel narrowband transmissions. By using orthogonal subcarriers whose spacing are integer multiples of the symbol rate *1/T*, OFDM is able to achieve great bandwidth saving over its FDM (frequency division multiplexing) counterpart while still avoiding inter-carrier interference (ICI) [10]. The low OFDM symbol rate achieved by transmitting data in parallel makes the use of a guard interval/cyclic prefix between OFDM symbols affordable, in order to handle the channel delay spread and thereby eliminate inter-symbol interference (ISI) [11]. OFDM is efficiently implemented digitally (baseband) through the use of fast Fourier transform (FFT) techniques [10].

The block diagram of a typical OFDM transmitter is as shown in Figure 5.1 wherein a serial bit stream (possibly with coding and interleaving) is mapped to a digital modulation symbol constellation (PSK or QAM) and demultiplexed into N parallel streams. These undergo inverse FFT (IFFT) processing from the frequency-domain (FD) to time-domain (TD) giving a set of N complex time-domain samples. These samples are converted back into a serial stream (P/S) and a cyclic prefix inserted, after which the real and imaginary parts of the samples are converted to analogue signals using digital-to-analogue converters (D/A). These analogue signals are then used to modulate the carrier frequency generated by the local oscillator (LO) respectively, wherein the resulting sum is the transmitted signal $x(t)$.

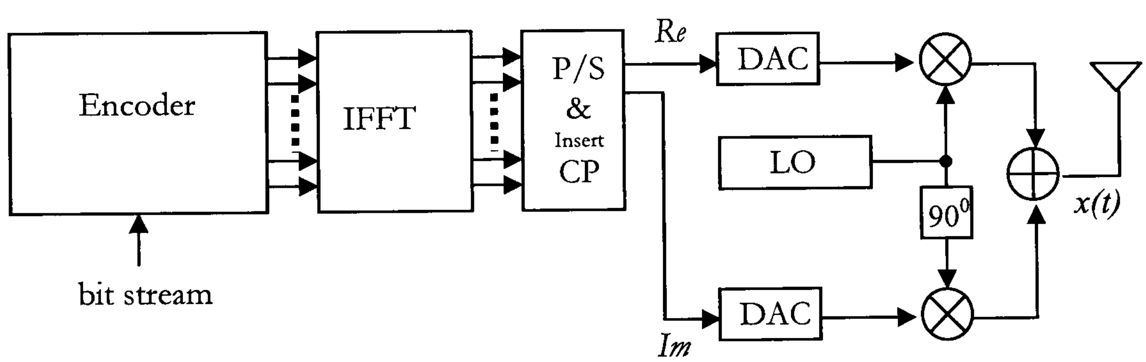

Figure 5.1: Block diagram of a typical OFDM transmitter

An OFDM receiver is illustrated in Figure 5.2, wherein the received signal $r(t)$ is quadrature-mixed down to baseband using the local oscillator (LO). This signal is then filtered after which the analogue-to-digital (A/D) converter provides real (Re) and imaginary (Im) samples of the signal. Synchronization is subsequently performed and the cyclic prefix removed before the serial-to-parallel conversion of the corrected samples of the received signal. These undergo FFT processing (TD to FD) to obtain N parallel streams, which are then demapped from the symbol constellation (after channel estimation and compensation) and multiplexed back to a serial binary stream (possibly with stages of decoding and de-interleaving).

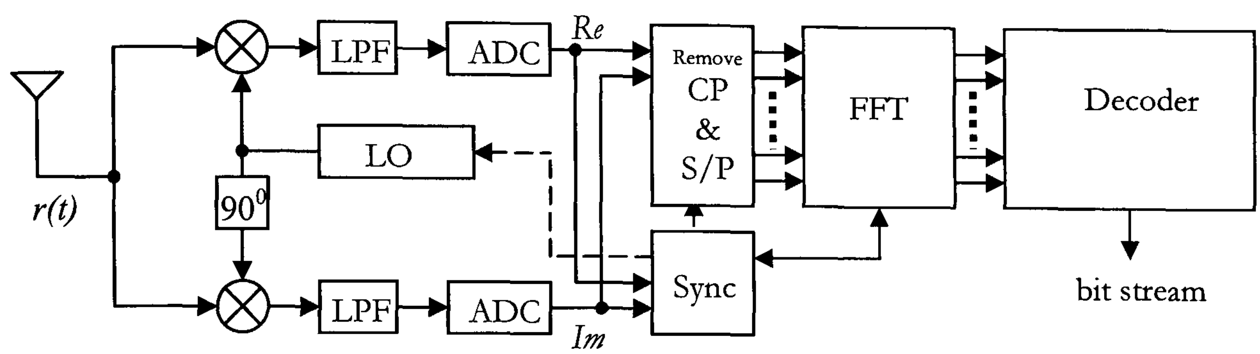

Figure 5.2: Block diagram of a typical OFDM receiver

Figure 5.3 shows the typical synchronization stages in an OFDM receiver. Firstly, a coarse timing estimate is obtained and used for fractional frequency offset estimation based on time-domain (TD) samples ($r(k)$) of the received signal. The fractional frequency offset is then corrected, after which integer frequency offset estimation and compensation are achieved using frequency-domain (FD) samples of the received signal, based on the coarse timing estimate. The coarse timing is then used to control the FFT window for data recovery. Alternatively, an optional fine timing synchronization may be achieved by estimating the channel impulse response using TD samples of the received signal.

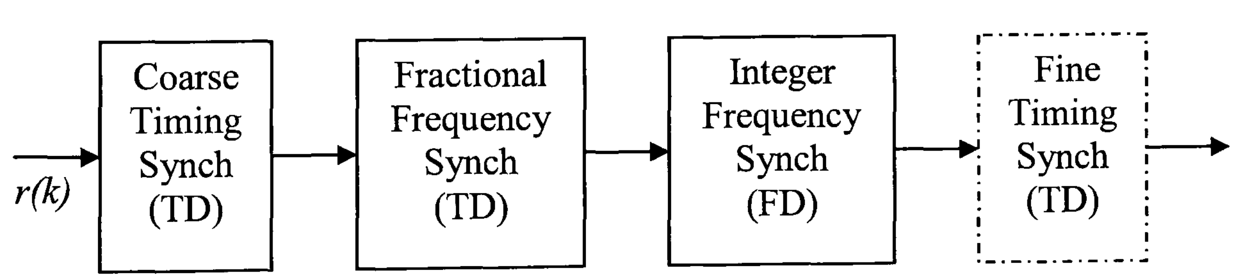

Figure 5.3: Block diagram of typical synchronization stages in OFDM

5.2 OFDM Signal Model

The OFDM samples at the output of the IFFT in the transmitter are given by:

$$x(k)=\frac{1}{\sqrt{N_{use}}}\sum_{n=0}^{N_{use}-1} X_n e^{j2\pi kn/N}; \qquad k=0,1,2,3,\ldots\ldots,N-1 \tag{5.1}$$

where N is the total number of subcarriers of which N_{use} are used. X_n represents the data symbol (PSK or QAM constellation) transmitted on the *nth* subcarrier while $x(k)$ represents the symbol samples after IFFT processing, with each symbol consisting N samples. However, the transmitted OFDM symbol can be denoted as $[x(N-G),x(N-G+1),\cdots,x(N-1),x(0),x(1),\cdots,x(N-1)]$ wherein the samples which precede $x(0)$ represent the cyclic prefix of length G which is used to eliminate the intersymbol interference (ISI) resulting from the multipath channel delay spread [10].

Figure 5.4 shows schematically a string of time-domain (TD) symbols in a transmitted OFDM frame. Each useful symbol consists of N samples and is preceded by either a guard interval (GI) or a cyclic prefix (CP) whose length is usually a fraction of the useful symbol length (e.g. $N/4$, $N/8$, $N/16$ or $N/32$). Preambles may be inserted at the beginning of the OFDM frame for the purpose of synchronization, wherein such preambles may also have a GI or CP appended.

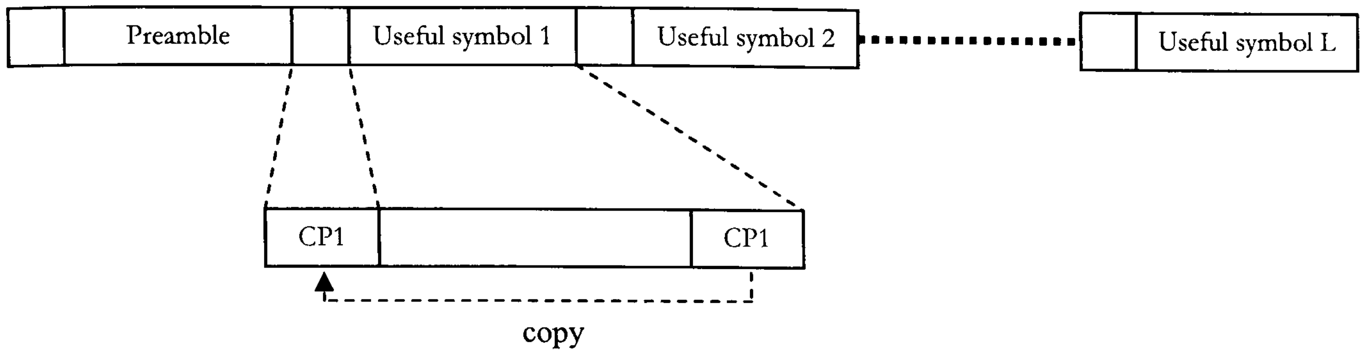

Figure 5.4: OFDM frame transmission showing cyclic prefix and preamble

At the receiver, the waveform after down-conversion and low-pass filtering is sampled with a frequency $1/T_s = N/T$ where $1/T$ is the subcarrier spacing. Assuming sampling precision, the complex samples of the received signal from an ISI (wideband) channel can be represented as:

$$r(k) = y(k-\varepsilon)e^{j2\pi\Delta f k/N} + \omega(k) \tag{5.2}$$

where ε is the integer symbol timing offset measured in samples, Δf is carrier frequency offset normalized to the subcarrier spacing, $\omega(k)$ represents the zero-mean complex additive white Gaussian noise (AWGN) and

$$y(k) = \sum_{m=0}^{L-1} h(m)x(k-m) \tag{5.3}$$

where $x(k)$ represents the transmitted OFDM samples and $h(m)$ is the impulse response of the wideband channel whose memory order is L-1 samples.

5.3 The Need for Timing Synchronization in OFDM

Timing synchronization in the OFDM receiver seeks to establish where the frame/symbol starts to ensure accurate positioning of the FFT window. Due to the use of a cyclic prefix (CP), OFDM exhibits some tolerance to symbol timing errors when the cyclic prefix length is longer than the maximum channel delay spread [33], [86]. In such instances, wherein the timing estimate falls within the ISI-free region of the CP, the timing errors introduce a linear phase shift into the data after FFT processing (in the frequency domain) and this can be corrected by the post-FFT channel estimation techniques used for equalization of the recovered data. However, an off-the-limit timing error (wherein the FFT window is positioned to include copies of either preceding or succeeding symbols) will result in intersymbol interference (ISI) which destroys the orthogonality of the subcarriers and consequently degrades the bit-error-rate (BER) performance [33].

Based on this reasoning, it is clear that timing synchronization constitutes a vital part of the OFDM receiver design and various techniques have been proposed in the literature for this purpose. Some of these techniques are data-aided (DA) wherein time-domain preamble structures are used in contrast to the non-data-aided (NDA) techniques which rely on inherent properties of the OFDM symbol (such as the CP) to achieve synchronization. It should be noted that in general, DA techniques produce faster and more reliable synchronization than NDA techniques and the choice of either is usually a trade-off between bandwidth, accuracy and processing delay. While continuous-mode applications such as digital video broadcasting (e.g. DVB-T [21]) may achieve symbol synchronization without the use of preambles, burst-mode applications such as in the wireless networks (e.g. WiFi [24] and WiMAX[25]) require preambles in the frame structure to achieve frame/symbol synchronization. Therefore, in this thesis, we concentrate on preamble-aided techniques for OFDM synchronization.

In [87], Nogami and Nagashima used a preamble consisting of one null training symbol (i.e. nothing transmitted for one symbol duration) to achieve symbol timing synchronization but this technique is only suitable for continuous applications, not for bursty transmissions where there can be silent intervals between transmissions. Classen and Meyr proposed a trial and error method for joint timing and frequency synchronization in [88] but the method is quite complex due to the exhaustive search that it requires. Schmidl and Cox [86] proposed using the autocorrelation of a training symbol with two identical parts to estimate timing and fractional frequency offset. An additional training symbol is then used along with the first to determine the integer frequency offset. However, Schmidl's timing metric has an uncertainty plateau and the method can yield timing estimates which are well beyond the ISI-free region, thus leading to degradation in BER performance [33]. Minn's method [89] uses the autocorrelation of a preamble with four, eight or sixteen 'signed' identical parts to achieve a sharp timing metric. However, its timing estimate is biased towards the strongest channel tap and an extrinsic technique is subsequently required to determine the channel impulse response and thereby adjust the timing estimate to the ideal start of frame. Shi's method [90] which uses a preamble with four 'signed' identical parts also experiences a similar timing bias which it accommodates by the use of a cyclic postfix. Although the methods proposed by Park [91] and Ren [92] show good performance in non-fading channels, they perform poorly in Rayleigh fading and strong-ISI channels and do not provide for reliable frequency estimation due to their preamble structures. In [93], Kasparis proposed a cross-correlation technique for improved timing estimation in OFDM systems but this method also experiences a similar problem with reliable frequency estimation. Other preamble-aided techniques have been proposed for OFDM timing recovery in [94]-[105]. However, these techniques are either unable to achieve an ideal BER with low overhead and low complexity in fading multipath channels or not suitable for reliable carrier frequency synchronization in ISI channels due to their preamble structures.

In order to solve these problems, we propose a novel low-complexity method for estimating the frame/symbol timing offset in OFDM systems. It uses a simple and conventional preamble structure and combines autocorrelation techniques with restricted cross-correlation to achieve a near-ideal timing accuracy (i.e. timing MSE approaching zero). Consequently, it achieves a BER performance similar to that of an ideal time-synchronized system in both AWGN and fading multipath channels. Moreover, its preamble structure is well-suited for reliable carrier frequency synchronization in OFDM systems using standard available techniques. As a result, both robust timing and reliable frequency synchronization can now be achieved with the minimum overhead of just one training symbol whose structure is compatible with current wireless network standards.

5.4 Existing Techniques for Timing Synchronization

In this section, some popular preamble-aided techniques for OFDM frame/symbol synchronization are discussed and their respective timing metrics are shown in a test scenario under ideal and wideband (ISI) channel conditions, with no additive noise.

5.4.1 Test Channel Specification

A test channel has been chosen to evaluate the performance of the existing and proposed OFDM synchronization algorithms. The OFDM signal parameters and the

ISI channel specifications are chosen based on the tutorial paper by Morelli, Kuo and Pun [33], wherein a fixed WiMAX test case (FFT size: N=256 and cyclic prefix: G=16) is used and the ISI channel consists of L=8 paths with path delays of τ_i = 0,1,2...L-1 sample periods and an exponential power delay profile having average power of $e^{(-\tau_i/L)}$. Each path in the ISI channel undergoes independent Rayleigh fading. Unless otherwise stated, N_{use} is assumed to be equal to N.

5.4.2 Schmidl's Method

Schmidl and Cox [86] proposed using the autocorrelation of one training symbol S_{Sch} with two identical parts in the time-domain as shown in (5.4), for OFDM timing synchronization. This training symbol is generated in the frequency-domain (FD) by transmitting a PN sequence (e.g. from a QPSK constellation) on the even subcarriers, while zeros are used on the odd subcarriers [86]. The PN sequence is appropriately scaled (e.g. by multiplying with $\sqrt{2}$) in order to maintain a unit signal energy for the OFDM symbol. The desired structure is then produced in the time domain via IFFT processing.

$$S_{Sch} = [A_{N/2} \; A_{N/2}] \tag{5.4}$$

where $A_{N/2}$ is a random sequence of length $N/2$.

The reasoning behind this preamble structure is that with the use of a CP whose length is greater than the channel delay spread, the identical parts of the training symbol will remain identical even after passing through a multipath (ISI) channel

[33],[86]. As such, Schmidl's method performs a simple autocorrelation $P_{Sch}(d)$ between the identical parts to obtain a timing metric $M_{Sch}(d)$ as follows:

$$P_{Sch}(d) = \sum_{k=0}^{N/2-1} r^*(d+k)\,r(d+k+N/2) \tag{5.5}$$

$$R_{Sch}(d) = \sum_{k=0}^{N/2-1} |\,r(d+k+N/2)|^2 \tag{5.6}$$

$$M_{Sch}(d) = |P_{Sch}(d)|^2 / (R_{Sch}(d))^2 \tag{5.7}$$

$$\hat{d} = \arg\max_{d} \{ M_{Sch}(d) \} \tag{5.8}$$

where d is the timing index/instant, $R_{Sch}(d)$ is an energy term used to normalize the autocorrelation $P_{Sch}(d)$ in order to achieve a timing metric $M_{Sch}(d)$ which is used for timing estimation and also preamble detection at instances wherein it exceeds a predetermined threshold based on the statistics of the autocorrelation as explained in [86]. $\hat{d}$ is the timing estimate which is determined at the maximum point of the timing metric.

Figure 5.5 shows the timing metric of Schmidl's method wherein a plateau is seen at its peak due to the presence of the cyclic prefix. The peak value can occur anywhere within this plateau depending on the channel noise. Therefore, in order to drive the timing estimate to the middle of such plateau, an averaging of timing points having a metric value greater than or equal to 90% of the peak value is recommended in [86]. It should be noted that Schmidl's method is a very popular technique for OFDM synchronization due to its low complexity and simplicity of implementation [89]-[94]. However, its major drawback is the BER degradation experienced in post-FFT data recovery when it yields timing estimates that are outside the ISI-free region [33] as will be shown in section 5.6.

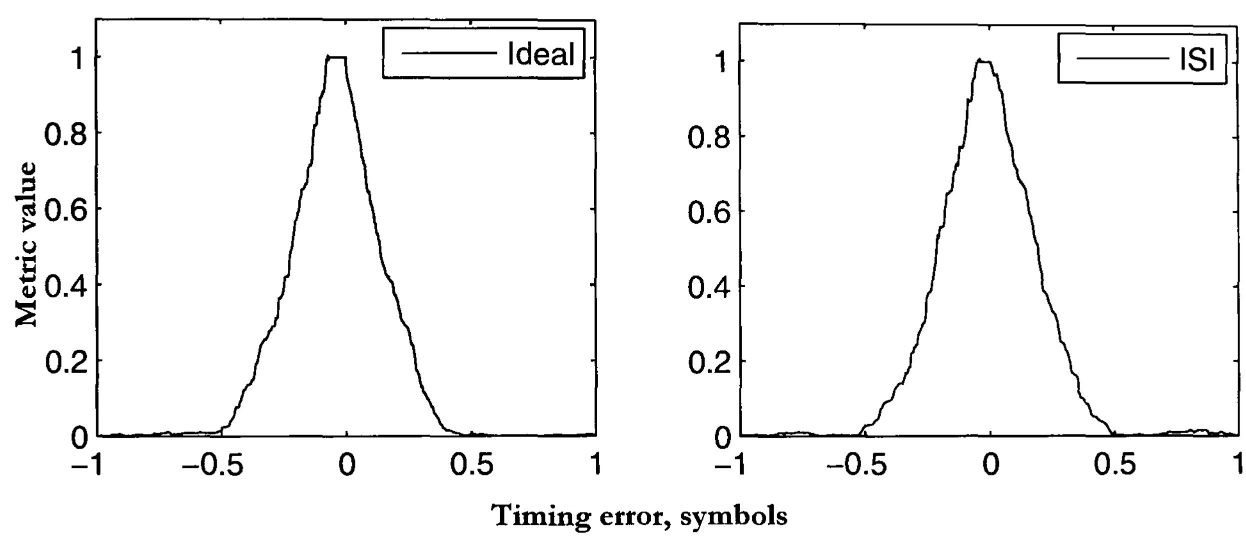

Figure 5.5: Timing metric for Schmidl's method (Eqn. 5.7); N=256, G=16

5.4.3 Minn's Method

In [89], Minn et al proposed an autocorrelation-based method which achieves a sharper timing metric than Schmidl's method. This method uses a training symbol which can have l = 4, 8 or 16 repeated segments with different signs in the time-domain. A 'signed' sixteen-segment symbol as proposed by Minn is shown in (5.9).

$$S_{Minn} = [+--+++--+-++-+--] \qquad (5.9)$$

where each segment is represented by its sign, i.e. a signed version of the same random sequence generated as specified in [89].

Minn's method performs an autocorrelation of the received signal $P_{Minn}(d)$ in order to obtain a timing metric $M_{Minn}(d)$ as follows:

$$P_{Minn}(d) = \sum_{m=0}^{l-2} b(m) \cdot \sum_{k=0}^{N/l-1} r^*(d + k + Nm/l)\, r(d + k + Nm/l + N/l) \tag{5.10}$$

$$R_{Minn}(d) = \left(\frac{l-1}{l}\right) \sum_{k=0}^{N-1} |r(d+k)|^2 \tag{5.11}$$

$$M_{Minn}(d) = |P_{Minn}(d)|^2 / (R_{Minn}(d))^2 \tag{5.12}$$

$$\hat{d} = \arg\max_{d} \{ M_{Minn}(d) \} \tag{5.13}$$

where *b(m)* is a sign which is equivalent to the product of signs for the two segments involved in each autocorrelation process of equation (5.10).

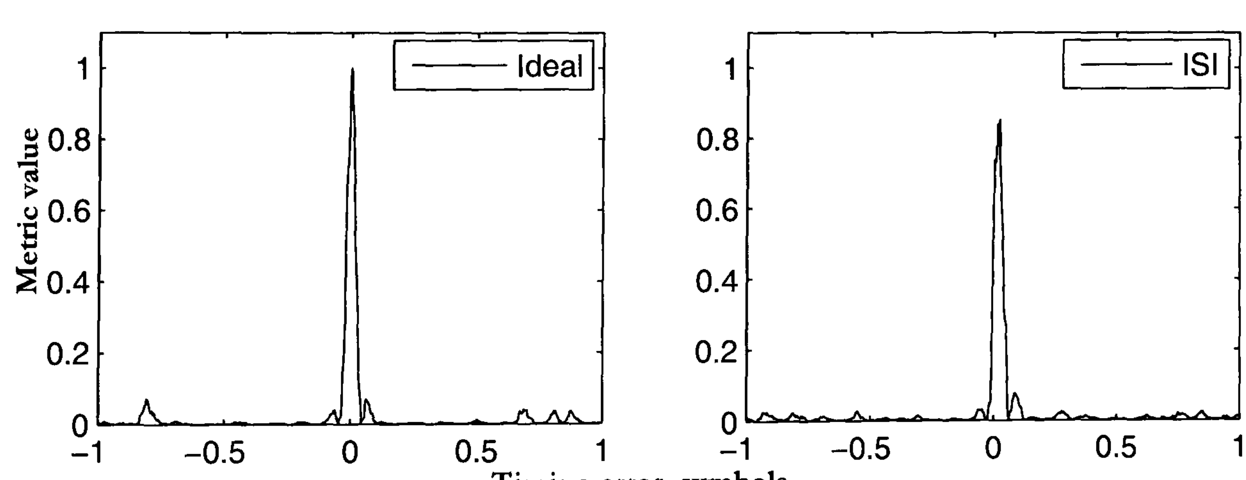

Figure 5.6: Timing metric for Minn's method (Eqn. 5.12); *N*=256, *G*=16

The timing metric of Minn's method as shown in Figure 5.6 is significantly sharper than that of Schmidl's method. However, its timing estimate tends to be biased towards strongest channel tap in an ISI channel. Therefore, it incorporates a fine timing adjustment stage which uses a computationally-intensive preamble-based channel estimation [89], in order to determine the channel impulse response and achieve an acceptable timing for post-FFT data recovery [89]. However, this preamble-based channel estimation is inappropriate in many OFDM systems where frequency-domain pilots must be inserted within the data for the purpose of channel estimation in a time-varying frequency-selective channel. Therefore, it constitutes a significant processing overhead.

5.4.4 Shi's Method

The method proposed by Shi and Serpedin [90] makes use of a training symbol with four repeated segments having different signs as shown in (5.14).

$$S_{Shi} = \quad [++-+] \tag{5.14}$$

where each segment is represented by its sign, i.e. a signed version of the same random sequence generated as specified in [90].

Shi's method performs an autocorrelation of the received signal $P_{Shi}(d)$ in order to obtain a timing metric $M_{Shi}(d)$ as follows:

$$P_{Shi}^{(i,j)}(d) = \sum_{k=0}^{N/4-1} r^*\left(d+k+(i-1)N/4\right) r\left(d+k+(j-1)N/4\right) \tag{5.15}$$

$$P_{Shi}(d) = \left|P_{Shi}^{(1,2)}(d) - P_{Shi}^{(2,3)}(d) - P_{Shi}^{(3,4)}(d)\right| + \left|P_{Shi}^{(2,4)}(d) - P_{Shi}^{(1,3)}(d)\right| + \left|P_{Shi}^{(1,4)}(d)\right| \quad (5.16)$$

$$R_{Shi}(d) = 1.5\sum_{k=0}^{N-1} \left| r(d+k) \right|^2 \quad (5.17)$$

$$M_{Shi}(d) = P_{Shi}(d)/R_{Shi}(d) \quad (5.18)$$

$$\hat{d} = \arg\max_{d} \{ M_{Shi}(d) \} \quad (5.19)$$

The timing metric achieved by Shi's method as shown in Figure 5.7 is sharper than that of Schmidl's method but its timing estimate is similarly biased towards the strongest channel tap as with Minn's method. Consequently, it also requires a timing adjustment technique to avoid degradation in the decoder error rate due to the ISI caused by such timing-errors. It achieves this by inserting a cyclic postfix to every transmitted OFDM symbol such as to accommodate its timing estimation bias [90]. However, such postfix is an additional overhead which reduces the bandwidth efficiency.

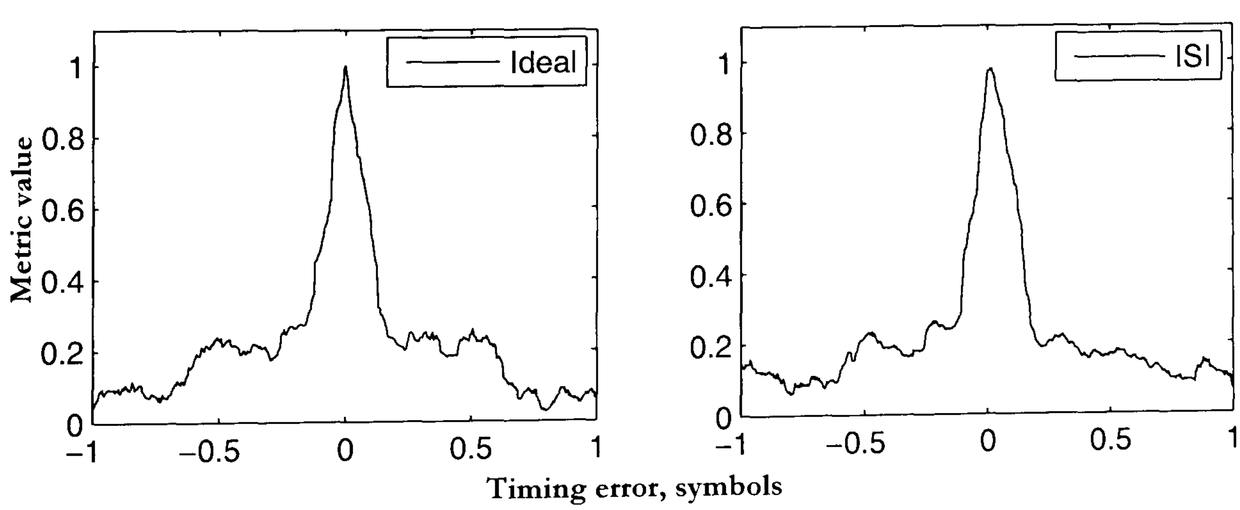

Figure 5.7: Timing metric for Shi's method (Eqn. 5.18); N=256, G=16

5.5 Improved Timing Synchronization for OFDM Systems

5.5.1 Introduction

An improved preamble-aided method for estimating the frame/symbol timing offset in OFDM systems is proposed as part of the work of this thesis. It uses a simple and conventional preamble structure and combines autocorrelation techniques with restricted cross-correlation to achieve a near-ideal timing performance (wherein the timing mean-square-error approaches zero) without significant increase in complexity when compared to the existing methods. Computer simulations show that the method is robust in both AWGN and fading multipath channels, achieving better accuracy than the existing methods such that a BER similar to that of an ideal time-synchronized OFDM system is achieved. The proposed method is multi-stage, wherein the preamble structure proposed by Schmidl and Cox [86] is re-used.

5.5.2 Cross-correlation Timing Detection in ISI Channels

In the AWGN channel, cross-correlation techniques (rather than autocorrelation) are widespread for frame detection [106]. Also, it has been shown in [59] that the ML timing estimation metric in such channel is cross-correlation based, under the assumption of negligible frequency offsets. It is assumed that the transmitted signal $x(k)$ consists of an infinite random sequence which exists for positive and negative values of k, with a known part $S(k)$ (having sharp autocorrelation) such that $x(k) = S(k);\quad k = 0,1,2\cdots,N-1$. A cross-correlation between the received signal r from an ISI channel and the known PN sequence can be derived as follows:

$$P_x(d,\Delta f) = \sum_{k=0}^{N-1} r\,(d+k,\Delta f)\; S^*(k) \tag{5.20}$$

$$= \sum_{k=0}^{N-1} \left(\left(\sum_{m=0}^{L-1} h(m) x(d+k-\varepsilon-m) \right) e^{j2\pi\Delta f k/N} + \omega(k) \right) S^*(k) \tag{5.21}$$

where d is the timing index/instant, Δf is the carrier frequency offset normalized to the subcarrier spacing, $h(m)$ is the impulse response of the wideband channel whose memory order is L-1 samples, ε is the integer symbol timing offset and $\omega(k)$ represents the zero-mean complex additive white Gaussian noise.

Equation (5.21) can be re-arranged to show a coherent part Γ_1 and a random part Γ_2 as follows:

$$P_x(d, \Delta f) = \Gamma_1(m = d-\varepsilon) + \Gamma_2(m \neq d-\varepsilon) \tag{5.22}$$

$$\Gamma_1(m = d-\varepsilon) = \sum_{k=0}^{N-1} h(d-\varepsilon) |S(k)|^2 e^{j2\pi\Delta f k/N} \tag{5.23}$$

$$\Gamma_2(m \neq d-\varepsilon) = \sum_{k=0}^{N-1} \left(\left(\sum_{m \neq d-\varepsilon} h(m) x(d+k-\varepsilon-m) \right) S^*(k) e^{j2\pi\Delta f k/N} + \omega(k) S^*(k) \right) \tag{5.24}$$

where ($d-\varepsilon$) is the timing error.

Assuming a negligible carrier frequency offset, it can easily be deduced from (5.22)-(5.24) that even in an ISI channel, cross-correlation is able to produce sharp frame/timing detection due to the coherent summation achieved in (5.23) at timing instants that correspond to the arrival of the known sequence $S(k)$ via the channel taps i.e. $h(0), h(1), \ldots, h(L-1)$. The strength of the cross-correlation corresponding to each channel tap depends primarily on the energy contained within that tap. The cross-correlation at all other timing instants will be lacking in the coherent part due to non-existent channel taps. Therefore a known random sequence (having a sharp autocorrelation property) can be used to achieve improved timing estimation via the sharp timing detection properties of cross-correlation. It is noted that the presence of significant frequency offsets in the received signal will degrade the performance of coherent cross-correlation [106] as the coherent summation in (5.23) will no longer be achievable.

Assuming the central limit theorem (CLT) holds, the cross-correlation $P_x(d)$ at all other timing instants apart from those corresponding to the arrival of the known sequence $S(k)$ via the channel taps (i.e. $d_{NC} \notin \{d_{ideal}, d_{ideal}+1, \cdots, d_{ideal}+L-1\}$) can be taken to be a zero-mean complex Gaussian variable. This implies that the absolute value of the cross-correlation at the non-coherent timing instants d_{NC} will follow a Rayleigh distribution whose PDF and expected value are given as:

$$p_R(|P_x(d_{NC})|) = \frac{|P_x(d_{NC})|}{\sigma^2}\, e^{-\frac{|P_x(d_{NC})|^2}{2\sigma^2}} \tag{5.25}$$

$$\mathrm{E}(|P_x(d_{NC})|) = \sigma\sqrt{\pi/2} \tag{5.26}$$

where $\mathrm{E}(\cdot)$ is the expected value operator and σ^2 is the variance of either the real or imaginary components of $P_x(d_{NC})$.

Assuming that sufficient observations are available:

$$\sigma \approx \sqrt{2/\pi} \cdot \left(\underset{d_{NC}}{mean} \left\{ \left| P_x(d_{NC}) \right| \right\} \right) \tag{5.27}$$

Deriving from the Rayleigh cumulative distribution function (CDF) as shown in (5.28), a threshold δ can be chosen in accordance with a desired probability that $|P_x(d_{NC})|$ does not exceed such threshold, wherein the reverse case is the probability of false alarm: P_{FA}.

$$\mathrm{P}\left(\left|P_x(d_{NC})\right| < \delta\right) = 1 - e^{\left(-\delta^2/2\sigma^2\right)} \tag{5.28}$$

$$\mathrm{P}\left(\left|P_x(d_{NC})\right| > \delta\right) = \mathrm{P}_{FA} = e^{\left(-\delta^2/2\sigma^2\right)} \tag{5.29}$$

$$\delta = \sqrt{-\ell n(\mathrm{P}_{FA}) 2\sigma^2} \tag{5.30}$$

At timing instants where the cross-correlation has a coherent part, the magnitude of such correlation is expected to exceed the chosen threshold while that of all other timing instants are expected to be below such threshold with high probability. This threshold crossing (TC) timing detection technique, which was proposed in [93], helps to identify the timing instants corresponding to the arriving channel paths and is incorporated into our novel method for improved timing estimation in OFDM systems.

5.5.3 Choice of Training Symbol

In choosing a training symbol for our proposed timing algorithm, we have considered the merits and demerits of both autocorrelation and cross-correlation approaches to OFDM timing estimation in ISI channels. In general, using cross-correlation for the preamble search process in an OFDM system is more computationally intensive than using autocorrelation techniques. This is in addition to the inability of coherent cross-correlation to operate under large frequency offsets in contrast to autocorrelation. However, the accuracy offered by coherent cross-correlation for symbol timing estimation is significantly better than what any autocorrelation technique can offer due to its impulse-shaped detection properties.

To solve the carrier frequency offset problem in OFDM, reliable techniques use a training symbol with repetitive blocks such as in Schmidl's [86] and Morelli's [107] methods, wherein the duration of each block is longer than the expected channel delay spread. In contrast, the best cross-correlation performance is achieved by using a purely random sequence as a repetitive structure will generate unwanted correlation peaks which degrade performance in the presence of channel noise.

In order to achieve a compromise and benefit from the advantages of both autocorrelation and cross-correlation, a preamble structure with two identical parts is chosen based on its observed properties as will be explained later. The training symbol S_{Sch} proposed by Schmidl in [86] fits perfectly into this design and will be implemented in our proposed algorithm.

5.5.4 Autocorrelation (Coarse Timing)

In the proposed method, the autocorrelation $P_{Sch}(d)$ of Schmidl's training symbol with two identical parts as shown in (5.4) and (5.5) is processed as follows:

$$M_c(d) = \frac{1}{G+1} \sum_{k=0}^{G} | P_{Sch}(d-k) |^2 \tag{5.31}$$

$$\hat{d}_c = \arg\max_d \{ M_c(d) \} \tag{5.32}$$

where $P_{Sch}(d)$ is Schmidl's autocorrelation which is integrated in (5.31) over the length of the cyclic prefix in order to eliminate its uncertainty plateau and achieve a coarse timing metric $M_c(d)$ whose peak indicates the coarse timing estimate $\hat{d}_c$.

Preamble detection is achieved using a similar concept to Schmidl's method [86]. The coarse timing estimate ($\hat{d}_c$) is subsequently used for frequency offset estimation (pre-FFT and/or post-FFT) via existing techniques such as Schmidl's [86] or Kim's [108] frequency estimators which are known to give reliable frequency estimates even with a coarse timing. The total frequency offset is then corrected in the stored received samples, after which cross-correlation is performed.

5.5.5 Restricted Cross-correlation (Fine Timing)

Cross-correlation techniques produce sharper detection properties than autocorrelation and have been proposed for OFDM synchronization in [93],[96]-[99], although these methods suffer from drawbacks such as a preamble structure unsuitable for reliable frequency estimation and/or poor timing performance in fading ISI channels. In a multipath environment, coherent cross-correlation between a frequency-corrected received preamble and its known version (i.e. a random sequence having sharp autocorrelation) will yield a set of very sharp peaks (impulses) which indicate all the arriving paths from the channel as discussed in section 5.5.2. For a preamble having two identical parts, the coherent cross-correlation will yield three distinct sets of impulses, where each set indicates the arriving paths.

Figure 5.8 shows an example coherent cross-correlation of the frequency-corrected received signal as implemented using (5.33) and (5.34) in the test scenario under ideal and ISI channel conditions, wherein there is a major peak in the middle corresponding to a full-symbol pattern match and two minor peaks at half a symbol away corresponding to a half-symbol pattern match. The minor peaks which are due to the symmetric structure in (5.4) constitute a major hindrance to using such preamble for cross-correlation timing in a fading and/or noisy channel since any of these peaks could instantaneously have the highest value. On the other hand, the symmetric structure is beneficial for low-complexity coarse timing and reliable frequency offset estimation [86],[108]. In order to solve this problem, we propose a novel approach to jointly optimize the cross-correlation and autocorrelation properties of the chosen preamble.

$$P_x(d) = \sum_{k=0}^{N-1} r_{corT}(d+k)\ S_{Sch}^{*}(k) \tag{5.33}$$

$$M_x(d) = |P_x(d)|^2 \tag{5.34}$$

where r_{corT} is the total frequency corrected signal, $P_x(d)$ is the coherent cross-correlation and $M_x(d)$ is the coherent cross-correlation timing metric.

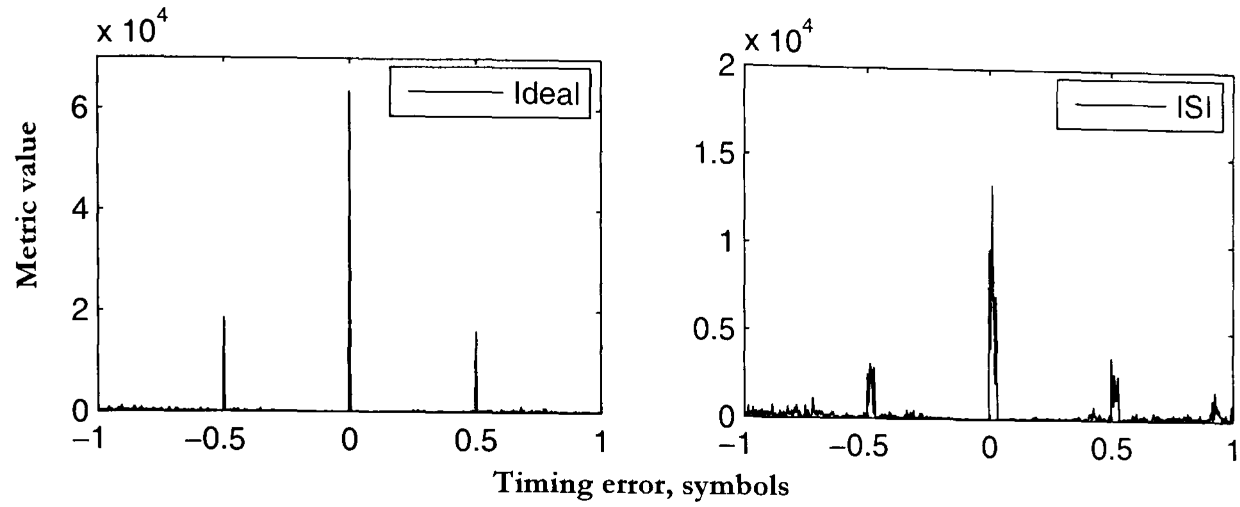

Figure 5.8: Cross-correlation metric (Eqn. 5.34); *N*=256, *G*=16

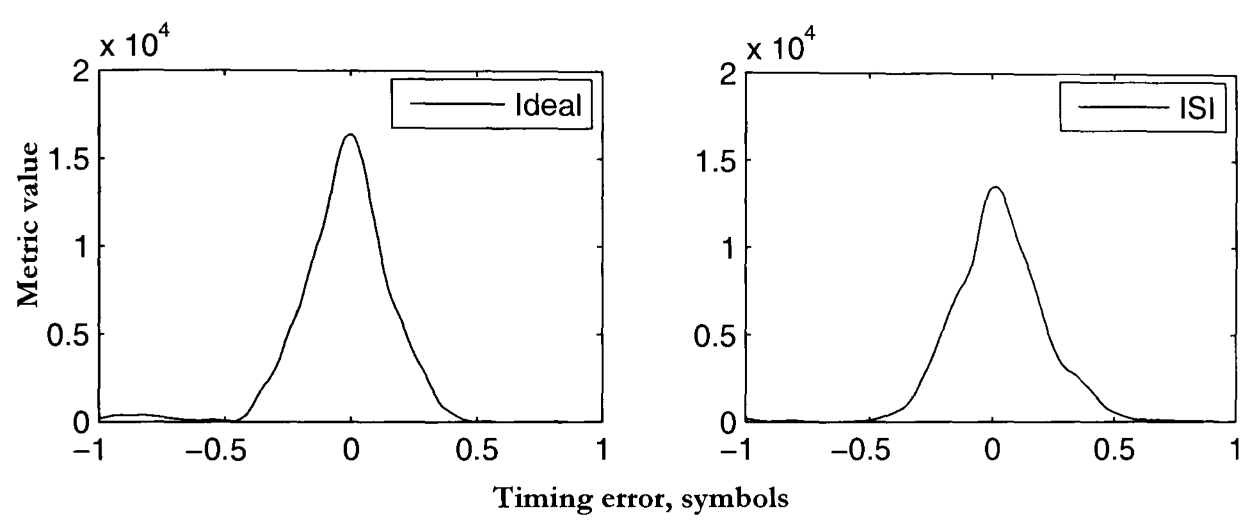

Figure 5.9: Autocorrelation metric (Eqn. 5.31); *N*=256, *G*=16

As illustrated in Figure 5.8, the location of the two minor cross-correlation peaks is fixed at a half-symbol timing error from the ideal timing peak. Also, the autocorrelation metric of (5.31) as shown in Figure 5.9 yields significantly low values at timing points which are in the region of a half-symbol timing error or more from the ideal timing point. Therefore the autocorrelation can be used to filter the unwanted minor peaks. One way to achieve this is to simply multiply both metrics together. This multiplication can be restricted to a timing window of one symbol length N, symmetric around the coarse timing estimate $\hat{d}_c$ in order to reduce computational complexity. An alternative approach which avoids multiplication is to use the autocorrelation peak value to define a timing window consisting of all timing points whose autocorrelation exceeds a pre-determined fraction of the peak value. This timing window is then used to restrict the cross-correlation computations accordingly. The filtering helps to determine the major peak which corresponds to the strongest arriving path. Figure 5.10 shows the resulting timing metric achieved by such filtering process.

A restricted timing adjustment window is also proposed for the chosen preamble structure in ISI channels, based on the known relative location of the minor and major cross-correlation peaks and the expected channel delay spread, in order to track the cross-correlation peak that corresponds to the first arriving channel path (which is not always the strongest arriving path) with high efficiency using a threshold criterion as discussed in section 5.5.2. This restricted timing adjustment window is illustrated in Figure 5.11 and implemented using equation (5.37) and (5.38).

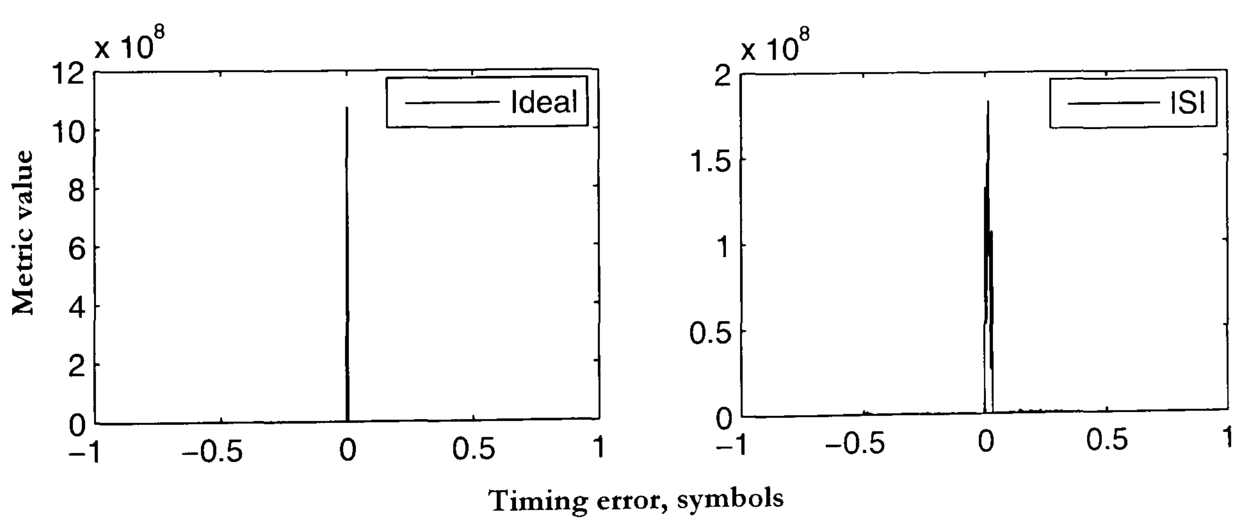

Figure 5.10: Filtered correlation metric (Eqn. 5.35); *N*=256, *G*=16

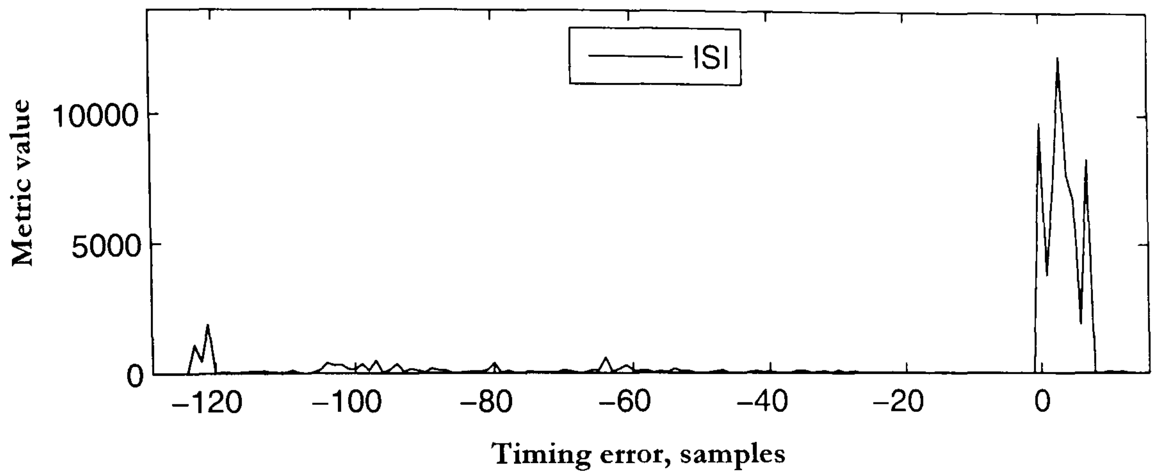

Figure 5.11: Timing adjustment window (Eqn. 5.37 and 5.38); *N*=256

The processing operations within the restricted cross-correlation stage are summarised as follows:

$$M_{opt}(d) = |P_x(d)|^2 \cdot M_c(d); \qquad d \in \{\hat{d}_c - N/2,\ \hat{d}_c + N/2\} \tag{5.35}$$

$$\hat{d}_{opt} = \arg\max_{d} \{M_{opt}(d)\}; \qquad d \in \{\hat{d}_c - N/2,\ \hat{d}_c + N/2\} \tag{5.36}$$

$$\hat{d}_{FFT} = \arg \mathop{first}_{d} \{|P_x(d)| > T_{th}\}; \qquad d \in \{\hat{d}_{opt} - \lambda,\ \hat{d}_{opt}\} \tag{5.37}$$

$$T_{th} = \alpha \cdot \left(\mathop{mean}_{d} \{|P_x(d)|\}\right); \qquad d \in \{\hat{d}_{opt} - N/2 + \lambda + 1,\ \hat{d}_{opt} - \lambda - 1\} \tag{5.38}$$

where M_{opt} is the filtered timing metric computed for a restricted set of timing points and d is chosen in (5.35) and (5.36) to ensure that all relevant timing points that could be the ideal timing are tracked. d is chosen in (5.37) such as to track the first arriving path ($\hat{d}_{FFT}$) which may not always be the strongest arriving path ($\hat{d}_{opt}$), wherein all channel paths are expected to be received within $\lambda+1$ samples: $(L-1 \le \lambda \le G)$. In (5.38), d is chosen such as to exclude major and minor coherent peaks and their multipath, in order to calculate a threshold T_{th} using the mean correlation of the non-coherent timing points as explained in section 5.5.2. P_{FA} is probability of false alarm (for which a non-coherent correlation peak exceeds the threshold) and $\alpha = \sqrt{-(4/\pi)\ell n(\mathrm{P}_{FA})}$. The first arriving channel path (or any other one) is expected to have a correlation which is greater than T_{th} with high probability. Deriving from extensive simulations, P_{FA} is chosen as 10^{-6} for timing adjustment purposes. The threshold T_{th} is used to detect the ideal timing $\hat{d}_{FFT}$.

5.6 Computer Simulations

Extensive computer simulations were performed in order to assess the performance of the proposed method in comparison with existing methods. Coherent QPSK sub-carrier modulation is used and ideal frequency synchronization is assumed. In Figure 5.12, a WiFi test case [24] (FFT size N=64 and cyclic prefix length G=16) is used in an AWGN channel with expected delay spread set to $\lambda = 0$ for the proposed method, whereas in Figure 5.13 - 5.15, a fixed WiMAX test case [25] (N=256 and G=16) is used in the test ISI channel described in section 5.4.1, with the expected delay spread set to $\lambda = G$ for the proposed method. For the uncoded BER results of Figure 5.15, a synchronization symbol and a data symbol are incorporated into the transmitted frame. 51 evenly-spaced frequency domain pilots are inserted into the data symbol for the purpose of channel estimation and equalization via linear interpolation. In order to keep the simulation model generic, no error control coding is used. A training symbol with sixteen identical parts is used with Minn's method.

The results of Figure 5.12 show that Minn and Shi's methods are able to achieve better performance than Schmidl's method (with 90% averaging), having a fractional timing mean-square-error (MSE) in an AWGN channel due to their sharp timing metrics. However, the proposed method shows a superior performance, as it is able to consistently determine the ideal start of the FFT window without error in our computer simulations for SNR values greater than 0dB due to its impulse-shaped timing metric. In the Rayleigh fading ISI channel, the timing estimators exhibit a different behaviour as shown in Figure 5.13 and 5.14. The proposed method maintains it superiority over the existing methods in such channel, as it achieves a fractional timing MSE and is also shown to be biased towards the ideal timing point (i.e. zero bias) in contrast to the other methods.

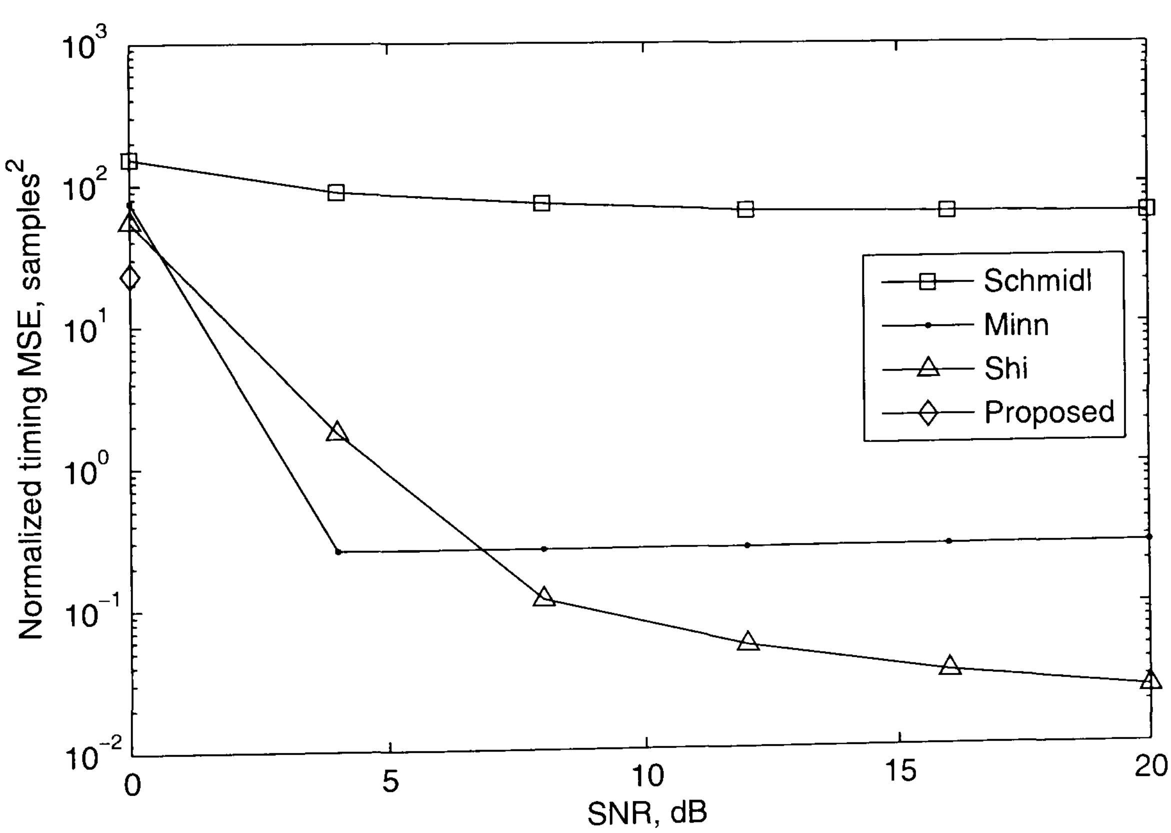

Figure 5.12: Timing MSE for the estimators in an AWGN channel; *N*=64

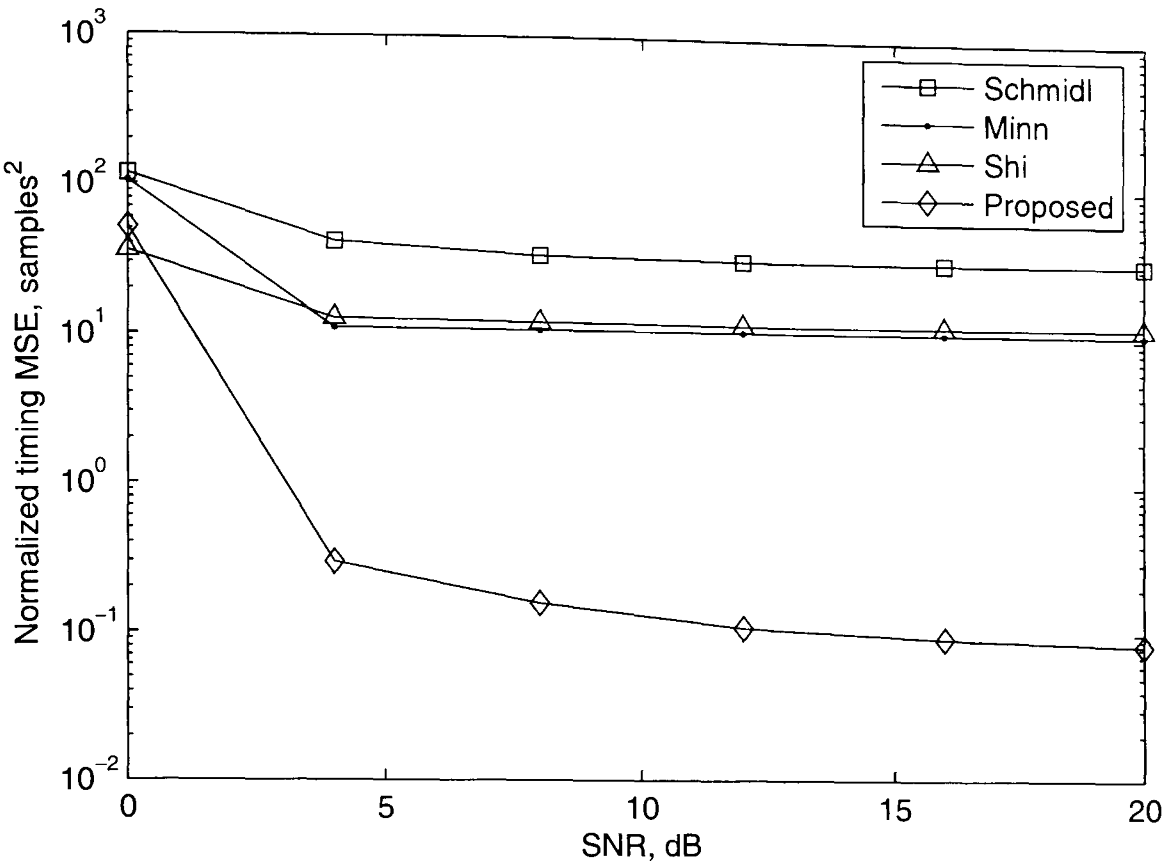

Figure 5.13: Timing MSE for the estimators in an ISI channel; N=256

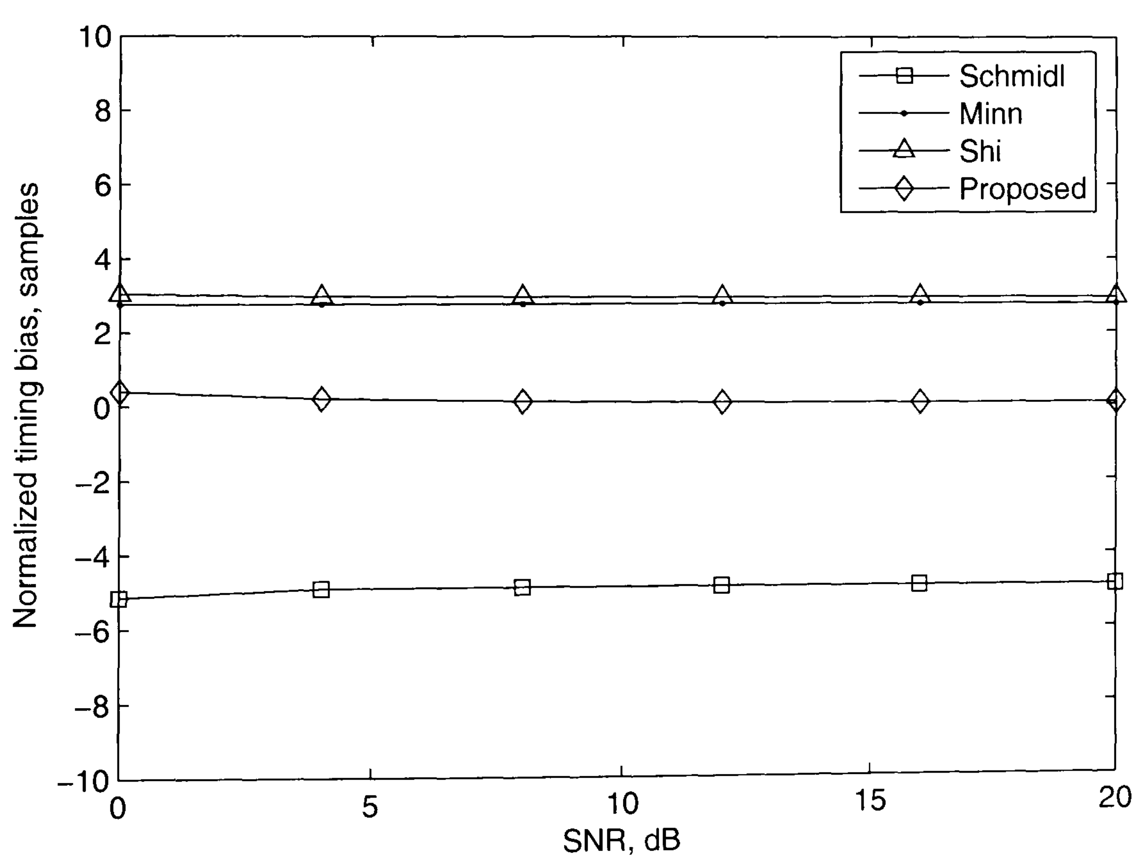

Figure 5.14: Timing bias for the estimators in an ISI channel; N=256

The accuracy of Minn and Shi's methods in ISI channels is compromised by their bias towards the strongest channel tap as opposed to the first arriving channel tap. It is also noted that the proposed method is less complex than both methods since it uses a simpler autocorrelation process and excludes computing an energy term or using such energy term to divide the autocorrelation at each timing point. Also, its cross-correlation processing is performed for only a restricted set of timing points.

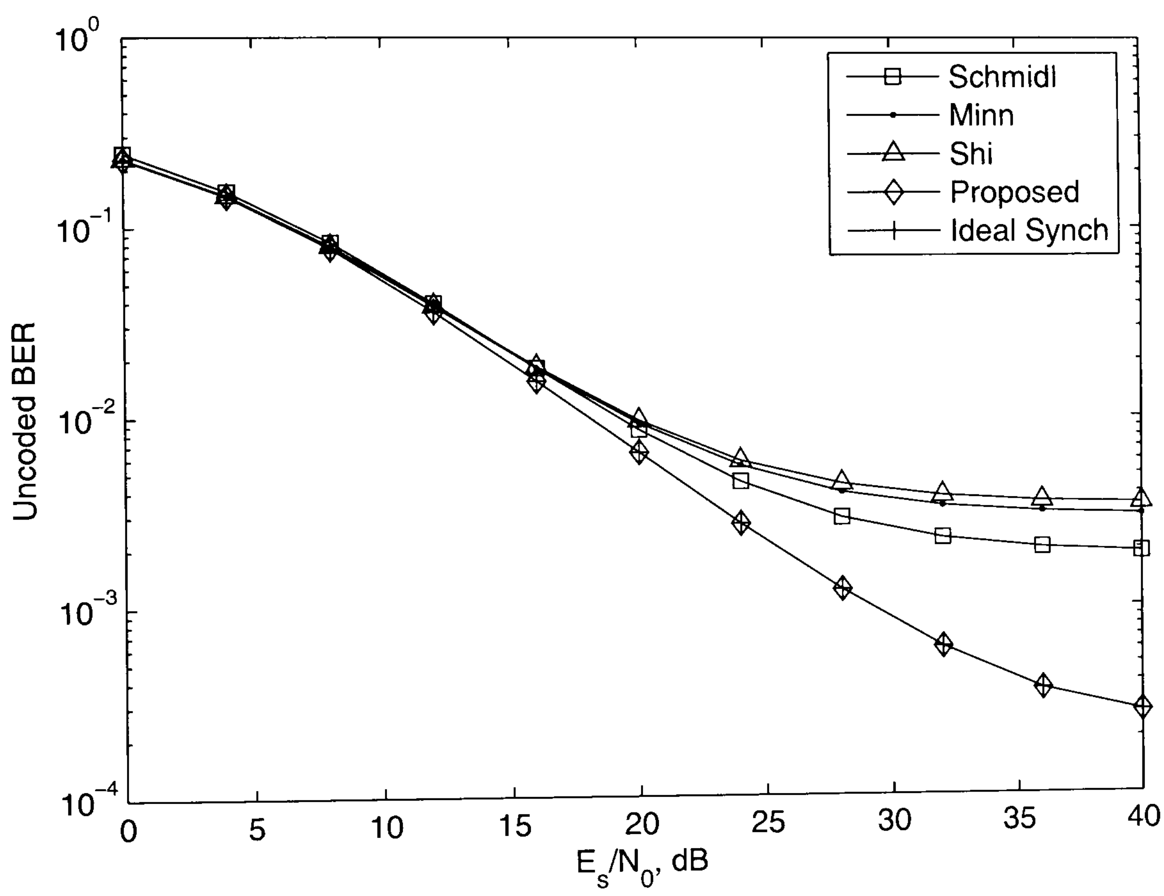

Figure 5.15: BER for the estimators in an ISI channel; *N*=256

As discussed in [89], timing MSE is not sufficient for determining the performance of a timing estimator in a CP-based OFDM system. This is because OFDM exhibits tolerance to timing errors within the ISI-free region as explained in section 5.3. Consequently, the uncoded BER performance of the timing estimators is shown in Figure 5.15, wherein the proposed method is seen to achieve the same performance as an ideal time-synchronized OFDM system. This means that the SNR degradation due to imperfect timing synchronization by the existing methods can now be fully recovered using a low-complexity technique. The error floor noticed in the ideal synchronization curve is due to the imperfect channel estimation technique implemented.

Despite its large timing MSE, Schmidl's method (with 90% averaging) achieves a better uncoded BER than the methods proposed by Minn and Shi in strong ISI channels. This is because Schmidl's timing estimates are biased towards the middle of the cyclic prefix as shown in Figure 5.14 and will still achieve a good BER performance provided they fall into the ISI-free region [86]. In contrast, Minn's and Shi's methods produce timing estimates which are biased towards the strongest time-varying channel tap as shown in Figure 5.14 and cannot achieve the ideal performance since such estimates will cause an overlap between copies of the current symbol and those of the succeeding OFDM symbol. Consequently, Minn's method requires preamble-based channel impulse response estimation while Shi's method requires the use of a cyclic postfix to solve this problem. Such extrinsic solutions constitute significant extra overhead and are not required by the proposed method.

5.7 Conclusions

In this chapter, we have reviewed the importance of timing synchronization in the OFDM receiver and discussed existing preamble-aided methods for frame/symbol timing in OFDM systems. It was shown that the cross-correlation approach is able to provide sharper timing detection than autocorrelation techniques in an ISI channel, although it encounters the challenge of degraded performance in the presence of a repetitive preamble structure and/or large frequency offsets.

In order to improve timing performance, a novel low-complexity technique which combines the advantages of autocorrelation and cross-correlation is proposed using a simple and conventional preamble structure with two identical parts. The method was compared with popular existing methods for OFDM timing synchronization in AWGN and Rayleigh fading multipath channels and computer simulation results for timing MSE and timing bias show that the proposed method achieves a superior performance to the existing methods, wherein its timing MSE and bias both approach the ideal value of zero. The proposed method is also shown to achieve the same BER as an ideal time-synchronized OFDM system which is not achievable by existing methods of comparable complexity and/or overhead. This means that the SNR degradation due to imperfect timing can now be fully recovered with a low complexity technique, leading to greater power-efficiency in OFDM systems.

Table 5.1: Summary table of improvement achieved by proposed method

Estimator	**Timing MSE (samples^2)** SNR=4dB	**Timing Bias (samples)** SNR=4dB
Proposed	0.29	0.21
Schmidl	41.68	-4.92
Minn	10.97	2.76
Shi	12.77	2.97

Table 5.1 summarizes the improvement achieved by the proposed OFDM timing algorithm over existing techniques in the tested multipath fading scenario. This improvement in timing estimation is achieved without compromising the repetitive

structure needed in the preamble to achieve reliable frequency offset estimation using standard available techniques. Consequently, robust timing and reliable frequency estimation are achieved with a minimum overhead of just one OFDM training symbol whose structure is compatible with commercial wireless network standards such as WiFi and WiMAX

Chapter 6

6 Time-Frequency Synchronization for OFDM Systems

6.1 Introduction

The previous chapter introduced OFDM modulation and its signal model in a wideband (ISI) channel. The importance of frame/symbol timing synchronization in the OFDM receiver and existing timing synchronization techniques were discussed and a novel low-complexity technique proposed to significantly enhance timing estimation accuracy. In this chapter, we focus on preamble-aided techniques for combined timing and frequency synchronization in OFDM systems using a minimum preamble overhead and optimising important parameters such as computational complexity, processing delay, estimation accuracy and estimation range. OFDM is very sensitive to carrier frequency offsets in the received signal due to its orthogonality requirements. Such frequency offsets may be caused by Doppler shifts and/or instabilities in the local oscillator (LO) and result in a shift in the OFDM subcarrier frequencies, which means that the subcarriers lose their orthogonality, thereby leading to inter-carrier interference (ICI). Consequently, it is usually required to reduce the frequency errors to a small fraction of the subcarrier spacing [34]. It is noted that consumer-grade crystal oscillators usually have a limit on the frequency accuracy they can provide. Assuming a 10ppm (parts per million) crystal operating in a WiMAX OFDM system of 5GHz carrier frequency, 1.25MHz bandwidth and 256-point FFT [89], the offset due to oscillator instabilities can be up to 10 subcarrier spacings. Therefore, in practice, the frequency offset can be many times the subcarrier spacing.

In addition to the importance of timing synchronization as established in the previous chapter, it is clear that frequency synchronization also constitutes a vital part of the OFDM receiver design in terms of accuracy and also estimation range. Various techniques have been proposed in the literature for OFDM carrier frequency synchronization but the data-aided approach is discussed in this thesis as the use of preambles is necessary for frame/symbol timing detection in burst-mode applications such as in the current wireless networks (e.g. WiFi [24] and WiMAX [25]).

Schmidl and Cox [86] proposed using the autocorrelation of a training symbol with two identical parts to estimate timing and fractional frequency offset with an estimation range of ± 1 subcarrier spacing. An additional training symbol is then used along with the first to determine the integer frequency offset in a range of $\pm N/2$ subcarrier spacings, where N is the FFT size. However, Schmidl's algorithm can yield timing estimates which are well beyond the ISI-free region, thus leading to degradation in the decoder error rate [33]. Morelli's method [107] uses one training symbol with l identical parts to achieve an improved frequency estimation, wherein the estimation range is $\pm l/2$ subcarrier spacings. Although it improves on the overhead efficiency of Schmidl's method, it uses the same error-prone timing approach as Schmidl's and its estimation range still falls far below the theoretical limit of $\pm N/2$ subcarrier spacings. Kim [108] proposed a similar method to Schmidl's, but using only its first training symbol with two identical parts to achieve both fractional and integer frequency estimation in a range of $\pm N/2$ subcarrier spacings. The method is efficient in preamble overhead but also suffers from the inaccuracies of Schmidl's timing algorithm. Other preamble-aided techniques have been proposed for OFDM timing and/or frequency synchronization in [97]-[105] and [109]-[113]. However, they suffer from various drawbacks in fading ISI channels such as limited frequency estimation range, poor timing accuracy and/or poor frequency accuracy.

In order to jointly solve the problems of timing and frequency synchronization in OFDM systems with minimum preamble overhead, such as to achieve a BER similar to that of an ideal time-frequency-synchronized system, we propose a novel low-complexity method based on autocorrelation, restricted cross-correlation and threshold-based time-frequency detection. This method uses only one training symbol, having a simple and conventional structure, to achieve robust, reliable and full-range time-frequency synchronization in OFDM systems. Consequently, OFDM receivers will be able to operate at lower SNR, since the degradation that was previously experienced due to imperfect timing and/or frequency synchronization using existing techniques can now be eliminated. Furthermore, the wide range frequency estimation achieved provides for cheaper OFDM receivers which incorporate low-grade oscillators, since they will be able to operate under larger frequency offsets.

6.2 Existing Techniques for Time-Frequency Synchronization

In this section, some popular preamble-aided techniques for combined timing and wide-range frequency synchronization in OFDM are discussed. Carrier frequency offset estimation in OFDM systems is usually achieved based on an estimate of the symbol timing. This means that the frequency estimation stage is generally preceded a suitable timing algorithm as illustrated in the synchronization block diagram of Figure 5.3. The most reliable techniques for fractional frequency synchronization in OFDM systems use identical blocks in the preamble, wherein each block is longer than the channel impulse response. This is because the recieved block patterns remain identical after passing through an ISI channel except for a phase shift introduced by the frequency offset, wherein such phase shift is proportional to the frequency offset.

6.2.1 Schmidl's Method

The training symbol with two identical parts (S_{Sch}) proposed by Schmidl [86] for timing estimation as discussed in section 5.4.2 is also used for carrier frequency recovery. However, its estimation range is ± 1 subcarrier spacing (i.e. $-1 \le \Delta f \le 1$). In order to successfully estimate frequency offsets which are beyond this range (i.e. $-N/2 \le \Delta f \le N/2$), Schmidl proposed using an additional training symbol with no repetitive structure (S_{Sch_2}), generated using PN sequences in the frequency domain as explained in [86]. In this scenario, the fractional frequency offset is estimated in the time-domain (pre-FFT) using the autocorrelation of Schmidl's first training symbol (P_{Sch}), after which the integer frequency offset is estimated in the frequency-domain (post-FFT data recovery) using a differential correlation between the two training symbols.

The fractional frequency offset is first computed by using the autocorrelation-based estimator proposed by Lank and Reed [71] for single frequency estimation over the identical halves of the first training symbol as shown in (6.1), based on the reasoning that these two halves will remain identical even after passing through an ISI channel [33],[86]. The fractional offset is then corrected in the received signal as shown in (6.2). Thus, the residual frequency offset becomes an integer multiple of 2, which means that the integer search window is reduced by half.

$$\Delta\hat{f}_f = \frac{1}{\pi}\angle\left\{P_{Sch}\left(\hat{d}\right)\right\} = \frac{1}{\pi}\angle\left\{\sum_{k=0}^{N/2-1} r^*\left(\hat{d}+k\right) r\left(\hat{d}+k+N/2\right)\right\} \tag{6.1}$$

$$r_{cor}(k) = r(k)e^{-j2\pi k\Delta\hat{f}_f/N} \tag{6.2}$$

where $\hat{d}$ is the timing estimate from Schmidl's timing algorithm, $\Delta\hat{f}_f$ is the fractional frequency offset estimate and $r_{cor}(k)$ is the fractional-frequency-corrected signal sample.

The integer frequency offset is computed after taking the FFT of the two training symbols (S_{Sch} and S_{Sch_2}) using the fractional-frequency-corrected received signal and Schmidl's timing estimate as shown in (6.3)-(6.5). By correcting the fractional frequency offset, inter-carrier interference (ICI) can be avoided and the residual integer frequency offset has the effect of displacing data into a wrong subcarrier bin, proportional to the amount of integer offset.

$$V_n = \sqrt{2}\, X_{2,2n} / X_{1,2n} \tag{6.3}$$

$$B_{Sch}(g) = \left\{ \frac{\left|\sum_{n\in H} Y_{1,2n+2g}^* V_n^* Y_{2,2n+2g}\right|}{2\left(\sum_{n\in H}\left|Y_{2,2n+2g}\right|^2\right)^2} \right\} \tag{6.4}$$

$$\Delta\hat{f}_i = 2 * \arg\max_g \{\, B_{Sch}(g) \,\} \tag{6.5}$$

where $\mathrm{H}=\{0,1,\ldots,N_{use}/2\}$, $g\in\{-N/4,\ldots,-1,0,1,\ldots,N/4\}$ and $n\in\mathrm{H}$. $X_{1,2n}$ and $X_{2,2n}$ represent the known PN sequences in the frequency-domain which are used to generate the two training symbols S_{Sch} and S_{Sch_2} respectively in the time-domain and V_n is a weighted differential between $X_{1,2n}$ and $X_{2,2n}$. $Y_{1,2n}$ and $Y_{2,2n}$ represent the FFTs of the received training symbols (fractional-frequency-corrected) as determined by the symbol timing estimate. $\Delta\hat{f}_i$ is the integer frequency offset estimate determined at the peak of the integer timing metric $B_{Sch}(g)$.

The timing estimate produced by Schmidl's timing algorithm is used for both stages of frequency recovery despite the errors associated with it [86]. This is due to the fact that the autocorrelation in (6.1) and the differential correlation in (6.4) are performed over a relatively large number of samples when compared with the standard deviation of the timing errors. Consequently, reliable frequency estimation is achievable by Schmidl's method despite its coarse timing estimate [86].

6.2.2 Morelli's Method

The method proposed by Morelli and Mengali [107] uses one training symbol with with l 'similarly signed' identical parts in the time-domain, wherein timing estimation can be achieved by using Schmidl's timing algorithm when the number of identical parts is even. Its frequency estimation uses a similar concept to the method earlier proposed by both authors for single frequency estimation [64], except that the autocorrelation is now taken over identical blocks and not every sample. The carrier frequency offset is computed as follows:

$$\Delta\hat{f} = \frac{l}{2\pi}\sum_{m=1}^{J} w(m)\angle\left\{R(m)R^{*}(m-1)\right\}; \qquad 1 \le m \le J \tag{6.6}$$

$$R(m) = \frac{1}{N-m\mathrm{M}}\sum_{k=mM}^{N-1} r\left(\hat{d}+k\right)r^{*}\left(\hat{d}+k-m\mathrm{M}\right); \qquad 0 \le m \le J \tag{6.7}$$

$$w_m \triangleq \frac{3(l-m)(l-m+1)-J(N-J)}{J\left(4J^2-6Jl+3l^2-1\right)} \tag{6.8}$$

where $R(m)$ represents the autocorrelation between the repeated segments, each consisting of $\mathrm{M} = N/l$ samples, w_m defines the BLUE weighting factors for optimal linear combination and J is a design parameter whose optimal value is $l/2$ [107].

By using the best linear unbiased estimation principle over many segments ($l > 2$), Morelli's method is able to achieve an improved frequency estimation accuracy compared to Schmidl's method. Also, it has a wide estimation range is given as $-l/2 \le \Delta f \le l/2$ in [107]. However, there is a limitation on the number of identical parts that can be used in the training symbol since each identical part should be as long as the channel delay spread in order to avoid the degradation caused by ISI. Hence, Morelli's method is unable to achieve full-range frequency estimation (i.e. $-N/2 \le \Delta f \le N/2$) in contrast to Schmidl's method, as in practice, $l << N$.

Minn's method [94] proposes to use Morelli's algorithm with a 'signed' training symbol for carrier frequency synchronization. However, since Minn's training symbol does not consist of 'similarly signed' identical parts, the ISI in the channel will degrade its frequency estimation performance. The same applies to Kasparis' method [93] wherein the identical structure in its training symbol is destroyed by multiplying it with a binary PN sequence in the time-domain.

6.2.3 Kim's Method

In [108], Kim proposed a method which uses Schmidl's first training symbol with two identical parts (S_{Sch}) to achieve full-range carrier frequency recovery (i.e. $-N/2 \le \Delta f \le N/2$). Timing and fractional frequency estimation are achieved using the same algorithms proposed by Schmidl [86]. However, Kim's method uses only one training symbol for integer frequency estimation, in contrast to the two symbols required by Schmidl's method. After the fractional frequency offset is corrected, integer frequency offset estimation is achieved in the frequency-domain (post-FFT data recovery) using a differential cross-correlation of the training symbol. The integer frequency offset is computed as follows:

$$\overline{V}_n = X_{1,2n} / X_{1,2n+2} \tag{6.9}$$

$$B_{Kim}(g) = \left\{ \frac{\left| \sum_{n\in \mathrm{H}} Y^*_{1,2n+2g+2} \overline{V}_n^* Y_{1,2n+2g} \right|}{\left(\sum_{n\in \mathrm{H}} \left| Y_{1,2n+2g} \right|^2 \right)^2} \right\} \tag{6.10}$$

$$\Delta\hat{f}_i = 2 * \arg\max_g \{ B_{Kim}(g) \} \tag{6.11}$$

where $\mathrm{H} = \{0,1,\ldots,N_{use}/2\}$, $g \in \{-N/4, \ldots, -1,0,1,\ldots,N/4\}$ and $n \in \mathrm{H}$. $X_{1,2n}$ represents the known PN sequence in the frequency-domain which is used to generate the training symbol S_{Sch} in the time-domain and $\overline{V}_n$ is a differential of $X_{1,2n}$. $Y_{1,2n}$ represents the FFT of the received training symbol (fractional-frequency-corrected). $\Delta\hat{f}_i$ is the integer frequency offset estimate determined at the peak of the integer timing metric $B_{Kim}(g)$.

It should be noted that Kim's method has a better overhead efficiency than Schmidl's method for carrier frequency recovery since it uses only one training symbol in contrast to the two required by the latter.

6.2.4 Fractional Frequency Synchronization Performance

Computer simulations were run in order to verify the performance of the existing methods for OFDM fractional frequency estimation. The performance of the full-range time-frequency estimation will be evaluated later in comparison with our proposed method. QPSK sub-carrier modulation is used and the received signal is given an initial frequency offset of Δf = -0.45. Figure 6.1 shows the normalized frequency mean-square-error (MSE) of the estimators in the test ISI channel specified in section 5.4.1, wherein the CRLB for the AWGN channel is also shown for comparison. It can be seen that Morelli's method with a training symbol consisting of l=8 identical parts achieves a slightly better accuracy than Schmidl's method (which is also equivalent to Morelli's method with l=2 [107]). Although both methods do not achieve the CRLB for single frequency estimation in the AWGN channel based on a data record of N samples as defined in chapter 3, their performance is nonetheless sufficient for the requirements of frequency synchronization in OFDM as discussed in [34]. This is also confirmed in BER results shown later.

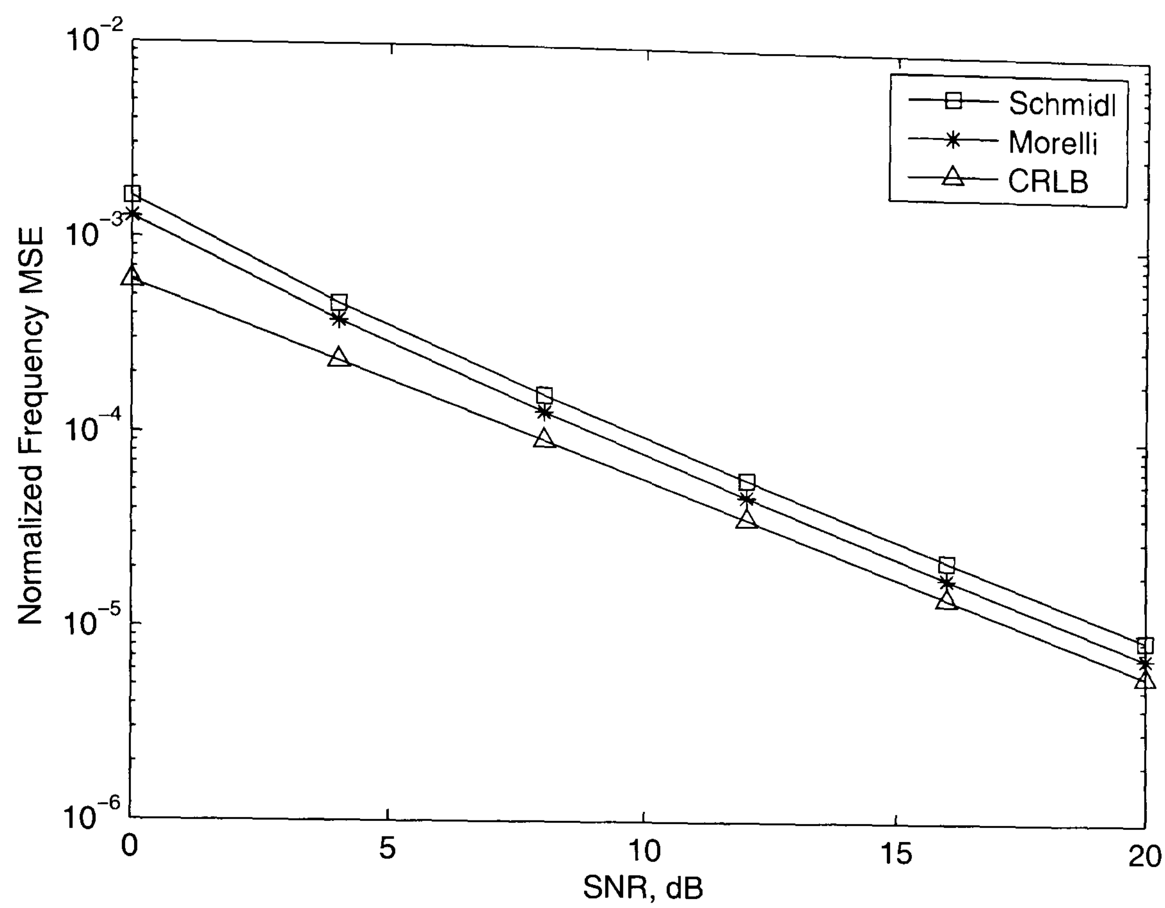

Figure 6.1: Fractional frequency MSE for the estimators; N=256

6.3 Robust and Efficient Time-Frequency Recovery for OFDM

6.3.1 Introduction

In this section, a robust and efficient technique for frame/symbol timing and carrier frequency recovery in OFDM systems is proposed. It uses a simple and conventional preamble structure, consisting of only one training symbol, to achieve near-ideal timing accuracy and full-range carrier frequency recovery. Figure 6.2 shows a block diagram of the proposed method wherein coarse timing and fractional frequency estimation are first achieved in similar fashion to Figure 5.3. These are then followed by the timing checkpoint, joint 'timing and integer frequency' and fine timing estimation stages respectively. All the processing operations are performed using time-domain samples without the need for post-FFT subcarrier data recovery. Hence, the training symbol can be designed using optimized sequences in either the time-domain (TD) or frequency-domain (FD).

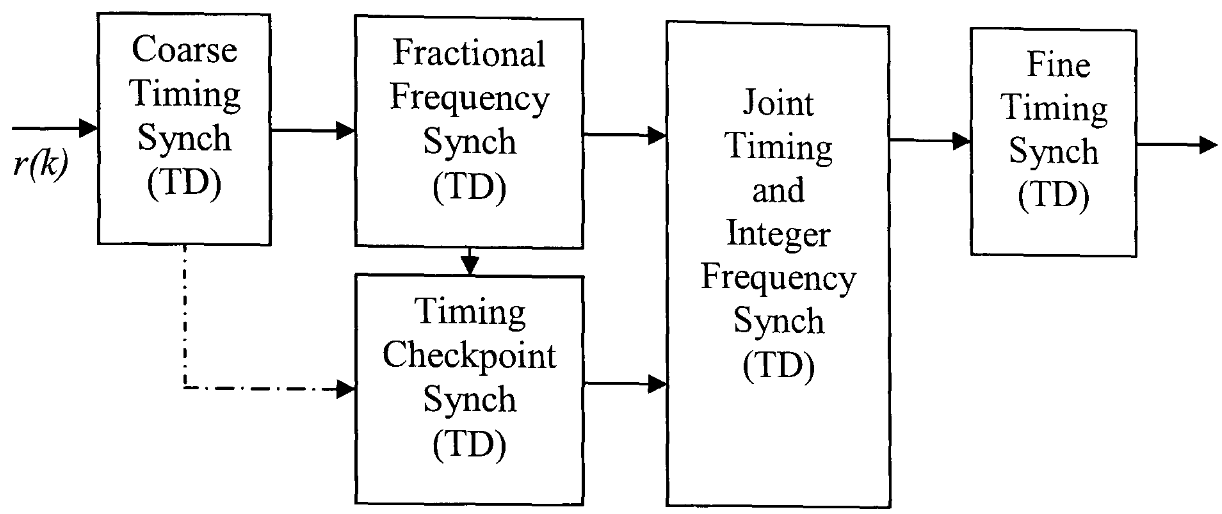

Figure 6.2: Block diagram of synchronization stages in the proposed method

6.3.2 Cross-correlation Time-Frequency Detection in ISI Channels

The usefulness of cross-correlation for timing detection in ISI channels has been discussed in the previous chapter (section 5.5.2). This concept is now extended to time-frequency detection in ISI channels. It can easily be deduced from (5.22)-(5.24) that even in an ISI channel, cross-correlation is able to achieve joint timing and frequency detection due to the coherent summation in (5.23), produced at timing instants that correspond to the arrival of a known random sequence $S(k)$ via the channel taps i.e. $h(0), h(1), \ldots, h(L-1)$ in the absence of significant frequency offsets. The cross-correlation at all other timing instants will be lacking in the coherent part due to non-existent channel taps. Also, the presence of significant frequency offsets will destroy the coherence in (5.23). For instance, assuming $S(k)$ has constant amplitude, the coherent summation in (5.23) reduces to zero for integer frequency offsets since the sum of a sinusoid over an integer number of full cycles is zero as shown below:

$$\sum_{k=0}^{N-1} e^{j2\pi\Delta f k/N} = 0; \qquad \Delta f \in (-N/2,\cdots,-1,0,1,\cdots,N/2), \;\; \Delta f \neq 0 \tag{6.12}$$

Therefore a known random sequence (having sharp autocorrelation) can be used to achieve robust joint timing and integer frequency estimation via the sharp detection properties of cross-correlation.

Assuming the central limit theorem (CLT) holds and sufficient frequency synchronization is achieved, the cross-correlation $P_x(d)$ at all other timing instants apart from those corresponding to the channel paths (i.e. $\forall d \notin \{d_{ideal}, d_{ideal}+1,\cdots,d_{ideal}+L-1\}$) can be taken to be a zero-mean complex Gaussian variable. Using the same CLT principle and assuming a timing instant that corresponds to the arrival of a channel path, the cross-correlation $P_x(\Delta f)$ at all other integer frequency corrections apart from that corresponding to the actual integer frequency offset correction can be taken to be a zero-mean complex Gaussian variable. This implies that the absolute value of the cross-correlation at the non-coherent instants in either the timing axis (i.e. $P_x(d_{NC})$) or the frequency axis (i.e. $P_x(\Delta f_{NC})$) will follow a Rayleigh distribution with a similar set of statistics as those given in (5.25) and (5.26).

Consequently, a timing or frequency threshold can be chosen based on the analysis in (5.27) – (5.30) such that the absolute value of the cross-correlation at the correct timing and integer frequency instants exceed the chosen threshold while that of all other timing or integer frequency instants fall below such threshold with high probability. This threshold crossing detection technique applied to both timing and frequency axis is one of the key components of our proposed joint timing and integer frequency estimator, such that reliable and low-complexity time-frequency synchronization in OFDM systems can be achieved.

6.3.3 Training Symbol, Coarse Timing and Fractional Frequency

A training symbol S_{Sch} consisting of two identical parts in the time-domain is chosen as preamble for the proposed time-freqency technique in similar fashion to the novel method proposed for timing estimation in section 5.5. Its simple structure as shown in equation (5.4) is implemented in Schmidl's method and also compatible with current wireless network standards such as WiFi [24] and WiMAX [25]. Its autocorrelation property helps to achieve reliable and low-complexity coarse timing and fractional frequency estimation [86] while its uniquely combined autocorrelation and cross-correlation properties are used in our proposed method to achieve enhanced time-frequency estimation performance in OFDM systems. The training symbol can be generated via IFFT processing from the frequency-domain (FD) as explained in section 5.4.2 or directly in the time domain (TD) via direct repetition using a suitable PN sequence of length $N/2$.

The proposed time-frequency synchronization technique is a multi-stage procedure as illustrated in Fig. 6.2. Firstly, preamble detection and coarse timing estimation are achieved in similar fashion to the novel method proposed for improved OFDM timing estimation in chapter 5, wherein a low-complexity autocorrelation $P_{Sch}(d)$ of the received signal samples is computed as shown in (5.5) and a coarse timing estimate derived accordingly as shown in (5.31) and (5.32). Fractional frequency offset estimation is then achieved using the autocorrelation $P_{Sch}(\hat{d})$ as shown in (6.1) based on the coarse timing estimate which may be pre-advanced towards the middle of the cyclic prefix zone (i.e. $\hat{d} = \hat{d}_c - 0.5G$) in order to increase the probability of using fully identical parts in (6.1), as this helps to improve accuracy. Such pre-advancement is not applicable where a cyclic prefix is not used. The fractional frequency offset is corrected in the stored received signal samples as shown in (6.2). Consequently, the residual frequency offset becomes an integer multiple of 2 since the estimator in (6.1) has an estimation range of ± 1 subcarrier spacing.

6.3.4 Restricted Differential Cross-correlation (Timing Checkpoints)

After preamble detection and coarse timing, differential cross-correlation between the received signal samples and the known preamble S_{Sch} is computed using a restricted set of timing instants as indicated by a timing filter window derived from the autocorrelation timing metric M_c. Differential cross-correlation is used in order to cope with large frequency offsets (i.e. $\Delta f \geq 1$) as coherent cross-correlation will fail under this condition [93],[97]. However, differential cross-correlation is not as reliable as coherent cross-correlation for timing detection purposes because the extra terms it incorporates increase the overall noise variance. Nevertheless, cross-correlation techniques produce sharper detection properties than autocorrelation and in an ISI environment, differential cross-correlation between a received preamble and its known version (i.e. a random sequence having sharp autocorrelation) can be used to detect a set of likely timing instants corresponding to the arriving channel paths.

Figure 6.3 shows an example differential cross-correlation of the fractional-frequency-corrected received signal as implemented using (6.13)-(6.15) in the test scenario under ideal and ISI channel conditions, wherein there is a major peak in the middle corresponding to a full-symbol pattern match and two minor peaks at half-symbol timing error corresponding to a half-symbol pattern match. The minor peaks result from the symmetric structure of the preamble and constitute a major hindrance to using such preamble in a noisy channel since any of these peaks could instantaneously have the highest value.

$$U(d,\, k) = r_{cor}(d+k)\, S^{*}_{Sch}(k); \qquad k \in \{0,\, N-1\} \tag{6.13}$$

$$P_{dx}(d) = \sum_{k=0}^{N-2} U^{*}(d,\, k)\, U(d,\, k+1) \tag{6.14}$$

$$M_{dx}(d) = |\, P_{dx}(d)|^{2} \tag{6.15}$$

where r_{cor} is the fractional-frequency-corrected received signal and $U(d,k)$ represents the samples of r_{cor} at timing point d multiplied by its corresponding complex conjugate in the known preamble $S_{Sch}(k)$. $P_{dx}(d)$ is the differential cross-correlation and $M_{dx}(d)$ is the different cross-correlation metric.

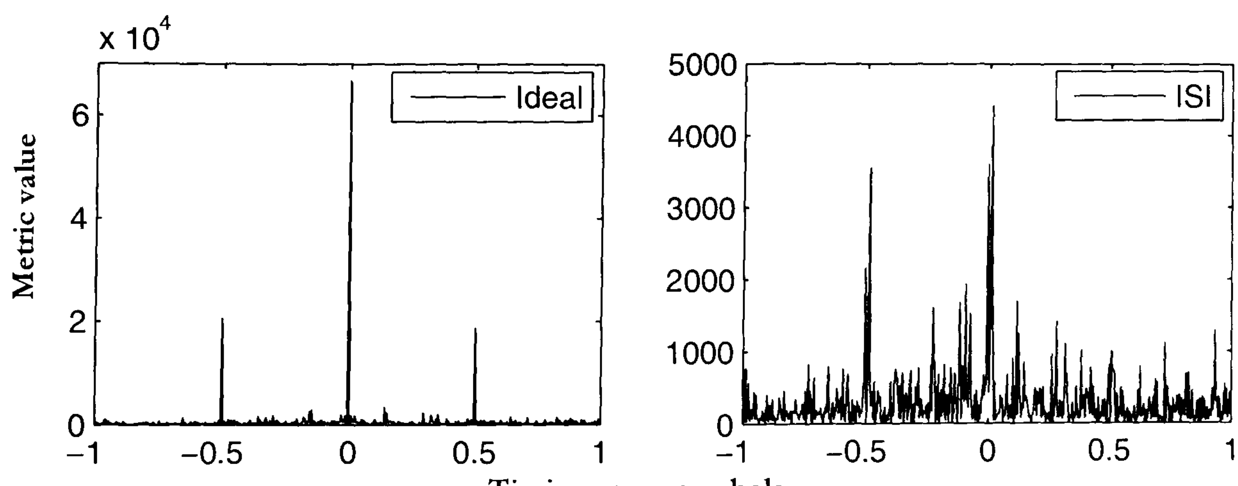

Figure 6.3: Differential cross-correlation metric (Eqn. 6.20) ; N=256

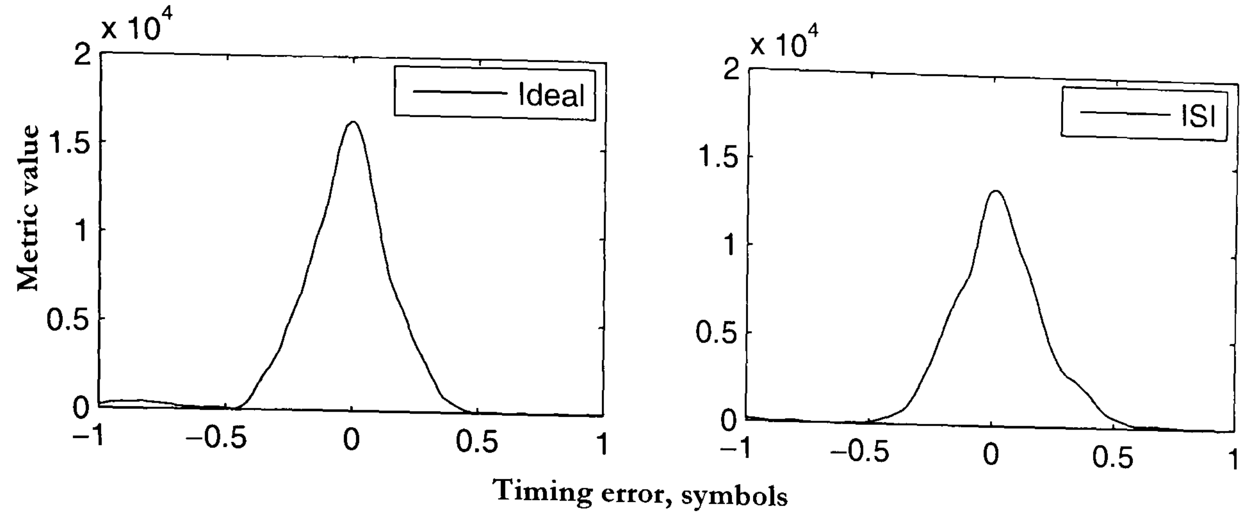

Figure 6.4: Autocorrelation metric (Eqn. 5.31); *N*=256

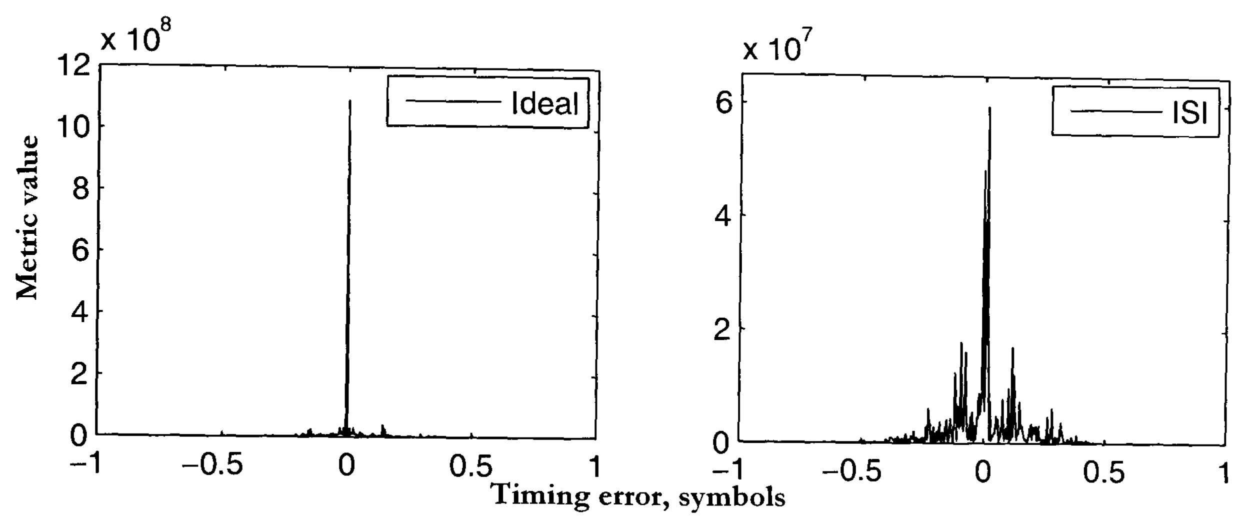

Figure 6.5: Filtered correlation metric (Eqn. 6.21); *N*=256

As previously discussed in chapter 5, the autocorrelation metric of the training symbol as shown in Figure 6.4 can be used to filter the unwanted minor peaks. One way to achieve this is to simply multiply both metrics together. This multiplication can be restricted to a timing window of one symbol length N, symmetric around the coarse timing estimate $\hat{d}_c$ in order to reduce complexity. An alternative approach which avoids multiplication is to use the autocorrelation peak value to define a timing window in terms of all timing points whose autocorrelation exceeds a pre-determined fraction of the peak value. This timing window is then used to restrict the differential cross-correlation accordingly. The filtering helps to determine a set of likely timing instants which correspond to the arriving channel paths. Figure 6.5 shows the resulting timing metric achieved by such filtering process.

The processing operations within the differential cross-correlation stage are summarised as follows:

$$M_{check}(d) = |P_{dx}(d)|^2 \cdot M_c(d)\,; \qquad d \in \left\{\hat{d}_c - N/2,\ \hat{d}_c + N/2\right\} \tag{6.16}$$

$$\hat{d}_{check} = \arg\max_{d} \left\{ M_{check}(d) \right\} \tag{6.17}$$

where $M_{check}(d)$ is the filtered timing-checkpoint metric computed for a restricted set of timing points and d is chosen in (6.16) to ensure that all relevant timing points that could be the ideal timing are tracked. $\hat{d}_{check}$ is the operational timing checkpoint, wherein all previously determined checkpoints are excluded from $M_{check}(d)$.

6.3.5 Restricted 2D/1D Cross-correlation (Joint Time-Frequency)

The next stage is an enhanced algorithm which can operate in the two dimensions (2D) of timing offset and frequency offset to jointly determine the best timing point and the integer frequency offset. This 2D estimator combines the strength of coherent cross-correlation for timing detection and for integer frequency detection as discussed in section 6.3.2. The fundamental concept is to use coherent cross-correlation over the frequency axis at the most probable timing instants (i.e timing checkpoints). This is done by correcting the received signal as indicated by each timing checkpoint, over all probable values of integer frequency offsets, before performing coherent cross-correlation with the known preamble. The peak value of the resulting 2D time-frequency metric indicates both the best timing point and the integer frequency offset.

The timing checkpoints are determined by sorting the filtered timing-checkpoint metric ($M_{check}(d)$) in descending order of strength. For each timing checkpoint starting from the strongest, the corresponding one-dimensional vector of N fractional-frequency-corrected samples undergoes coherent cross-correlation with the known preamble over all possibilities of integer frequency offset correction. This is computed efficiently by the use of the FFT algorithm [104] as shown in (6.18) which can either be implemented independently or via the existing FFT module in the OFDM receiver.

$$I\left(\hat{d}_{check}, i\right) = \left| FFT\left\{U\left(\hat{d}_{check}, k\right)\right\}\right|; \qquad k \in \{0, N-1\} \tag{6.18}$$

where $I\left(\hat{d}_{check}, i\right)$ is the 1D integer frequency offset metric at a timing checkpoint $\hat{d}_{check}$, determined using the fast Fourier transform (FFT).

The proposed 2D time-frequency estimator is adaptive in terms of complexity as it uses both threshold crossing (TC) and maximum value (MAX) detection criteria [106]. The TC criterion is implemented over the 1D integer frequency offset metric at each timing checkpoint while the MAX criterion is implemented over the complete 2D time-frequency metric. For each timing checkpoint starting from the strongest, the algorithm derives a 1D integer frequency offset metric according to

(6.18). This is illustrated in Figure 6.6 which shows the metric for both ideal and ISI channel conditions as specified in section 5.4.1.

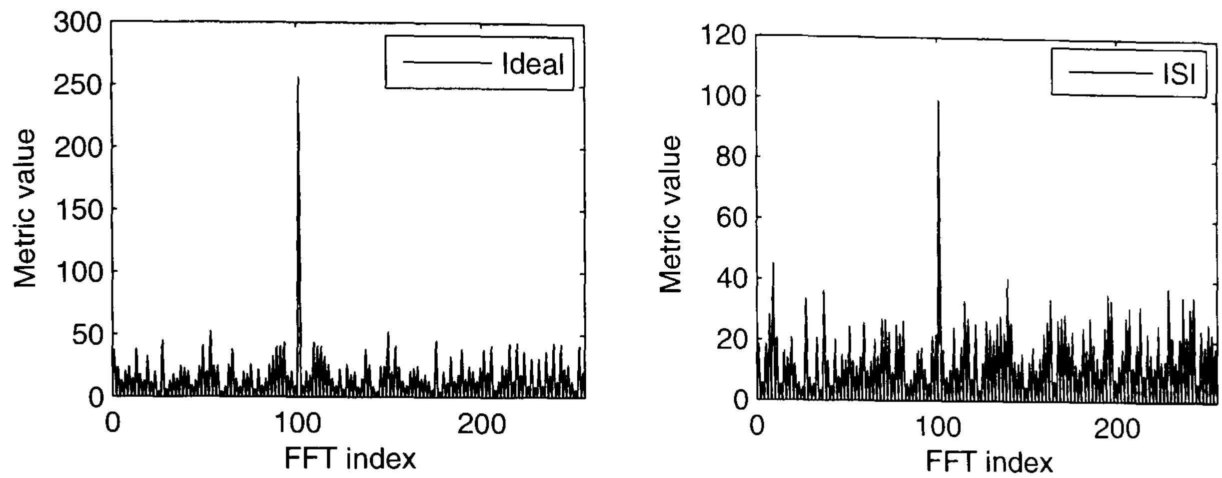

Figure 6.6: 1D integer frequency metric (Eqn. 6.23); N=256 and Δf =100

The peak value of the 1D metric at a timing checkpoint is compared with a threshold F_{th}. If this threshold is exceeded, a successful estimation is declared for both timing and integer frequency at that peak instant. Otherwise the next timing checkpoint is used and the process repeated until there is either success or the complete 2D time-frequency metric is formed and its maximum value determined as the successful estimate. This is implemented as follows:

$$\Delta\hat{f}_i = \hat{i} = \arg\max_{i}\left\{I\left(\hat{d}_{check}, i\right)\right\} \tag{6.19}$$

$$\hat{d}_{opt} = \arg\max_{d_{check}}\left\{I\left(\hat{d}_{check}, i\right)\right\} \tag{6.20}$$

where $\Delta\hat{f}_i$ is the integer frequency offset estimate and $\hat{d}_{opt}$ is the timing estimate which corresponds to a strong arriving channel path. $I\left(\hat{d}_{check}, i\right)$ is either the 1D integer frequency offset metric at any timing checkpoint where the TC criterion indicates successful estimation or the complete 2D time-frequency metric wherein all timing checkpoints have been tested and the MAX criterion used.

The threshold F_{th} determined based on the statistics of coherent cross-correlation as explained in section 6.3.2 and 5.5.2 is given as:

$$F_{th} = \sqrt{-(4/\pi)\ell n(\mathrm{P}_{FA})}\ \underset{i \neq \hat{i}}{mean}\left(I\left(\hat{d}_{check}, i\right)\right) \tag{6.21}$$

where P_{FA} is the designed probability of false alarm. This probability must be low enough to avoid a synchronization failure since a missed detection can still be recovered via the MAX criterion of the 2D metric. It should be noted that P_{FA} is dependent on the FFT size. Based on extensive simulations, a value of $\mathrm{P}_{FA} = 10^{-8}$ is chosen for N=256 and $\mathrm{P}_{FA} = 10^{-9}$ for N=1024.

The maximum number of timing checkpoints ($n_{checkpoints}$) needed for reliable joint time-frequency estimation is inversely proportional to the FFT size and the SNR since these parameters directly affect the accuracy of cross-correlation. Nonetheless, for a small FFT size, an increase in $n_{checkpoints}$ is balanced out by the reduction in computational complexity since N is small. Ultimately, the pre-determined design value to be used depends on the tolerable processing delay for synchronization. Based on extensive simulations, the following range is recommended, without loss of generality.

$$1 \leq n_{checkpoints} \leq 64 \tag{6.22}$$

It is noted that under favourable channel conditions, the first timing checkpoint is usually sufficient to achieve reliable synchronization. After estimating the integer frequency offset, compensation is made for the total frequency offset in the received signal as follows:

$$r_{corT}(k) = r_{cor}(k) e^{-j2\pi k \Delta\hat{f}_i / N} = r(k) e^{-j2\pi k \Delta\hat{f}_T / N} \tag{6.23}$$

$$\Delta\hat{f}_T = \Delta\hat{f}_i + \Delta\hat{f}_f \tag{6.24}$$

where $\Delta\hat{f}_T$ is the total frequency offset and r_{corT} is the total-frequency-corrected received signal sample.

6.3.6 Restricted Cross-correlation (Fine Timing)

In order to adjust the timing estimate to the ideal start of frame which corresponds to the first arriving channel path with significant strength (rather than the strongest or any other arriving channel tap path as determined by the joint time-frequency algorithm), a modified version of the timing adjustment technique proposed in chapter 5 is used, since $\hat{d}_{opt}$ has already been determined via the 2D/1D time-frequency algorithm. The processing operations within the final coherent cross-correlation stage are summarised as follows:

$$P_x(d) = \sum_{k=0}^{N-1} r_{corT}(d+k)\ S^*_{Sch}(k); \qquad d \in \left\{\hat{d}_{opt} - N/2 + \lambda + 1,\ \hat{d}_{opt}\right\} \tag{6.25}$$

$$\hat{d}_{FFT} = \arg \underset{d}{first} \left\{ |P_x(d)| > T_{th} \right\}; \qquad d \in \left\{ \hat{d}_{opt} - \lambda, \hat{d}_{opt} \right\} \tag{6.26}$$

$$T_{th} = \alpha \cdot \left(\underset{d}{mean} \left\{ |P_x(d)| \right\} \right); \qquad d \in \left\{ \hat{d}_{opt} - N/2 + \lambda + 1, \hat{d}_{opt} - \lambda - 1 \right\} \tag{6.27}$$

where d is chosen in (6.25) to ensure that all relevant timing points that could be the ideal timing are tracked. d is chosen in (6.26) such as to track the first arriving path ($\hat{d}_{FFT}$) which rather any strong arriving path ($\hat{d}_{opt}$), wherein all channel paths are expected to be received within $\lambda + 1$ samples: ($L - 1 \leq \lambda \leq G$). In (6.27), d is chosen such as to exclude major and minor coherent peaks and their multipath, in order to calculate a threshold T_{th} using the mean correlation of the non-coherent timing points as explained in section 5.5.2. P_{FA} is probability of false alarm (for which a non-coherent correlation peak exceeds the threshold) and $\alpha = \sqrt{-(4/\pi)\ell n(P_{FA})}$. The first arriving channel path (or any other one) is expected to have a correlation which is greater than T_{th} with high probability. Deriving from extensive simulations, P_{FA} is chosen as 10^{-6} for timing adjustment purposes. The threshold T_{th} is used to detect the ideal timing $\hat{d}_{FFT}$.

6.4 Computer Simulations

Extensive computer simulations were run in order to assess the performance of the proposed method in comparison to the existing methods for time-frequency synchronization in OFDM. Coherent QPSK sub-carrier modulation is used in all tested scenarios with a random normalized frequency offset uniformly distributed in the range $-N/2 < \Delta f < N/2$. Morelli's method [107] is not included in this section because its frequency estimation range falls far below the tested range. The expected delay spread is set to $\lambda = G$ for the proposed method.

6.4.1 Test case A: Terrestrial

The results of Figure 6.7 – 6.10 were produced based on a terrestrial WiMAX OFDM system in the Rayleigh fading ISI channel specified in section 5.4.1. These results compare the performance of the proposed method with existing methods in terms of timing MSE, frequency MSE and bit-error-rate (BER). The CRLB for single frequency estimation in the AWGN channel (discussed in chapter 3) is included in Figure 6.8 and 6.9 for comparison purposes. For the uncoded BER results of Figure 6.10, a synchronization symbol and a data symbol are incorporated into the transmitted frame. 51 evenly-spaced frequency domain pilots are inserted into the data symbol for the purpose of channel estimation and equalization via linear interpolation. In order to keep the simulation model generic, no error control coding is used.

In Figure 6.7, it is seen that the proposed method achieves a fractional timing MSE in similar fashion to the improved method proposed for timing estimation in chapter 5. This performance is significantly better than that of Schmidl's timing algorithm. Figure 6.8 shows that the proposed method is superior to Schmidl's frequency method in terms of integer frequency estimation accuracy, although Kim's method achieves the same performance in this scenario. However, when the number of used subcarriers is reduced from 256 to 200, Schmidl and Kim's method produce unreliable integer frequency estimates for large frequency offsets as shown in Figure 6.9 while the proposed method maintains a robust performance.

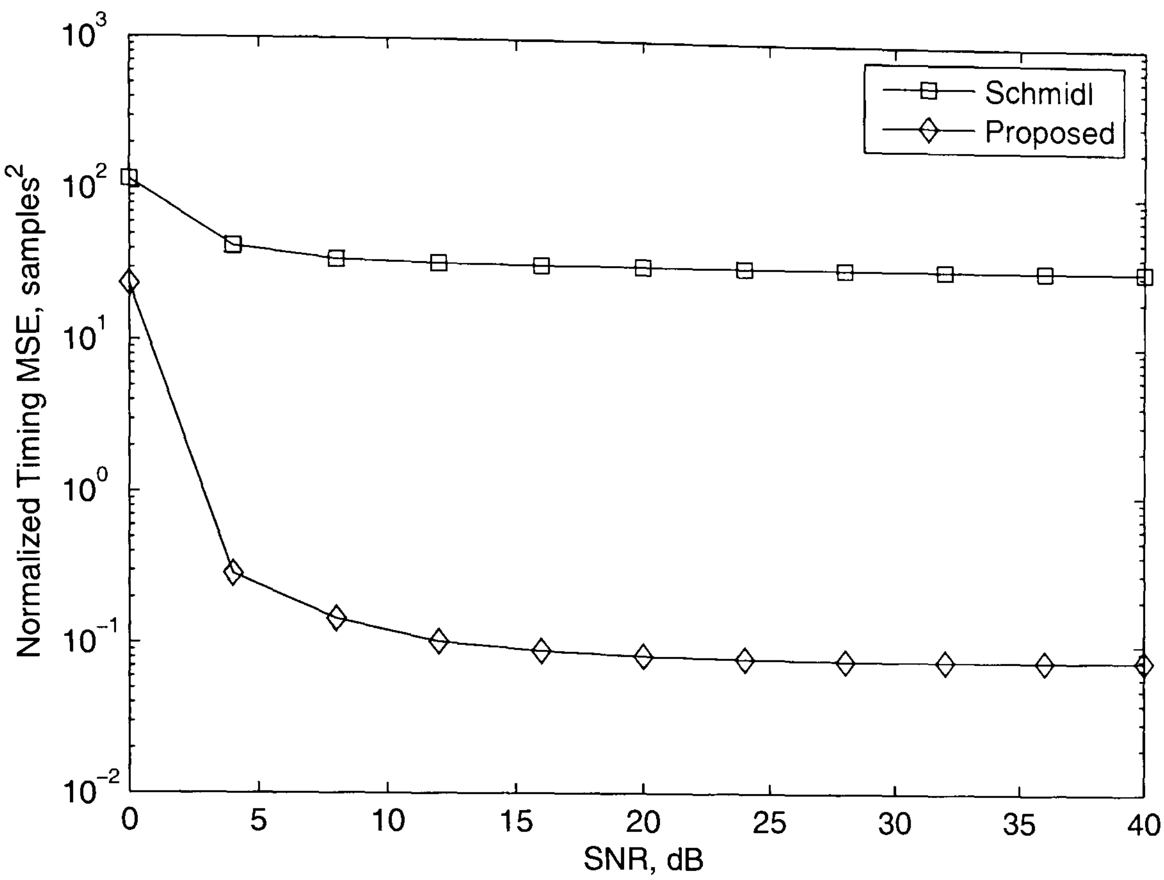

Figure 6.7: Timing MSE for the estimators; N=256

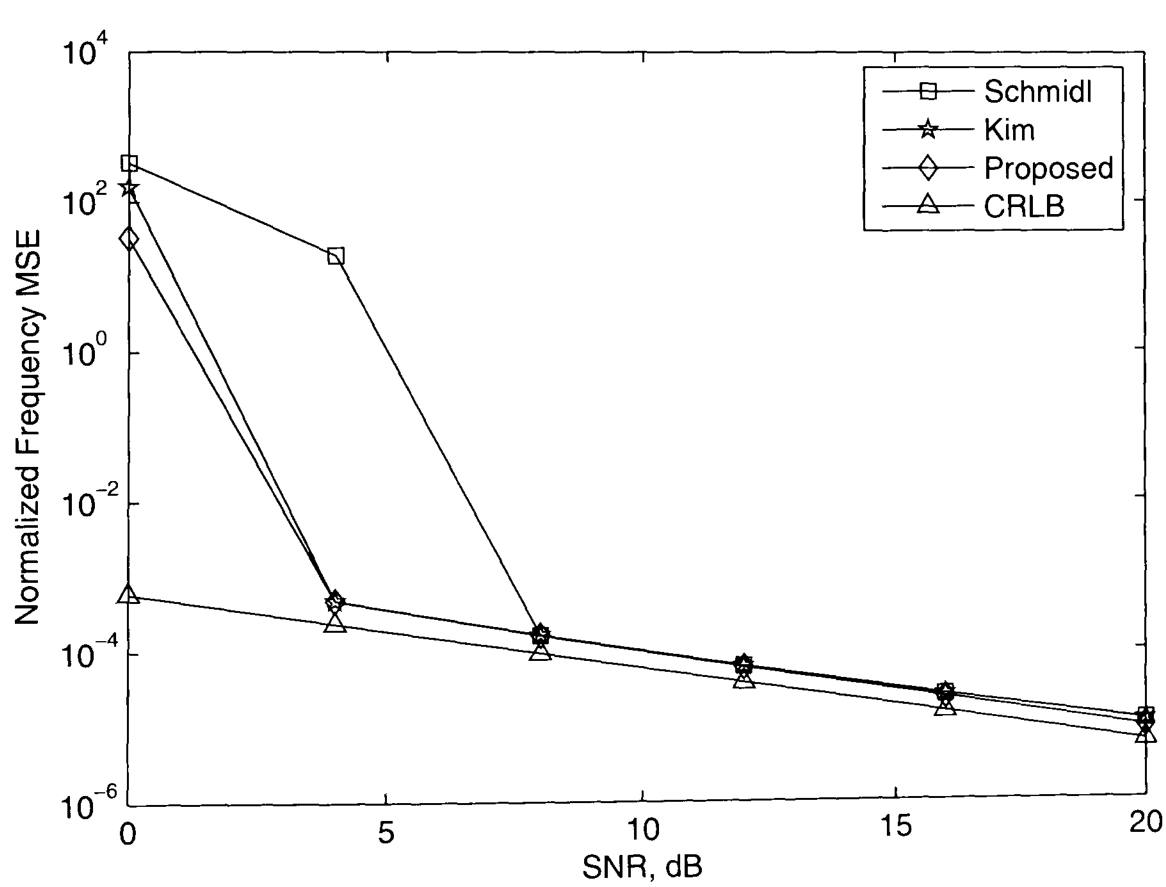

Figure 6.8: Frequency MSE for the estimators; N=256

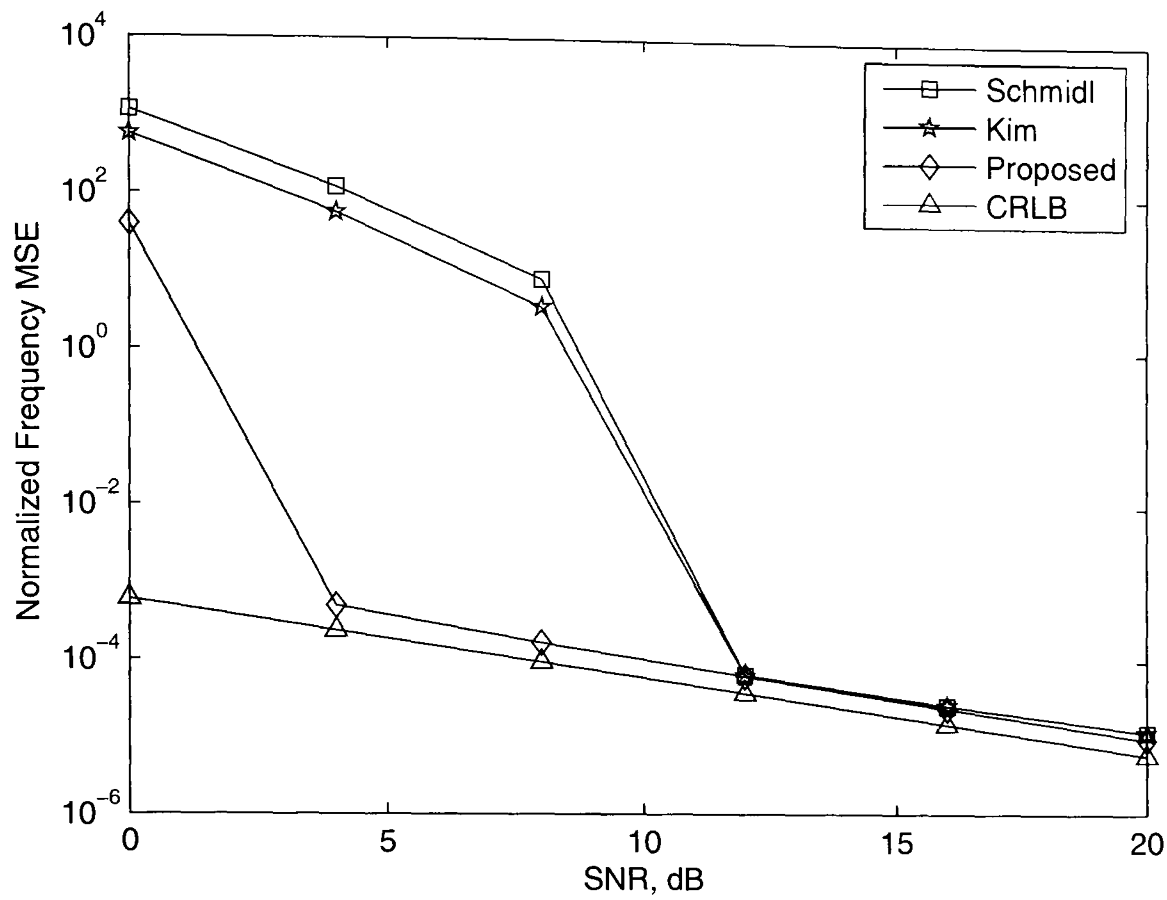

Figure 6.9: Frequency MSE for the estimators; N=256, N_{use}=200

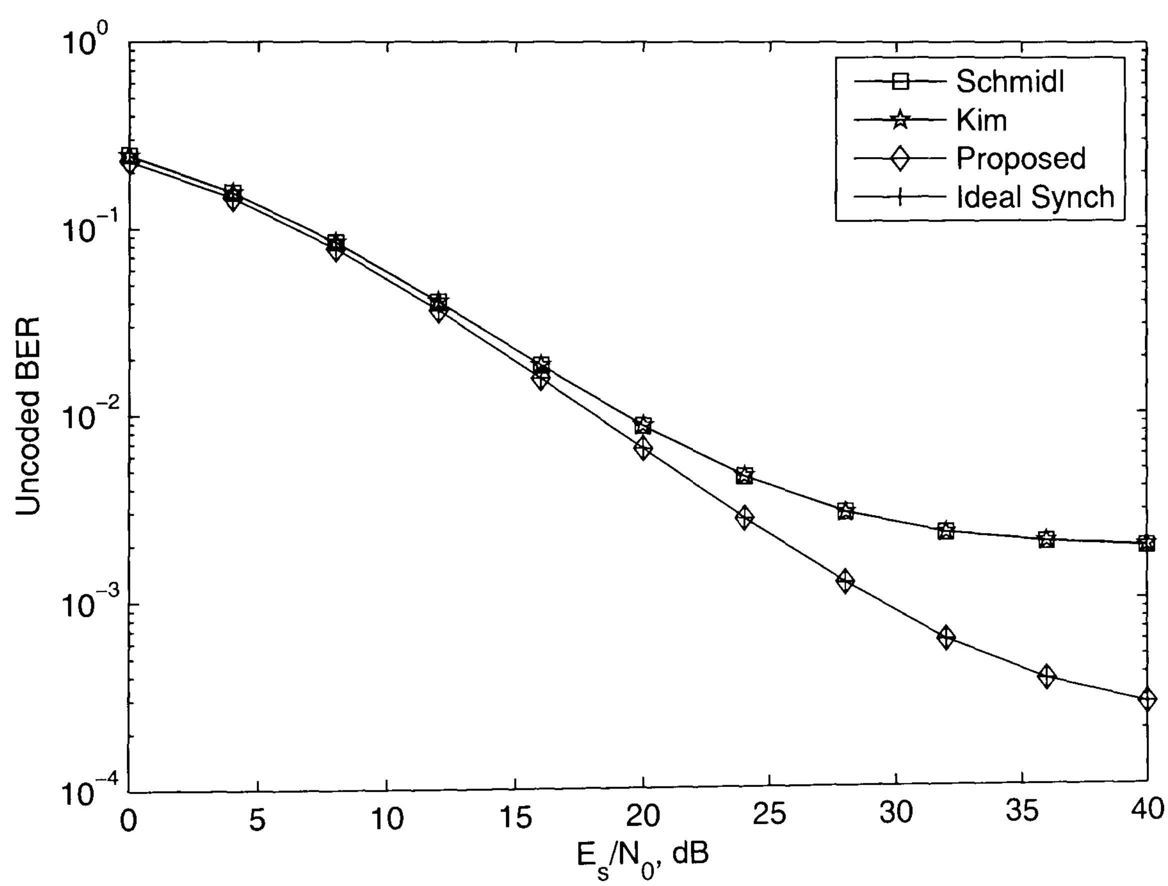

Figure 6.10: BER performance for the estimators; N=256

The uncoded BER results of Figure 6.10 confirm the robustness of the proposed method as it achieves the same decoder error rate as an ideal time-frequency-synchronized system in contrast to the existing methods. It is seen that Schmidl's and Kim's methods achieve a similar BER whose degradation is dominated by the poor performance of their timing algorithm. In terms of complexity, the proposed method is less computationally intensive than the existing ones for wide-range integer frequency estimation since its integer frequency metric is implemented efficiently using the FFT algorithm unlike the other methods. Table 6.1 shows the mean value of the actual number of timing checkpoints used in the joint time-frequency stage to achieve the BER results shown, where it can be deduced that the first timing checkpoint is usually sufficient to achieve successful estimation.

Table 6.1: Mean value of checkpoints used for successful estimation; *N*=256

SNR (dB)	4	8	12	16	20
Mean checkpoints	1.7502	1.1933	1.1048	1.0812	1.0700

6.4.2 Test case B: Satellite-Terrestrial Hybrid

The results of Figure 6.12 were produced using a validated link-level simulator developed under a collaborative research project between the University of Surrey, UK and ETRI, Korea in 2006 in order to assess the performance of timing and frequency synchronization algorithms within an overall OFDM-based S-UMTS downlink [114]. The block diagram of this simulator is as shown in Figure 6.11 and its OFDM signal parameters as specified in [114] were chosen based on a 3GPP feasibility study [115] with FFT/IFFT size: $N = 1024$, number of used subcarriers: $N_{use} = 705$, CP length: $G = 64$, symbol rate: $R_s = 6.528 Msym/s$ and carrier frequency: $f_c = 2GHz$. QPSK modulation is used for subcarrier data and a vehicle speed of 150km/h is assumed with the MAESTRO 5 (satellite + three terrestrial repeaters) urban channel profile implemented. The power-delay-profile (PDP) of this channel is as shown in Table 6.2.

Table 6.2: PDP for MAESTRO 5 satellite-terrestrial-hybrid channel

Tap	Relative delay (ns)	Mean power (dB)	Rice k-factor (dB)
1	0.0	-91.8	7
2	1692.7	-67.8	-1000
3	1757.8	-80.7	-1000
4	2278.6	-67.5	-1000
5	2343.7	-72.8	-1000
6	2408.8	-69.6	-1000
7	3190.0	-73.1	-1000
8	8203.0	-74.8	-1000
9	8268.1	-78.4	-1000
10	8788.9	-81.6	-1000

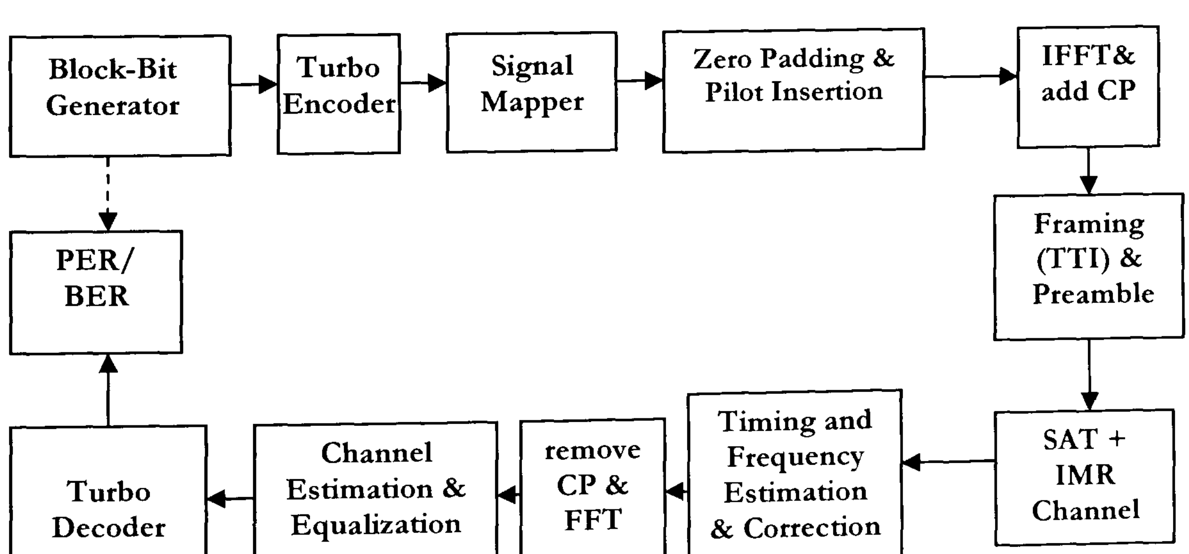

Figure 6.11: Block diagram showing the OFDM link-level simulator

The turbo encoder implements a systematic rate 1/3 parallel concatenated code while the log-map algorithm is used for decoding. Each frame or TTI (transmit time interval) consists of 12 OFDM symbols, preceded by the preamble needed for synchronization as defined for each tested method. Frequency-domain pilot symbols are placed within each TTI for the purpose of channel estimation and equalization via 2D time-frequency interpolation. 5 out of the 12 OFDM symbols in a frame contain such pilots (i.e. symbols 1, 4, 7, 10 and 12). For each of these 5 symbols, 107 out of the 705 active (i.e. ~6.3%) sub-carriers are used as pilot tones. Also 10% of the total transmit power is allocated to the pilots and 90% to useful data.

Figure 6.11 shows the performance of the proposed method in comparison to Schmidl's and Kim's methods in terms of packet-error-rate (PER). The proposed method is shown to achieve the same PER as an ideal time-frequency-synchronized system in contrast to the performance loss experienced by both existing methods due to their associated timing and frequency errors.

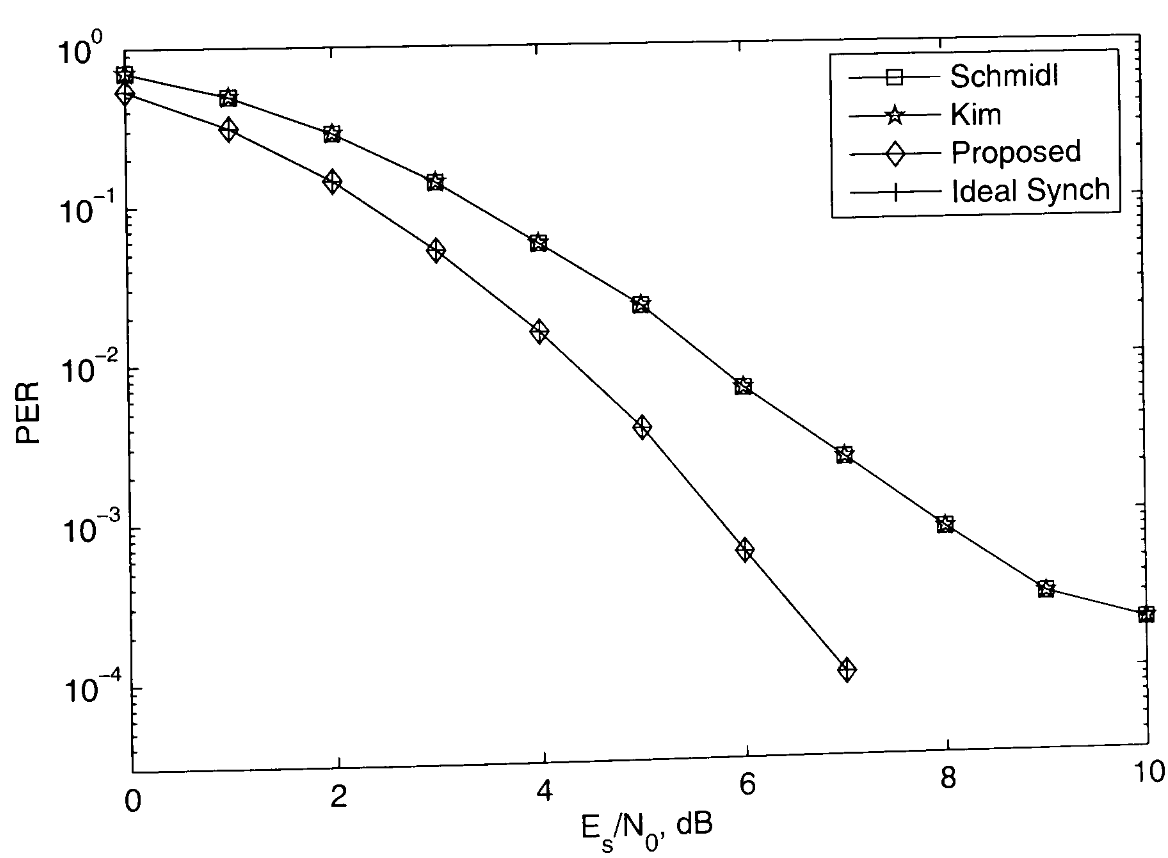

Figure 6.12: PER for the estimators; N=1024

Table 6.3 shows the mean value of the actual number of timing checkpoints used in the joint time-frequency stage to achieve the PER results shown, where it can be deduced that the first timing checkpoint is usually sufficient to achieve successful estimation. In comparison to Table 6.2, it can be seen that the number of timing checkpoints required for successful estimation reduces as the FFT size increases.

Table 6.3: Mean value of checkpoints used for successful estimation; N=1024

SNR (dB)	2	4	6	8	10
Mean checkpoints	1.0111	1.0049	1.0001	1.0000	1.0000

6.5 Conclusions

In this chapter, we have reviewed time-frequency synchronization for OFDM systems and discussed existing preamble-aided carrier frequency offset estimators having wide acquisition range. However, these methods suffer from different drawbacks such as estimation inaccuracy, overhead inefficiency, computational complexity and limited estimation range.

In order to jointly solve the problems of timing and frequency synchronization in OFDM systems with minimal preamble overhead, such as to achieve a BER similar to that of an ideal time-frequency-synchronized system, we have proposed a novel low-complexity method based on autocorrelation, restricted cross-correlation and threshold-based time-frequency detection. This method uses only one training symbol, having a simple and conventional structure, to achieve robust, reliable and full-range time-frequency synchronization in OFDM systems.

The method was compared with the popular existing methods in both terrestrial and satellite-terrestrial ISI channels. Computer simulation results for timing MSE and frequency MSE show that the proposed method achieves a superior performance to the existing ones, wherein its timing MSE is fractional and approaches the ideal value of zero while its integer frequency estimation is reliable even when the N_{use}/N ratio less than 100%. The proposed method is also shown to achieve the same BER and PER as an ideal time-frequency-synchronized OFDM system, which is not achievable by the existing methods due to their timing and/or frequency errors. By using the proposed algorithm, OFDM receivers will be able to operate at lower SNR, since the degradation that was previously experienced due to imperfect timing and/or frequency synchronization using existing techniques can now be eliminated. Also, there will be reduced hardware complexity and/or processing delay due to the use of the efficient FFT algorithm in the OFDM receiver to compute the integer frequency metric in contrast to the existing methods. Furthermore, the wide-range frequency estimation achieved by the proposed method provides for cheaper OFDM receivers which incorporate low-grade oscillators, since they will be able to operate under larger frequency offsets. An additional advantage is that the training symbol structure is compatible with current wireless network standards such as WiFi and WiMAX.

Table 6.4 summarizes the improvement achieved by the proposed OFDM time-frequency algorithm over existing techniques in the tested terrestrial multipath fading scenario.

Table 6.4: Summary table of improvement achieved by proposed method

Estimator	**Timing MSE (samples^2) SNR=4dB**	**Frequency MSE (Δf^2) SNR=4dB, $N_{use}=N$**	**Frequency MSE (Δf^2) SNR=4dB, $N_{use}<N$**
Proposed	0.29	$4.75\text{x}10^{-4}$	$4.95\text{x}10^{-4}$
Schmidl	41.68	19.26	120.89
Kim	-	$4.80\text{x}10^{-4}$	57.07

Chapter 7

7 Conclusions and Future Work

7.1 Conclusions

In this thesis, we have investigated robust synchronization algorithms for DVB-S2 and OFDM systems, as these technologies address the increasing demand for broadband applications and user mobility in modern wireless communications.

Firstly, single frequency estimation was discussed. The existing feed-forward techniques with practical computational complexity, such as Kay's WPA and M&M's methods are unable to achieve the full theoretical estimation range, which limits their application. Therefore, we have proposed two new feedforward techniques to solve this problem. The proposed WNLP and WNALP have a lower computational complexity than Kay's WPA and M&M's methods respectively and achieve the CRLB in similar fashion to the latter. Furthermore, they are able to achieve the full frequency estimation range which is ~50% of the sampling rate. Consequently, the proposed techniques are more robust for single frequency estimation since they achieve optimal accuracy and a full estimation range without compromising computational efficiency.

Secondly, carrier frequency synchronization for DVB-S2 systems which operate at very low SNR, have a stringent frequency accuracy requirement and tolerate large frequency offsets was examined. The existing techniques use a closed-loop FED for coarse frequency acquisition and a modified L&R's estimator for frequency fine-tuning, over a large number of pilot fields, in order to achieve the required estimation accuracy at very low SNR while maintaining a low complexity.

The use of two stages over multiple pilot fields leads to large synchronization delays. Consequently, we have proposed a modified version of the novel WNALP for wide-range single-stage DVB-S2 frequency synchronization. The proposed method achieves an improvement over the existing techniques in terms of reduced synchronization delays and increased estimation range. The improvement achieved by our proposed technique has increased significance for DVB-S2 mobile systems which may experience larger frequency offsets due to the Doppler effect and may need frequent carrier frequency re-synchronization due to severe signal fading (e.g. in railway tunnels).

Thirdly, we have reviewed the importance of timing synchronization and discussed existing preamble-aided methods for frame/symbol timing in OFDM systems. In order to improve timing performance, we have proposed a novel low-complexity technique which combines the advantages of autocorrelation and cross-correlation using a simple and conventional preamble structure with two identical parts. The method was compared with existing methods for OFDM timing synchronization in AWGN and Rayleigh fading multipath channels and computer simulation results for timing MSE and timing bias show that the proposed method achieves a superior performance to the existing methods, wherein its timing MSE and bias both approach the ideal value of zero. The proposed method is also shown to achieve the same BER as an ideal time-synchronized OFDM system which is not achievable by existing methods of comparable complexity and/or overhead. This means that the SNR degradation due to imperfect timing can now be fully recovered with a low complexity technique, leading to greater power-efficiency in OFDM systems. The improvement in timing estimation is achieved by the proposed method without compromising the repetitive structure needed in the preamble to achieve reliable frequency offset estimation using existing techniques. Consequently, robust timing and reliable frequency estimation are achieved with a minimum overhead of just one OFDM training symbol whose structure is compatible with commercial wireless network standards such as WiFi and WiMAX.

Lastly, we have reviewed time-frequency synchronization for OFDM systems and discussed existing preamble-aided carrier frequency offset estimators having wide acquisition range. It was noted that these methods suffer from different drawbacks such as timing estimation inaccuracy, overhead inefficiency, computational complexity and limited estimation range. In order to jointly solve the problems of timing and frequency synchronization in OFDM systems with minimum preamble overhead, we have proposed a novel low-complexity method based on autocorrelation, restricted cross-correlation and threshold-based time-frequency detection. This method uses only one training symbol, having a simple and conventional structure, to achieve robust, reliable and full-range time-frequency synchronization in OFDM systems. The method was compared with the existing methods in both terrestrial and satellite-terrestrial ISI channels wherein the proposed method is shown to achieve the same BER and PER as an ideal time-frequency-synchronized OFDM system, which is not achievable by the existing methods due to their timing and/or frequency errors. By using the proposed algorithm, OFDM receivers will be able to operate at lower SNR, since the degradation that was previously experienced due to imperfect timing and/or frequency synchronization using popular existing techniques can now be eliminated. Also, there will be reduced hardware complexity and/or processing delay due to the use of the efficient FFT algorithm in the OFDM receiver to compute the integer frequency metric in contrast to the existing methods. Furthermore, the wide-range frequency estimation achieved by the proposed method provides for cheaper OFDM receivers which incorporate low-grade oscillators, since they will be able to operate under large frequency offsets. An additional advantage is that the training symbol structure is compatible with current wireless network standards such as WiFi and WiMAX.

7.2 Future work

Based on the achievements of this thesis, we propose some future research work as follows:

- The novel algorithms for timing and time-frequency synchronization in OFDM systems make use of threshold-crossing (TC) detection based on simplifying assumptions. In the future, an in-depth analytical analysis of the TC detection criteria in ISI channels for OFDM systems should be performed. This will help to determine more accurately how the probability of false alarm P_{FA} varies with FFT size N and expected delay spread λ. An advantage of this in-depth analysis will be a proper choice of values for P_{FA} such that the occurrence of 'missed detection' is minimized, resulting in reduced processing delay in the proposed time-frequency algorithm.
- Single-user OFDM systems are evolving into various multi-user systems based on OFDMA (Orthogonal Frequency Division Multiple Access) [26],[33], wherein OFDM subcarriers are assigned to different users. This presents a new challenge to OFDM synchronization, especially in the uplink, since transmissions by different users may experience different frequency offsets and propagation delays. Some techniques have already been proposed for these scenarios but there is still room for improvement. Therefore, future research work should investigate OFDM synchronization in the multi-user

environment with the goal of achieving an enhanced efficiency in synchronization performance.

- A variant of OFDM is MIMO-OFDM, wherein the multiple-input-multiple-output (MIMO) techniques are combined with OFDM in order to achieve an increase in capacity while maintaining robustness against frequency-selective fading in the channel. This opens up another opportunity for further research, wherein robust and low-complexity synchronization techniques can be investigated.
- The work done within this thesis on OFDM synchronization can also be extended to OFDM channel estimation. In particular, the development of robust and efficient algorithms for joint time-frequency synchronization and channel estimation in OFDM systems can be explored.

List of Publications

- Awoseyila A.B., Kasparis C. and Evans B.G, "Frame timing and carrier frequency recovery for frequency selective signals," *UK Patent Application No. GB0803333.4*, April 2008.
- Awoseyila A.B., Kasparis C. and Evans B.G, "Robust and efficient time-frequency synchronization for OFDM systems," Submitted for publication in *IEEE Transactions on Wireless Communications*, 2008.
- Awoseyila A.B., Kasparis C. and Evans B.G, "Improved preamble-aided timing estimation for OFDM systems," *IEEE Communications Letters*, vol. 12, no. 11, pp. 825-827, Nov. 2008.
- Awoseyila A.B., Kasparis C. and Evans B.G, "Improved single frequency estimation with wide acquisition range," *Electronics Letters*, vol. 44, no. 3, pp. 245-247, Jan. 2008.
- Awoseyila A.B., Kasparis C. and Evans B.G, "Carrier synchronization for DVB-S2 systems in a Rician mobile channel," *25th AIAA International Communications Satellite Systems Conference*, Korea, Apr. 2007.
- Awoseyila A.B., Kasparis C. and Evans B.G, "Low-complexity frequency estimation for DVB-S2 systems at low SNR," *25th AIAA International Communications Satellite Systems Conference*, Korea, Apr. 2007.

Bibliography

1. Morello A. and Mignone V., "DVB-S2: The second generation standard for satellite broadband services," *Proceedings of the IEEE*, vol. 94, no. 1, pp. 210-227, Jan. 2006.
2. Teo K.H., Tao Z. and Zhang J., "The mobile broadband WiMAX standard," *IEEE Signal Processing Magazine*, vol. 24, no. 5, pp. 144 – 148, Sep. 2007.
3. Saunders S.R., *Antennas and Propagation for Wireless Communication Systems*, John Wiley, 1999.
4. Rappaport T.S., *Wireless Communications, Principles and Practice*, 2nd edition, Prentice Hall, 2002.
5. Parsons J. D., *The Mobile Radio Propagation Channel*, 2nd edition, John Wiley, 2002.
6. Evans B.G., *Satellite Communication Systems*, 3rd edition, the Institution of Electrical Engineers, 1999.
7. Maral G. and Bousquet M., *Satellite Communications Systems*, 3rd edition, John Wiley, 1998.
8. Reimers U. and Morello A., "DVB-S2, the second generation standard for satellite broadcasting and unicasting," *International Journal of Satellite Communications and Networking*, vol. 22, no. 3, pp. 249–268, May-June 2004.
9. ETSI EN 302 307, *Digital Video Broadcasting (DVB); Second Generation Framing Structure, Channel Coding and Modulation Systems for Broadcasting, Interactive Services, News Gathering and other Broadband Satellite Applications*, v1.1.1, June 2004.

10. Van Nee R. and Prasad R., *OFDM for Wireless Multimedia Communications*, Artech House, 1999.

11. Bahai A.R.S., Saltzberg B.R. and Mustafa E., *Multi-carrier Digital Communications: Theory and Applications of OFDM,* Springer-Verlag, New York Inc., 2004.

12. Schulze H. and Luders C., *Theory and Applications of OFDM and CDMA: Wideband Wireless Communications,* John Wiley and Sons Ltd., 2005.

13. Hanzo L., Muenster M., Choi B.J. and Keller T., *OFDM and MC-CDMA for Broadband Multi-user Communications, WLANs and Broadcasting,* John Wiley and Sons Ltd., 2003.

14. Keller T. and Hanzo L., "Adaptive multi-carrier modulation: A convenient framework for time-frequency processing in wireless communications," *Proceedings of the IEEE*, vol. 88, no. 5, pp. 611–640, May 2000.

15. Weinstein S. B. and Ebert P. M., "Data transmission by frequency division multiplexing using the discrete Fourier transform," *IEEE Transactions on Communications*, vol. 19, no. 10, pp. 628–634, Oct. 1971.

16. Bingham J. A. C., "Multi-carrier modulation for data transmission: An idea whose time has come," *IEEE Communications Magazine*, vol. 28, pp. 5–14, May 1990.

17. Cimini L. J., "Analysis and simulation of a digital mobile channel using orthogonal frequency division multiplexing," *IEEE Transactions on Communications*, vol. 33, no. 7, pp. 665–675, Jul. 1985.

18. ETSI EN 301 790, *Digital Video Broadcasting (DVB); Interaction Channel for Satellite Distribution Systems*, v1.3.1, Mar. 2003.

19. Vincent P. et al, "Mobile Wideband Global Link System (MOWGLY) – aeronautical, train and maritime global high-speed satellite services," *Proceedings of AIAA ICSSC conference*, Rome, Sep. 2005.

20. ETSI EN 300 401, *Radio Broadcasting Systems: Digital Audio Broadcasting to Mobile, Portable and Fixed Receivers*, 1995.

21. ETSI EN 300 744, *Digital Video Broadcasting (DVB); Frame Structure, Channel Coding and Modulation for Digital Terrestrial Television*, v.1.5.1, Nov. 2004.

22. ETSI EN 302 304, *Digital Video Broadcasting (DVB); Transmission System for Handheld Terminals*, v.1.1.1, Nov. 2004.

23. ETSI EN 302 583, *Digital Video Broadcasting (DVB); System Specifications for Satellite services to Handheld devices (SH) below 3 GHz*, v.1.1.1, Jul. 2007.

24. IEEE 802.11a, *Wireless LAN Medium Access Control (MAC) and Physical Layer (PHY) Specifications*, 1999.

25. IEEE 802.16.2004, *IEEE Standard for Local and Metropolitan Area Networks, Part 16: Air Interface for Fixed Broadband Wireless Access System*, 2004.

26. 3GPP Long Term Evolution, *http://www.3gpp.org/Highlights/LTE/LTE.htm*

27. Li B., Qin Y., Low C.P. and Gwee C.L., "A survey on mobile WiMAX," *IEEE Communications Magazine*, vol. 45, no. 12, pp. 70-75, Dec. 2007.

28. Mengali U., D'Andrea A. N., *Synchronization Techniques for Digital Receivers*, Plenum Press, New York, 1997.

29. Meyr H., Moeneclaey M. and Fechtel S., *Digital communication receivers: synchronization, channel estimation and signal processing*, Wiley, New York, 1997.

30. Proakis, J.G., *Digital Communications*, McGraw-Hill, New York, 1983.

31. Casini E., De Gaudenzi R. and Ginesi A., 'DVB-S2 modem algorithms design and performance over typical satellite channels', *International Journal of Satellite Communications and Networking*, vol. 22, no. 3, pp. 281-318, May-Jun. 2004.

32. Wu N. et al, "A modified carrier frequency estimator for DVB-S2 system," *IEEE Wireless Communications and Networking Conference (WCNC)*, pp. 2428-2432, 2007.

33. Morelli, M., Kuo, C.-C.J. and Pun, M.-O., "Synchronization techniques for orthogonal frequency division multiple access (OFDMA): a tutorial review," *Proceedings of the IEEE*, vol. 95, no. 7, pp. 1394-1427, Jul. 2007.

34. Pollet T., Van Bladel M. amd Moeneclaey M., "BER sensitivity of OFDM systems to carrier frequency offset and weiner phase noise," *IEEE Transactions on Communications*, vol. 43, pt.1, pp. 191-193, Feb.-Apr. 1995.

35. Awoseyila A.B., Kasparis C. and Evans B.G, "Low-complexity frequency estimation for DVB-S2 systems at low SNR," *25th AIAA International Communications Satellite Systems Conference*, Korea, Apr. 2007.

36. Awoseyila A.B., Kasparis C. and Evans B.G, "Carrier synchronization for DVB-S2 systems in a Rician mobile channel," *25th AIAA International Communications Satellite Systems Conference*, Korea, Apr. 2007.

37. Awoseyila A.B., Kasparis C. and Evans B.G, "Improved single frequency estimation with wide acquisition range," *Electronics Letters*, vol. 44, no. 3, pp. 245-247, Jan. 2008.

38. Awoseyila A.B., Kasparis C. and Evans B.G, "Improved preamble-aided timing estimation for OFDM systems," *IEEE Communications Letters*, vol. 12, no. 11, pp. 825-827, Nov. 2008.

39. Awoseyila A.B., Kasparis C. and Evans B.G, "Robust and efficient time-frequency synchronization for OFDM systems," Submitted for publication in *IEEE Transactions on Wireless Communications*, 2008.

40. Gardner F.M., "Demodulator reference recovery techniques suited for digital implementation," *European Space Agency Final Report*, ESTEC contract no. 6847/86/NL/DG, Aug. 1988.

41. Luise M. and Reggiannini R., "Carrier frequency recovery in all-digital modems for burst-mode transmission," *IEEE Transactions on Communications*, vol. 43, no. 3, pp.1169-1178, Mar. 1995.

42. Albertazzi G. et al, "On the adaptive DVB-S2 physical layer: design and performance," *IEEE Wireless Communications*, vol. 12, no. 6, pp. 62-68, Dec. 2005.

43. C. Shannon, *A Mathematical Theory of Communication*, Bell System Technical Journal, 1948.

44. ETSI TR 101 112, *Selection Procedures for the Choice of Radio Transmission Technologies of the UMTS*, v3.2.0, Apr. 1998.

45. Sweeney, P., *Error Control Coding: from Theory to Practice*, John Wiley, 2002.

46. Kay S., *Fundamentals of Statistical Signal Processing: Estimation Theory*, Prentice-Hall, Englewood Cliffs, N.J., 1993.

47. Papoulis A. and Pillai S., *Probabilities, Random Variables and Stochastic Processes*, 4th edition, McGraw-Hill, 2002.

48. Kay S., *Modern Spectral Estimation: Theory and Applications*, Prentice-Hall, Englewood Cliffs, N.J., 1988.

49. Van Trees H.L., *Detection, Estimation and Modulation: Part 1*, John Wiley, New York, 1968.

50. D'Andrea A.N., Mengali U. and Reggiannini R., "The modified Cramer-Rao bound and its applications to synchronization problems," *IEEE Transactions on Communications*, vol. 42, no. 2/3/4, pp. 1391-1399, Feb./Mar./Apr. 1994.

51. Rife, D.C. and Boorstyn, R.R., "Single tone parameter estimation from discrete time observations," *IEEE Transactions on Information Theory*, vol. IT-20, pp. 591-598, Sep. 1974.

52. Kay S., "A fast and accurate single frequency estimator," *IEEE Transactions on Acoustics, Speech and Signal Processing*, vol. 37, no.12, pp. 1987-1990, Dec. 1989.

53. Gardner, F.M, "Properties of frequency difference detectors," *IEEE Transactions on Communications*, vol. 33, pp. 131-138, Feb. 1985.

54. D.G. Messerschmitt, "Frequency detectors for PLL acquisition in timing and carrier frequency recovery," *IEEE Transactions on Communications*, vol. 36, pp. 1035-1043, Sep. 1988.

55. D'Andrea A.N. and Mengali U., "Noise performance of two frequency-error detectors derived from maximum likelihood estimation methods," *IEEE Transactions on Communications*, vol. 42, pp.793-802, Feb./Mar./Apr. 1994.

56. Franks L.E., "Carrier and bit Synchronization in data communication – a tutorial review," *IEEE Transactions on Communications*, vol. 28, pp. 1107-1121, Aug. 1980.

57. Gardner, F.M., *Phase Lock Techniques*, 2nd edition, John Wiley, New York, 1979.

58. Scholtz R.A., "Frame synchronization techniques," *IEEE Transactions on Communications*, vol. COM-28, no. 8, pp. 1204-1213, Aug. 1980.

59. Massey J.L., "Optimum frame synchronization," *IEEE Transactions on Communications*, vol. COM-20, no. 2, pp. 115-119, April 1972.

60. Oppenheim A. and Schafer R.W., *Discrete-Time Signal Processing*, Prentice-Hall, Englewood Cliffs, NJ, 1989.

61. Brown T. and Wang M.M., "An iterative algorithm for single frequency estimation," *IEEE Transactions on Signal Processing*, vol. 50, no. 11, pp. 2671-2682, Nov. 2002.

62. Zakharov Y.V. and Tozer T.C., "Frequency estimator with dichotomous search of periodogram peak," *Electronic Letters*, vol. 35, pp. 1608-1609, Sep. 1999.

63. Fitz M.P, "Further results in the fast estimation of a single frequency," *IEEE Transactions on Communications*, vol. 42, no. 2-4, pp. 862–864, Feb-Apr. 1994.

64. Mengali U. and Morelli M., "Data-aided frequency estimation for burst digital transmission," *IEEE Transactions on Communications,* vol. 45, no. 1, pp. 23-25, Jan. 1997.

65. Tretter S., "Estimating the frequency of a noisy sinusoid by linear regression," *IEEE Transactions on Information Theory*, vol. IT-31, pp. 832–835, Nov. 1985.

66. Kim D., Narasimha M., and Cox D., "An improved single frequency estimator," *IEEE Signal Processing Letters*, vol. 3, pp. 212–214, Jul. 1996.

67. M. Fowler and J. Johnson, "Extending the threshold and frequency range for phase-based frequency estimation," *IEEE Transactions on Signal Processing*,

vol. 47, pp. 2857–2863, Oct. 1999.

68. Leung S.H and Lau W.H., "Modified Kay's method with improved frequency estimation," *Electronic Letters*, vol. 36, no. 10, pp. 918-920, May 2000.

69. Zhang Z., Jakobsson A., Macleod M.D. and Chambers J.A., "A hybrid phase-based single frequency estimator," *IEEE Signal Processing Letters*, vol. 12, no. 9, Sep. 2005.

70. Fu, H. and Kam, P.Y., "Improved weighted phase averager for frequency estimation of single sinusoid in noise," *Electronics Letters*, vol. 44, no. 3, pp. 247-248, Jan. 2008.

71. Lank G., Reed I. and Pollon G., "A Semicoherent detection and Doppler estimation statistic," *IEEE Transactions on Aerospace and Electronic Systems*, vol. AES-9, no. 2, pp. 151–165, Mar. 1973.

72. Classen, F., Meyr, H. and Sehier, P., "Maximum likelihood open loop carrier synchronizer for digital radio," *IEEE International Conference on Communications*, vol.1, pp. 493-497, 1993.

73. Volcker B. and Handel P., "Frequency estimation from proper sets of correlation," *IEEE Transactions on Signal Processing*, vol. 50, no. 4, pp. 791-802, Apr. 2002.

74. Wang Z. and Abeysekera S. S., "Efficient frequency estimation using the pulse-pair method at different lags," *Proceedings of the IEEE International Conference on Acoustics, Speech and Signal Processing*, Hong Kong, pp. 517–520, Apr. 2003.

75. Dongming B. and Xinying Y., "An improved Fitz carrier frequency offset estimation algorithm," *International Conference on Communication Technology (ICCT) Proceedings*, vol. 2, pp. 778-781, 2003.

76. Wang Z. and Abeysekera S. S., "Frequency estimation from multiple lags of correlations in the presence of MA colored noise," *Proceedings of the IEEE International Conference on Acoustics, Speech and Signal Processing*, Philadelphia, pp. 693–696, 2005.

77. Rezki M., Kale I. and Sabel L., "Reduced complexity feed forward frequency estimator for AWGN Channels," *14th International Conference on Digital Signal Processing*, vol. 2, pp. 1313-1316, Jul. 2002.

78. Sun F-W, Jiang Y, Lee L-N., "Frame synchronization and pilot structure for second generation DVB via Satellites," *International Journal of Satellite Communications and Networking*, vol. 22, no. 3, pp. 319–339, May-Jun. 2004.

79. Jakes W. C., *Microwave Mobile Communications*, IEEE press, New York, 1994.

80. Holzbock M. et al., "Aeronautical Channel Characterization Measurements at K band," *4th Ka band Conference*, pp. 263-269, 1998.

81. Hagenauer, J et al., "The maritime satellite communication channel - channel model, performance of modulation and coding," *IEEE Journal on selected areas in communications*, vol. SAC-5, no. 4, pp. 701-713, May 1987.

82. Patzold, M. et al., "A study of a land mobile satellite channel model with Assymetrical Doppler Spectrum and lognormally Distributed Line of Sight Component," *IEEE Transactions on Vehicular Technology*, vol. 47, no. 1, pp. 297-310, Feb. 1998.

83. Sciascia, G. et al., "Statistical characterization of the railroad satellite channel at Ku-band," *Proceedings of the International Workshop of COST Actions 272 and 280,* May 2003.

84. Diaz, M.A. et al, "DVB-S air interface over railroad satellite channel: performance and extensions," *Sixth Baiona Workshop on Signal Processing in Communications*, pp. 277-282, 2003.

85. Faraj Z. et al, "Mobility and fading impacts on DVB-RCS systems," *3rd Advanced Satellite Mobile Systems (ASMS) Conference*, Germany, May 2006.

86. Schmidl, T., and Cox, D.C., "Robust frequency and timing synchronization for OFDM," *IEEE Transactions on Communication,* vol. 45, no. 12, pp. 1613 – 1621, Dec. 1997.

87. Nogami H. and Nagashima T., "A frequency and timing period acquisition technique for OFDM systems," *Personal, Indoor and Mobile Radio Communications (PIMRC) conference*, vol. 3, pp. 1010–1015, Sep. 1995.

88. Classen F. and Meyr H., "Frequency synchronization algorithms for OFDM systems suitable for communication over frequency selective fading channels," *IEEE Vehicular Technology Conference*, vol. 3, pp. 1655–1659, Aug. 1994.

89. Minn H., Bhargava V. K. and Letaief K. B., "A robust timing and frequency synchronization for OFDM systems," *IEEE Transactions on Wireless Communications*, vol. 2, no. 4, pp. 822–839, Jul. 2003.

90. Shi K. and Serpedin E., "Coarse frame and carrier synchronization of OFDM systems: A new metric and comparison," *IEEE Transactions on Wireless Communications*, vol. 3, no. 4, pp. 1271–1284, Jul. 2004.

91. Park, B., Cheon, H., Kang, C., and Hong, D., "A novel timing estimation method for OFDM systems," *IEEE Communication Letters,* vol. 7, no. 5, pp. 239-241, May 2003.

92. Ren, G., Chang, Y., Zhang, H., and Zhang, H., "Synchronization methods based on a new constant envelope preamble for OFDM systems," *IEEE Transactions on Broadcasting,* vol. 51, no. 1, pp.139-143, Mar. 2005.

93. Kasparis C. and Evans B.G., "A cross-correlation approach for improved timing estimation in OFDM broadcasting systems," *24th AIAA International. Communication Satellite Systems Conference (ICSSC)*, pp. 1039-1048, Jun. 2006.

94. Minn, H., Zeng, M., and Bhargava, V.K., "On timing offset estimation for OFDM systems," *IEEE Communication Letters,* vol. 4, pp. 242-244, Jul. 2000.

95. Yang B., Letaief K. B., Cheng R. S. and Cao Z., "Timing recovery for OFDM transmission," *IEEE Journal on Selected Areas in Communication*, vol. 18, no. 11, pp. 2278–2291, Nov. 2000.

96. Fort A. et al "A performance and complexity comparison of auto-correlation and cross-correlation for OFDM burst synchronization," *IEEE International Conference on Acoustics, Speech and Signal Processing,* vol. 2, pp. 341-344, Apr. 2003.

97. Kim H.W., Kunseok K. and Ahn D-S., "Efficient time and frequency synchronization for OFDM based wireless indoor communication over Rician fading channel," *IEEE 10th International Symposium on Consumer Electronics (ISCE)*, pp. 1-5, 2006.

98. Ai S., Leung S-H and Leung C-S., "A novel synchronization scheme for OFDM over fading channels," *IEEE International Conference on Acoustics, Speech and Signal Processing (ICASSP)*, vol. 4, pp. IV-401-404, May 2006.

99. Balamurali N. and Jalihal D., "Robust timing and frequency synchronization algorithm for IEEE 802.16 OFDM systems," *International Conference on Signal Processing and Communications (SPCOM)*, pp. 234-238, 2004.

100. Speth M., Fechtel S., Fock G. and Meyr H., "Optimum receiver design for wireless broadband systems using OFDM, Part I," *IEEE Transactions on Communications*, vol. 47, no. 11, pp. 1668–1677, Nov. 1999.

101. Tufvesson F., Edfors O. and Faulkner M., "Time and frequency synchronization for OFDM using PN-sequence preambles," *IEEE Vehicular Technology Conference*, vol. 4, pp. 2202–2207, Sep. 1999.

102. Coulson A. J., "Maximum likelihood synchronization for OFDM using a pilot symbol: Algorithms," *IEEE Journal on Selected Areas in Communication*, vol. 19, no. 12, pp. 2486–2494, Dec. 2001.

103. Coulson A. J., "Maximum likelihood synchronization for OFDM using a pilot symbol: Analysis," *IEEE Journal on Selected Areas in Communication*, vol. 19, no. 12, pp. 2495–2503, Dec. 2001.

104. Wu F. and Abu-Rgheff A. M., "Time and frequency synchronization for OFDM systems operating in Gaussian and fading channels: a tutorial," *8th Annual Postgraduate Symposium on the Convergence of Telecommunications, Networking and Broadcasting (PGNET)*, June 2007.

105. Keller T., Piazzo L., Mandarini P. and Hanzo L., "Orthogonal frequency division multiplex synchronization techniques for frequency-selective fading channels," *IEEE Journal on Selected Areas in Communication*, vol. 19, no. 6, pp. 999–1008, June 2001.

106. Kim et al, "Enhanced frame synchronization for DVB-S2 system under a large frequency offset," *Wireless Communications and Networking Conference (WCNC) 2007*, pp. 1184 – 1188, Mar. 2007.

107. Morelli, M., and Mengali, U., "An improved frequency offset estimator for OFDM systems," *IEEE Communication Letters,* vol. 3, no. 3, pp. 239-241, Mar. 1999.

108. Kim Y. H., Song I., Yoon S. and Park S., "An efficient frequency offset estimator for OFDM systems and its performance characteristics," *IEEE Transactions on Vehicular Technology,* vol. 50, no. 5, pp. 1307-1312, Sep. 2001.

109. Moose P. H., "A technique for orthogonal frequency division multiplexing frequency offset correction," *IEEE Transactions on Communications*, vol. 42, no. 10, pp. 2908–2914, Oct. 1994.

110. Lambrette U., Speth M. and Meyr H., OFDM burst frequency synchronization by single carrier training data, *IEEE Communication Letters*, vol. 1, no. 2, pp. 46–48, Mar. 1997.

111. Song H. K., You Y. H., Park J. H. and Cho Y. S., "Frequency-offset synchronization and channel estimation for OFDM-based transmission," *IEEE Communication Letters*, vol. 4, no. 3, pp. 95–97, Mar. 2000.

112. Daffara F. and Adami O., "A novel carrier recovery technique for orthogonal multicarrier systems," *European Transactions on Telecommunications*, vol. 7, pp. 323–334, Jul./Aug. 1996.

113. Morelli M. and Mengali U., "Carrier Frequency Estimation for Transmissions over Selective Channels," *IEEE Transactions on Communications*, vol. 48, no. 9, pp. 1580-1589, Sep. 2000.

114. Evans B.G, Thompson P.T., Kasparis C. and Janaaththanan S., "Analysis of the S-UMTS specification for B3G," *UniS and ETRI Project Deliverable D3- Final Report on downlink performance of OFDM-based S-UMTS*, March 2006.

115. 3GPP TR 25.892, *3rd Generation Partnership Project; Technical Specification Group Radio Access Network; Feasibility Study for OFDM for UTRAN enhancement*, v.6.0.0, June 2006.